

Biomedical Application of Piezoelectric Micro Diaphragm Pumps

Zur Erlangung des akademischen Grades eines
DOKTORS DER INGENIEURWISSENSCHAFTEN (DR.-ING.)

von der KIT-Fakultät für Chemieingenieurwesen und Verfahrenstechnik des Karlsruher Instituts für Technologie (KIT)

genehmigte
DISSERTATION

von
Agnes Beate Bußmann, M. Sc.
aus Heppenheim, Deutschland

Tag der mündlichen Prüfung: 27.04.2022

Erstgutachter: Prof. Dr. Jürgen Hubbuch

Zweitgutachter: Prof. Dr. Christoph Kutter



This document is licensed under a Creative Commons
Attribution-Non Commercial 4.0 International License (CC BY-NC 4.0):
<https://creativecommons.org/licenses/by-nc/4.0/deed.en>

Acknowledgements

This dissertation is the result of several years of research and development and would not have been feasible without the support of numerous people to whom I would like to express my thanks.

First and foremost, I would like to thank Professor Jürgen Hubbuch for the supervision of my doctoral project. He was always available for technical discussions, interested in my work outside of his core field of research and eager to support me in any possible way. Being based at Fraunhofer in Munich, I was always welcome in Karlsruhe and happily included into the team. I am very grateful for the excellent supervision.

A large thank you also goes to Professor Christoph Kutter, the second assessor of my dissertation. No matter how busy he was, he would make time to discuss my plans and ideas. His suggestions and ideas were indispensable, and his support extends far beyond my dissertation.

Special thanks go to Dr. Carsten Radtke, who was my very first point of contact with the MAB institute. I genuinely appreciate his open mind, the time he took to introduce the MAB and its research as well as to get to know me and my project. His interest in my work was very encouraging and his technical input most helpful.

The whole MAB-team was a great support to my work. During several stays to perform experiments in their labs, everybody was always keen to help me wherever needed. Especially I would like to thank Nils Hillebrandt and Dennis Weber, who helped me plan, organize, and conduct my experiments and supported me with all the lab equipment. But not only the MAB-team's input during experimental work was most helpful, I also appreciated their comments and ideas during seminar sessions where I had the pleasure to present my research to the team. Unfortunately, due to the pandemic situation I could only join one face to face "Seminarfahrt", which was a great experience. But also, during online sessions, the added ideas and comments to my work were extremely helpful. And even though, the in-person contact was greatly restricted during the last two years, I always felt most welcome in the MAB-Team and would like to thank the whole team for that.

Special thanks go to Polina Mednikova and Nicole Beckert, as I could not imagine any better collaboration within our shared EU-project Moore4Medical. I really enjoyed working with them and hope to carry on the good collaboration during the second half of the project.

It is a great pleasure to work in the department of microdosing at Fraunhofer EMFT and I am happy to have had the chance to conduct the research for my dissertation here. Many thanks go to Dr. Martin Richter for this opportunity.

Microdosing in general and micropumps in particular are a topic that is impossible to tackle for a single person and I am more than happy that the whole DOS-team supported me during my thesis. It was not only great to share ideas, receive so many suggestions and always have somebody to support me in the laboratory. I additionally really appreciate the personal relationship within the team and am happy to have such great co-workers. It is impossible to name all the individual contributions and I hope that each and every team member knows how grateful I am for their support.

I am especially grateful for the support of Christian Wald during the whole process. Not only has he happily discussed technical details with me, but also never hesitated

to provide time and resources to forward my research. I was lucky to have such a great supporter with him.

Furthermore, I would like to thank Lorenz Grünerbel, not only for being the perfect office mate, partner in crime in each step of the dissertation, and irreplaceable co-worker, but also for being the friend I needed so often within the last four years. I would not be where I am right now without his support.

Special thanks also go to Claudia Durasiewicz and Thomas Thalsofer. Starting (nearly) at the same point in time at DOS, we spent a great deal of time with similar problems. It was great to always count on their support each step of the way and to enjoy such a good time together. Furthermore, I would like to thank Martin Wackerle, since without him, nothing ever works. His patient and kind support with countless experimental setups and data analysis was irreplaceable. I am also grateful to Yücel Congar, who was the very first to patiently introduce me to our equipment and processes in the lab. His calm and focused way of working was always a big support and extraordinary help. Additionally, I would like to thank Dr. Sebastian Kibler for his support, though specifically for his targeted and skillful demotivation work.

Obviously not only the microdosing department supported me during my dissertation, but also many other colleagues from EMFT. I am thankful for the technical support from other departments, as well as the administrative support during each phase of my work. We can be happy to have such a great team.

A large thank you goes to Til Friebe, Sophie Hoffmann, Philipp Korzer, Florina Pommerening, William Bittner, Richard Ganser, and Maximilian Schumann, who supported my work during their Bachelor and Master thesis. Furthermore, I'd like to thank Thalia Hoffmann, Sophia Güntner, Philipp Maier, and Nivedha Surendran for their support during their internship, and Doris Zhou and Oliver Zett for their great help as working students. All of them were in one or the other way involved in the technical work of this dissertation. They have all done a great job in their individual projects and I was more than happy to have the chance to work with them. Besides their excellent technical work, I would also like to thank all of them for the good team work; it was a pleasure.

During my thesis I had the chance to work in many industrial and research projects. It was great to be able to forward such interesting topics together with many partners. I am very grateful for the interesting research, but also for the great time we spent together. I can only say thank you for four interesting and fun years to each one of them.

Lots of work went into proof reading my dissertation before I handed it in. I would like to thank Lorenz Grünerbel, Dr. Sebastian Kibler, Christian Wald, Alexandre Capone, Claudia Durasiewicz, my sister, and my father for their support during the writing process.

Last but not least, it remains to say thank you to all the private support that I have received from my friends and family within the last years. All the motivation, encouragement and time spent together were an indispensable support of this work.

Agnes Bußmann, München, 03.05.2022

Abstract

Fluid transport is a ubiquitous task in biomedical applications. Controlled flow is required by different various devices, e.g., hydraulic implants, drug delivery units, laboratory equipment for analysis and assay automatization, or even three dimensional bioprinting. State-of-the-art fluid transport methods rely on large, costly pumps with comparatively high power consumption, and the lack of small pump systems hinders the development of handheld devices, fully automated disposables, implants, or patch pumps. A possible solution are micropumps: miniaturized, energy-efficient fluidic actuators that enable the transport of small amounts of fluid. A promising type of micropumps are piezoelectrically actuated micro diaphragm pumps that combine many advantageous properties: they are extremely miniaturizable, the actuation is energy-efficient, the setup is comparatively easy and allows tailored solutions for specific requirements. Thus, piezoelectric micro diaphragm pumps offer great potential for improved biomedical devices.

The change from a macroscopic pump system to a micropump and the implied switch from fluidic to **microfluidic** systems results in significant challenges. This work distinguishes safety relevant requirements, flow properties and system-specific needs. Micropump research has revealed elaborate solutions for specific risks and challenging specifications. However, there are important requirements that have not yet been investigated, which hinders the technology's market breakthrough.

One important aspect that has been scarcely investigated is the **dosing precision** and **accuracy** of micropumps. Often a pump's **single stroke volume**, the volume that is displaced with one single oscillation of the actuator diaphragm, is stated as achievable limit of resolution. However, there is usually no information on the repeatability of single strokes or their sensitivity to changing conditions, e.g., backpressure or temperature. The fluctuation of the **stroke volume** limits the accuracy of a closed-loop control system, especially if the aimed volume is in the order of magnitude of a single stroke. Consequently, a detailed analysis of the **dosing precision** as well as design improvements towards more repeatable dosing are necessary. A change of medium can have a significant impact on the precision, since medium properties such as surface interaction, viscosity, or surface tension can impact the fluid transport in **microfluidic** devices. Therefore, it is required to perform experimental analysis with the application's target medium in addition to commonly used surrogate fluids, e.g., deionised water. The pump's dosing precision can also vary over time, for instance due to degradation of the actuator or the valve structures. This degradation can for instance be caused by gradual occlusion.

Due to the small geometries of **microfluidic** devices with a high surface to volume ratio, moving parts in the fluid paths, and fragile mechanical structures such as spring valves, the interaction between a micropump and the dosed medium can be more severe than in macroscopic pumps. For instance, protein agglomeration within a dosed drug solution can impair the therapeutic effect of the medication and lead to gradual occlusion of the pump system. For a reliable use of **microfluidic** actuators in the biomedical field, the investigation of any interaction that can damage the pump and impact the dosed medium is therefore indispensable.

In addition to technological challenges discussed above, economical requirements hinder the widespread implementation of micropumps in biomedical applications, even though they offer evident advantages compared to conventional pumps. There are large initial costs for development, detailed examination, and initial approval process of a new

technology in a medical product. Therefore, advances in medical device technology are slow and only incremental improvements based on already implemented technologies instead of completely new developments are introduced.

It is the aim of this thesis to advance the biomedical application of piezoelectric micro diaphragm pumps by improving the technology developed at the [Fraunhofer EMFT](#) Research Institution for Microsystems and Solid State Technologies. There are two main pump types, small silicon and larger stainless-steel pumps. In this thesis, both are evaluated and optimised in terms of fluidic properties, biocompatibility of the used material, and medium interaction.

To achieve better fluidic performance, an increase of the negative actuation voltage is evaluated. For piezoelectric actuation, the negative voltage amplitude is commonly limited to prevent depolarisation. However, higher negative actuation voltages are particularly interesting; due to the nonlinearity of the piezoelectric elongation, they lead to an overproportional increase of the diaphragm stroke. Therewith the achieved flow rate is overproportionally increased. For experiments with higher negative actuation voltages, the exact knowledge of the [coercive field](#), i.e., of the electric field where the polarisation switches its direction, is necessary. In this thesis, the [coercive field](#) of 1 kV/mm is determined with a custom-made setup. By increasing the negative actuation of steel and silicon micro diaphragm pumps from the commonly used 40 % to 90 % of the negative [coercive field](#), two fundamental pump characteristics are improved: the maximal flow rate due to an increased [stroke height](#), and the achievable air backpressure due to the increased [compression ratio](#). Without backpressure, the air flow rate increases by 30%, while at 30 kPa backpressure, it increases by 160 %. To detect depolarisation caused by the additional negative field, the [actuator stroke](#) is continually monitored for one million cycles. Even with a negative amplitude of -1 kV/mm, no depolarisation is visible due to regular repolarisation by the high positive amplitude of 1.5 kV/mm. The results indicate that negative voltages higher than those used conventionally can be employed, resulting in improved fluidic performance. This performance increase is implemented in a new silicon micropump for drug delivery that therewith reaches the required flow performance.

This adapted micropump of $5 \times 5 \times 0.6 \text{ mm}^3$, introduced and evaluated in this thesis in terms of performance and [dosing precision](#), aims to advance the development of miniaturized drug delivery units. The pump achieves a water flow rate of $74 \pm 6 \text{ }\mu\text{L/min}$, which is suitable for subcutaneous drug delivery. Its [blocking pressure](#) of approximately 51 kPa is sufficient to overcome additional backpressure, e.g., by occlusion of the injection site. Furthermore, the [precision](#) of volume package dosing is investigated with water and an insulin solution. This allows to determine problems caused by the change of transported liquid. Indeed, the higher surface tension of the insulin solution causes more stable air-liquid interfaces and thus increases the effort to transport a bubble through the pump. Nevertheless, the achieved [precision](#) is high compared to commercially available pump systems, also with the insulin solution. The standard deviation stays below the generally accepted 5%, even for extremely small packages of 0.5 mg, which can enable the dosage of higher concentrated drugs in future. The results of this study are promising for the development of further miniaturized patch pumps or even implantable systems that can increase the patients' comfort and enable better treatment.

An implantable application imposes even more material requirements than extracorporeal biomedical devices. For instance, the used material should not cause any arte-

facts in medical imaging such as nuclear magnetic resonance imaging or computed tomography scanning. This requirement is unproblematic for silicon pumps, though the steel micropumps developed for larger flow rates can cause artefacts in imaging. Therefore, part of this thesis is dedicated to the transfer of the pump technology to a titanium platform. The resulting novel pump performs equally well compared to state-of-the-art steel pumps. It achieves a water flow rate of 14.0 ± 2.2 mL/min and **blocking pressure** of 75 kPa, which is suitable for implantable devices such as hydraulic implants. The new pump is part of a titanium-based **microfluidic** technology platform that additionally contains two active valves. This platform allows for flexible development of several **microfluidic** biomedical devices and therewith distributes the initial effort to introduce a new technology on several parallel developments. Consequently, the platform can help promote the industrialisation of micro diaphragm pumps for biomedical applications.

In addition to implantable devices, the flexible applicability of the titanium technology platform enables the development of biomedical equipment, e.g., analysis systems, automated cell culture or three dimensional bioprinting. For utilization in this field, the influence of the pump on the transported medium should be minimal. Therefore, this thesis investigates the impact of transport with micro diaphragm pumps on cells in solution. Preliminary experiments show a significant impact of the small silicon micropump with an increase of dead cells of 30 percentage points compared to non-pumped cell solution. The larger metal pump causes less damage. Nevertheless, the influence is significant if a rectangular waveform, which is the fluidically most efficient actuation, is used. To limit the impact without loss in performance, an adapted actuation is investigated. The mixed signal, a rectangular waveform with 60 Hz sinusoidal flanks, shows similar properties in fluid transport as it achieves the same single **stroke volume** as the rectangular signal. The experimental analysis of the cell transport reveals a lower impact of the mixed signal compared to rectangular actuation. The decrease of viable cells compared to the non-pumped samples is small and the impact is similar to sinusoidal actuation. The adapted actuation signal therefore enables gentler cell transport than rectangular actuation.

The use of pumps within applications that require the transport of liquids containing cells, particles, fibres, or other solid substances, can cause severe damage to the **microfluidic** actuator. The pump includes narrow flow paths and sensitive structures, such as passive valves. To enable reliable transport of, e.g., cell solution, an experimental analysis of the particle tolerance of the pumps is necessary. To this end, the model of polystyrene particles enables a detailed experimental understanding. Optical imaging shows deposition in the valve structures, and fluidic as well as electromechanical analysis reveal a loss in performance. The impact of particles with a diameter of $16 \mu\text{m}$ is more severe than that of particles with a diameter of $1 \mu\text{m}$. Nevertheless, none of the tested pumps fails, even though the particle concentration is extremely high. The experimental evaluation reveals the need for geometric improvements, such as the avoidance of 90° angles, narrow paths and areas of zero flow.

The developments presented in this thesis address pressing, unsolved challenges of biomedical **microfluidic** applications and provide significant learnings that can be used in future to further improve the introduced micropumps. The detailed experimental analysis proves the benefit of implemented design adjustments and highlights necessary future adaptations. This work is therefore a step towards the biomedical application of micro diaphragm pumps and advances the development of improved treatment possibilities.

Zusammenfassung

Der Transport von Flüssigkeiten ist eine allgegenwärtige Aufgabe in biomedizinischen Anwendungen. Die Dosierung von Arzneimitteln ist ein geläufiges Beispiel für die Notwendigkeit einer präzisen und zuverlässigen Dosierung. Darüber hinaus ist kontrollierter Medientransport für verschiedene biomedizinische Anwendungen erforderlich. Beispiele sind hydraulische Implantate, Laborgeräte für die Analyse und Automatisierung von Versuchen oder sogar das dreidimensionale Bioprinting. Bisher werden für den Transport von Fluiden große, teure Pumpen mit vergleichsweise hohem Stromverbrauch verwendet und der Mangel an kleinen Pumpensystemen behindert die Entwicklung von Handgeräten, vollautomatischen Einmalgeräten, Implantaten oder Patch-Pumpen. Eine mögliche Lösung sind Mikropumpen: miniaturisierte, energieeffiziente fluidische Aktoren, die den Transport von kleinen Flüssigkeitsmengen ermöglichen. Ein vielversprechender und gut erforschter Mikropumpentyp sind piezoelektrisch betriebene Mikromembranpumpen. Diese vereinen viele vorteilhafte Eigenschaften: Sie sind extrem miniaturisierbar, energieeffizient, vergleichsweise einfach aufgebaut und ein flexibles Design erlaubt eine Anpassung an spezifische fluidmechanische Anforderungen. Daher bieten piezoelektrische Mikromembranpumpen ein großes Potenzial für verbesserte biomedizinische Geräte.

Der Wechsel von einem makroskopischen Pumpensystem zu einer Mikropumpe und der beinhaltete Wechsel von fluidischen zu mikrofluidischen Systemen führt zu erheblichen Herausforderungen. In dieser Arbeit wird zwischen sicherheitsrelevanten Aspekten, fluidischen Anforderungen und systemspezifischen Eigenschaften unterschieden. Die bisherige Mikropumpenforschung hat raffinierte Lösungen für mikrofluidische Problemstellungen sowie gut durchdachte Designanpassungen zur Steigerung der fluidischen Leistung hervorgebracht. Allerdings gibt es wichtige Anforderungen, die noch nicht untersucht wurden, was den Marktdurchbruch der Technologie behindert.

Ein wichtiger Aspekt, der bisher kaum untersucht wurde, ist die Präzision sowie die Genauigkeit der Dosierung. Oft wird das Einzelhubvolumen einer Pumpe, also das Volumen, das mit einer einzigen Schwingung der Antriebsmembran verdrängt wird, als erreichbare Auflösungsgrenze angegeben. Es gibt jedoch in der Regel keine Informationen über die Wiederholbarkeit der Einzelhübe oder ihre Empfindlichkeit gegenüber wechselnden Bedingungen, wie wechselnder Gegendruck oder Änderungen der Temperatur. Die Schwankung des Hubvolumens begrenzt jedoch die Genauigkeit eines Regelsystems, insbesondere wenn das angestrebte Volumen in der Größenordnung eines Einzelhubs liegt. Folglich sind eine detaillierte Analyse der Dosierpräzision sowie Designverbesserungen in Richtung einer wiederholbareren Dosierung erforderlich. Ein weiterer Aspekt ist, dass ein Wechsel des Mediums sich erheblich auf die Präzision der Dosierung auswirken kann, da die Eigenschaften des Mediums wie Oberflächenwechselwirkung, Viskosität oder Oberflächenspannung den mikrofluidischen Flüssigkeitstransport beeinflussen können. Daher ist es erforderlich, experimentelle Analysen zusätzlich zu den üblicherweise verwendeten Ersatzflüssigkeiten, wie demineralisiertes Wasser, mit dem Zielmedium der Anwendung durchzuführen.

Aufgrund der kleinen Geometrien mikrofluidischer Geräte mit einem hohen Verhältnis von Oberfläche zu Volumen, beweglichen Teilen in den Fluidpfaden und empfindlichen mechanischen Strukturen wie beispielsweise Federventile, kann die Wechselwirkung zwischen einer Mikropumpe und dem dosierten Medium stärker sein als bei makroskopischen Pumpen. So kann beispielsweise eine Proteinagglomeration in einer dosierten Medikamentenlösung die therapeutische Wirkung des Medikaments beeinträchtigen und zu einer allmählichen Verstopfung des Pumpensystems führen. Für einen

zuverlässigen Einsatz von mikrofluidischen Aktoren im biomedizinischen Bereich ist daher die Untersuchung aller Wechselwirkungen, die die Pumpe schädigen und das dosierte Medium beeinflussen können, unerlässlich.

Neben den oben genannten technologischen Herausforderungen behindern auch wirtschaftliche Anforderungen den breiten Einsatz von Mikropumpen in biomedizinischen Anwendungen, obwohl sie im Vergleich zu herkömmlichen Pumpen deutliche Vorteile bieten. Die Kosten für die Entwicklung, die eingehende Prüfung und den Zulassungsprozess einer neuen Technologie in einem Medizinprodukt, sind hoch. Daher sind die Fortschritte in der Medizintechnik langsam und es werden nur inkrementelle Verbesserungen auf der Grundlage bereits implementierter Technologien eingeführt. Völlig neuen Entwicklungen bleiben dabei aus.

Ziel dieser Arbeit ist es, die biomedizinische Anwendung piezoelektrischer Mikromembranpumpen durch Verbesserung der an der Fraunhofer Einrichtung für Mikrosysteme und Festkörpertechnologien (Fraunhofer EMFT) entwickelten Technologie voranzutreiben. Die EMFT arbeitet an zwei Pumpentypen: kleine Siliziumpumpen und größere Edelstahlpumpen. Beide werden in dieser Arbeit hinsichtlich ihrer fluidischen Eigenschaften, der Biokompatibilität des verwendeten Materials und der Wechselwirkung mit dem Medium bewertet und optimiert.

Um eine bessere fluidische Leistung zu erreichen, wird eine Erhöhung der negativen Ansteuerspannung untersucht. Bei der piezoelektrischen Aktuierung wird die Amplitude der negativen Spannung in der Regel begrenzt, um eine Depolarisierung zu verhindern. Höhere negative Ansteuerspannungen sind jedoch besonders interessant, da sie aufgrund der Nichtlinearität der piezoelektrischen Dehnung zu einer überproportionalen Erhöhung des Membranhubs und damit der erreichten Durchflussrate führen. Für Experimente mit höheren negativen Ansteuerspannungen ist die genaue Kenntnis des Koerzitivfeldes, also des elektrischen Feldes, bei dem die Polarisation ihre Richtung wechselt, notwendig. In dieser Arbeit wird das Koerzitivfeld von 1 kV/mm mit einem maßgeschneiderten Aufbau bestimmt. Durch die Erhöhung der negativen Ansteuerung von Stahl- und Siliziummikromembranpumpen von den üblicherweise verwendeten 40 % auf 90 % des negativen Koerzitivfeldes werden zwei grundlegende Pumpeneigenschaften verbessert: die maximale Fördermenge durch eine größere Hubhöhe, sowie der erreichbare Luftgegendruck durch das erhöhte Kompressionsverhältnis. Ohne Gegendruck steigt die Luftflussrate um 30 %, während bei 30 kPa Gegendruck sogar eine Steigerung um 160 % erreicht wird. Um eine durch das zusätzliche negative Feld verursachte Ablagerung zu erkennen, wird der Hub des Aktuators kontinuierlich über eine Million Zyklen überwacht. Selbst bei einer negativen Amplitude von -1 kV/mm ist aufgrund der regelmäßigen Repolarisation durch die hohe positive Amplitude von 1,5 kV/mm keine Depolarisation sichtbar. Die Ergebnisse zeigen, dass höhere negative Spannungen zur Aktuierung verwendet werden können, was zu einer verbesserten fluidischen Leistung führt. Diese Leistungssteigerung wird in einer neuen Siliziummikropumpe zur Medikamentendosierung umgesetzt, die damit die erforderliche Durchflussleistung erreicht.

Diese angepasste $5 \times 5 \times 0.6 \text{ mm}^3$ große Mikropumpe, die in dieser Arbeit vorgestellt und hinsichtlich Leistung und Dosiergenauigkeit bewertet wird, soll die Entwicklung von miniaturisierten Dosiereinheiten vorantreiben. Die Pumpe erreicht eine Wasserdurchflussrate von $74 \pm 6 \text{ } \mu\text{L}/\text{min}$ und ist damit für die subkutane Dosierung von Medikamenten geeignet. Ihr Blockierdruck von etwa 51 kPa reicht aus, um zusätzlichen Gegendruck, z. B. durch Verschließen der Injektionsstelle, zu überwinden. Darüber hinaus wird die Dosierpräzision mit Wasser und einer Insulinlösung untersucht. Dadurch lassen sich Probleme feststellen, die durch den Wechsel der transportierten Flüssigkeit verursacht werden. Die höhere Oberflächenspannung der Insulinlösung führt nämlich zu stabileren Grenzflächen, wodurch sich der Aufwand für den Transport einer Blase durch die

Pumpe erhöht. Dieses Ergebnis ist für künftige Verbesserungen von entscheidender Bedeutung. Dennoch ist die erreichte Präzision im Vergleich zu handelsüblichen Pumpensystemen auch mit der Insulinlösung hoch. Die Standardabweichung bleibt selbst bei extrem kleinen Volumenpaketen von 0,5 mg unter den allgemein akzeptierten 5 %, was in Zukunft die Dosierung von höher konzentrierten Lösungen ermöglichen kann. Die Ergebnisse dieser Studie sind vielversprechend für die Entwicklung miniaturisierter Patch-Pumpen oder sogar implantierbarer Systeme, die den Komfort für die Patienten erhöhen und eine bessere Behandlung ermöglichen.

Eine implantierbare Anwendung stellt noch höhere Anforderungen an das Material als extrakorporale biomedizinische Geräte. So darf das verwendete Material beispielsweise keine Artefakte in der medizinischen Bildgebung, wie beispielsweise bei einer Kernspin- oder Computertomographie verursachen. Diese Anforderung ist für Siliziumpumpen unproblematisch, schränkt aber die Nutzung von Stahlpumpen, die für größere Flussraten entwickelten wurden, ein. Daher ist ein Teil dieser Arbeit der Übertragung der Pumpentechnologie auf eine Titanplattform gewidmet. Die daraus resultierende neuartige Pumpe hat ähnliche fluidische Eigenschaften wie bekannte Stahlpumpen. Sie erreicht eine Wasserdurchflussrate von $14,0 \pm 2,2$ ml/min und einen Blockierdruck von 75 kPa, was für Medizinprodukte wie hydraulische Implantate geeignet ist. Die neue Pumpe ist Teil einer titanbasierten mikrofluidischen Technologieplattform, die zusätzlich zwei aktive Ventile enthält. Diese Plattform ermöglicht die flexible Entwicklung mehrerer mikrofluidischer biomedizinischer Geräte und verteilt damit den anfänglichen Aufwand zur Einführung einer neuen Technologie auf mehrere parallele Entwicklungen. Somit kann die Plattform dazu beitragen, die Industrialisierung von Mikromembranpumpen für biomedizinische Anwendungen voranzutreiben.

Die flexible Anwendbarkeit der Titan-Technologieplattform ermöglicht neben implantierbaren Geräten auch die Entwicklung von biomedizinischen Geräten, wie beispielsweise Analysesysteme, automatisierte Zellkultur oder dreidimensionales Bioprinting. Für den Einsatz in diesem Bereich sollte der Einfluss der Pumpe auf das transportierte Medium minimal sein. Daher wird in dieser Arbeit der Einfluss des Transports mit Mikromembranpumpen auf Zellen in Lösung untersucht. Vorläufige Experimente zeigen einen signifikanten Einfluss der kleinen Siliziumpumpe mit einem Anstieg des Anteils an toten Zellen um 30 Prozentpunkte im Vergleich zur nicht gepumpten Zelllösung. Die größere Metallpumpe verursacht weniger Schäden. Dennoch ist der Schaden signifikant, wenn eine rechteckige Wellenform, die fluidisch effizienteste Aktuierung, verwendet wird. Um die Auswirkungen zu begrenzen, ohne an Leistung zu verlieren, wird eine angepasste Ansteuerung untersucht. Das gemischte Signal, eine rechteckige Wellenform mit sinusförmigen 60-Hz-Flanken, zeigt ähnliche Eigenschaften beim Flüssigkeitstransport wie das Rechtecksignal, da das gleiche Einzelhubvolumen erreicht wird. Die experimentelle Analyse des Zelltransports zeigt eine geringere Auswirkung des gemischten Signals im Vergleich zur rechteckigen Schwingung. Der Rückgang der lebensfähigen Zellen im Vergleich zu den nicht gepumpten Proben ist gering und die Auswirkungen sind ähnlich wie bei sinusförmiger Ansteuerung. Das angepasste Ansteuersignal ermöglicht daher einen sanfteren Zelltransport als die rechteckige Ansteuerung.

Der Einsatz von Pumpen in Anwendungen, die den Transport von Flüssigkeiten mit Zellen, Partikeln, Fasern oder anderen festen Stoffen erfordern, kann zu schweren Schäden am mikrofluidischen Aktor führen. Die Pumpe enthält enge Fluidpfade und empfindliche Strukturen, wie passive Ventile. Um einen zuverlässigen Transport beispielsweise von Zelllösungen zu ermöglichen, ist eine experimentelle Analyse der Partikeltoleranz der Pumpen notwendig. Ein Experimentelles Modell mit Polystyrolpartikeln ermöglicht ein detailliertes Verständnis. Die optische Analyse zeigt Ablagerungen in den Ventilstrukturen, und sowohl die fluidische als auch die elektromechanische Evaluierung

weisen auf einen Leistungsverlust hin. Die Auswirkungen von Partikeln mit einem Durchmesser von 16 μm sind gravierender als die von Partikeln mit einem Durchmesser von 1 μm . Dennoch fällt keine der getesteten Pumpen aus, obwohl die Partikelkonzentration extrem hoch ist. Die experimentelle Auswertung zeigt die Notwendigkeit geometrischer Verbesserungen, wie die Vermeidung von 90 °-Winkeln, engen Pfaden und strömungsfreien Bereichen.

Die in dieser Arbeit vorgestellten Entwicklungen adressieren drängende, ungelöste Herausforderungen biomedizinischer mikrofluidischer Anwendungen und liefern wichtige Erkenntnisse, die in Zukunft eine weitere Verbesserung der vorgestellten Mikropumpen ermöglichen. Die detaillierte experimentelle Analyse beweist den Nutzen der implementierten Designanpassungen und zeigt notwendige zukünftige Anpassungen auf. Diese Arbeit ist daher ein Schritt in Richtung der biomedizinischen Anwendung von Mikromembranpumpen und treibt die Entwicklung verbesserter Behandlungsmöglichkeiten voran.

Contents

Acknowledgements	i
Abstract	i
Zusammenfassung	v
Contents	ix
1. Introduction	1
1.1. Challenges and Requirements for Biomedical Microfluidic Application	2
1.2. Experimental Evaluation of Microfluidic Dosing Accuracy	7
1.3. State of the Art of Microfluidic Actuators	9
1.3.1. Micropump Research for Biomedical Application	13
1.3.2. Piezoelectric Micro Diaphragm Pumps developed at Fraunhofer EMFT19	
2. Thesis Outline	21
2.1. Research Proposal	21
2.2. Research Results	23
3. Optical Evaluation of the Large-Signal Behaviour of Piezoelectric Disc Actuators to Increase the Precision of Micro Diaphragm Pumps	29
Abstract	29
3.1. Introduction	29
3.2. Materials and Methods	31
3.3. Results and Discussion	31
3.4. Conclusion	34
Acknowledgements	34
4. Increasing Piezo Micro Diaphragm Pump Performance by Optimizing Piezoelectric Actuation	35
Abstract	35
4.1. Introduction	35
4.2. Materials and Methods	36
4.3. Results and Discussion	36
4.4. Conclusion	38
Acknowledgement	38
5. Piezoelectric Silicon Micropump for Drug Delivery Applications	39
Abstract	39
5.1. Introduction	39
5.2. Materials and Methods	41
5.2.1. Basic Characterization	43
5.2.2. Bolus Characterization	44
5.3. Results and Discussion	45
5.3.1. Standard Characterization	45
5.3.2. Bolus Precision Investigation	47
5.4. Conclusions	50
Data Availability Statement	51
Acknowledgments:	51

6.	Piezoelectric Titanium-Based Microfluidic Pump and Valves for Implantable Medical Applications.....	53
	<i>Abstract</i>	53
6.1.	<i>Introduction</i>	53
6.2.	<i>Micropump and valve design</i>	55
6.2.1.	<i>Titanium pump</i>	56
6.2.2.	<i>Normally open valve</i>	56
6.2.3.	<i>Normally closed valve</i>	57
6.3.	<i>Materials and methods</i>	58
6.3.1.	<i>Stroke measurements</i>	58
6.3.2.	<i>Fluidic test</i>	59
6.3.3.	<i>Simulation</i>	59
6.3.4.	<i>Data Statement</i>	60
6.4.	<i>Experimental results and discussion</i>	60
6.4.1.	<i>Titanium pump</i>	60
6.4.2.	<i>Normally open valve</i>	63
6.4.3.	<i>Lifetime investigation normally open valve</i>	64
6.4.4.	<i>Normally closed valve</i>	64
6.4.5.	<i>Spring foil investigation normally closed valve</i>	65
6.5.	<i>Conclusion</i>	67
	<i>Acknowledgements</i>	68
7.	Cell Transport Using Piezoelectric Micro Diaphragm Pumps	69
	<i>Abstract</i>	69
7.1.	<i>Introduction</i>	69
7.2.	<i>Materials and Methods</i>	70
7.2.1.	<i>Micropumps</i>	70
7.2.2.	<i>Cell Transport</i>	71
7.2.3.	<i>Propidium iodide cell viability by flow cytometry</i>	72
7.2.4.	<i>Analysis</i>	72
7.3.	<i>Results and Discussion</i>	72
7.4.	<i>Conclusion</i>	74
	<i>Acknowledgements</i>	75
8.	Microfluidic Cell Transport with Piezoelectric Micro Diaphragm Pumps.....	77
	<i>Abstract</i>	77
8.1.	<i>Introduction</i>	77
8.2.	<i>Materials and Methods</i>	79
8.2.1.	<i>Piezoelectric Micro Diaphragm Pumps</i>	79
8.2.2.	<i>Cell Transport</i>	81
8.3.	<i>Results and Discussion</i>	82
8.3.1.	<i>Pump Characterisation</i>	82
8.3.2.	<i>Cell Transport</i>	85
8.4.	<i>Conclusion</i>	89
	<i>Data Availability Statement</i>	90
	<i>Acknowledgments</i>	90

9.	Particle Tolerance of Metal Micro Diaphragm Pumps.....	91
	<i>Abstract</i>	91
	9.1. <i>Introduction</i>	91
	9.2. <i>Materials and Methods</i>	92
	9.2.1. <i>Optical Examination of the Valve Structure</i>	93
	9.2.2. <i>Stroke measurements</i>	93
	9.2.3. <i>Fluidic test</i>	94
	9.2.4. <i>Particle Transport</i>	94
	9.3. <i>Results and Discussion</i>	95
	9.3.1. <i>Optical Valve Inspection</i>	95
	9.3.2. <i>Actuator Stroke Measurement</i>	97
	9.3.3. <i>Flow Characterisation</i>	97
	9.4. <i>Discussion and Conclusion</i>	99
	<i>Acknowledgement</i>	100
	<i>Data availability</i>	100
10.	Conclusion and Outlook.....	101
11.	References.....	xiii
	Abbreviations.....	xxvii
	Glossary.....	xxix
	Appendix.....	xxx
	A. <i>Supplementary Material Chapter 5</i>	xxxi
	B. <i>Supplementary Material Chapter 8</i>	xxxi

1. Introduction

adapted from a review article by Bußmann, Agnes; Grünerbel, Lorenz; Durasiewicz, Claudia; Thalhofer, Thomas; Wille, Axel; and Richter, Martin
Elsevier, Sensors and Actuators A: Physical, Volume 330, 2021, 112820

The precise dosage of liquid is crucial in many biomedical tasks. Often small volumes need to be transported, such as for sample transport in analysis systems, or medical devices for drug delivery, **microfluidic** systems to move body fluids, and hydraulic implants [1–3]. An automated fluid transport is advantageous, especially if slow, regular, or constant delivery is required, which can potentially be achieved with **microfluidic** actuators.

A prominent drug dosing application is the insulin therapy that patients suffering from diabetes require to manage their blood sugar carefully [4]. Research shows that continuous subcutaneous insulin injection with pump systems improves the patients' health compared to multiple daily injections, e.g., with pen injectors [5, 6]. To further ameliorate the treatment, patch pumps were developed [3]. They aim to increase the patients' compliance and reduce the need for disconnection, enabling a constant insulin supply, which promotes the therapeutic success. Additionally, a patch pump can limit the large deviations in delivered insulin that the vertical position of the infusion set in relation to the pump can cause due to hydrostatic pressure differences [7]. However, existing products are still large enough to be noticeable and some studies claim less accuracy for certain patch systems compared to durable pumps [8–10]. Similar to insulin therapy, medical research on cancer treatment shows that continuous drug delivery to specific tissue can achieve therapeutic effects while limiting side effects [11–13] by minimizing exposure to toxic drug levels [14]. Furthermore, adapting the treatment to the circadian rhythm can be beneficial [11, 12]. It is obvious, that precise, automated, and reliable dosing with a small system would improve patients' care tremendously and enable the use of adapted medication, such as higher concentrated doses.

In addition to drug delivery, the fluidic actuation of medical implants is a challenging medical task. In the united states, more than 15 % of men and 53 % of women aged over 20 suffers from urinary incontinence [15] and severe cases have to be treated with artificial sphincter implants. However, within the last decades, innovation in this field was scarce. State of the art are manually operated systems that are mostly used for the treatment of men, since the pump system is difficult to implant in women [16]. The pressure is set by the physician and cannot be adapt according to the patient's activity. The resulting high stress on the tissue can cause damage and require follow-up operations. An automated dosing unit would be a major invention to improve patients' comfort, though requires high pressure, flow and low leakage combined in an energy-efficient, small and reliable device.

Microdosing is also of high importance when it comes to animal treatment or testing. Medical studies on test animals are a crucial part of pharmaceutical research [17]. However, especially in the case of small test animals (e.g., rodents), extremely small volumes must be dosed. Furthermore, dosing units fixed to or implanted in the animal should

not be of excessive size or weight to minimize animal strain. Even though there are several solutions on the market [18–20], improvement towards smaller systems or more flexible administration is required

The introduced applications are diverse, though share the need for small, precise, energy-efficient, and reliable dosing units, which makes biomedical technology a focus of **microdosing** research [21, 22]. Already early publications on micropumps aim to improve drug delivery using those devices [23–26]. Within the last 45 years, work on **microfluidic** actuators continued and a variety of driving technologies has been developed. Many different microactuation principles have been investigated to create even smaller and more efficient **microfluidic** pumps [21, 22, 27–30].

Considering the great opportunities leading to a vast amount of research, the number of inventions, and especially the evident improvement of treatment, the question arises why **microfluidic** actuation is not yet common in medical products. There are only few commercially available **microdosing** units in analysis systems, human treatment, or for animal testing purposes. Other products are planned for market launch soon. Though, for many promising techniques, industrialization is still pending and progress towards products appears slow.

To enable a better understanding of the limited usage and slow industrialization, the specific challenges of biomedical **microdosing** are analysed. Furthermore, this work gives an overview of approaches within various types of microactuators to meet these very specific requirements. The status of development and general applicability of a **microfluidic** actuation technology in medical application is assessed. Based on this extensive literature work, unsolved requirements and need for technological improvement are identified.

1.1. Challenges and Requirements for Biomedical Microfluidic Application

Microdosing systems, e.g., based on micro electro mechanical system (MEMS) pump technologies, enable the delivery of smaller volumes and minimized size and weight of the system compared to current large-scale products. However, the small dimensions implicate several fields of challenges. Environmental conditions, such as variations in backpressure or temperature, have an impact on the pump and its microactuator. Due to smaller dimensions, surface scaled disturbances like the damping effect of bubbles, capillary forces, or particles become more influential compared to the volume scaled forces that drive the pump. Additionally, the space to include safety measures is limited. Despite all additional disturbances, microscale systems need to meet all current requirements for medical products, such as biocompatibility, flow accuracy, or lifetime [31]. Table 1.1 summarizes important requirements, divided in safety aspects, flow aspects of **microdosing**, and application specific requirements.

Table 1.1 Overview of requirements for pumps in biomedical applications

Requirements	General Requirements	Microdosing Specific Challenges
Safety Aspects		
Freeflow Stop	Uncontrolled flow caused by an overpressure at the reservoir can have severe consequences for the patient. In larger scale	Many microdevices show freeflow (e.g., micro diaphragm pumps). An integrated freeflow stop needs to fulfil size and weight constraints while

	products, the freeflow prevention can be implemented more easily.	functioning over a large pressure range.
Backflow: Leakage and Diffusion	Backflow, caused by diffusion or backpressure leading to leakage, can lead to clogging of injection sites, damage of the pump, pressure loss or dosing inaccuracy.	Leak tight valves are challenging due to geometric limitations.
Bubble Tolerance	Small bubbles can always occur in dosed liquids and the dosing unit needs to be capable of transporting them without failure.	Due to increased capillary forces and the dampening effect of air, depending on the actuation mechanism, bubbles can lead to failure of micropumps [32].
Interaction with Medium / Clogging	Dosing units must not influence the dosed medium or occlude during long use periods. Aggregation during storage or use is unacceptable.	Small channels with high surface to volume ratio and sharp edges are likely to influence the dosed medium and can promote obstruction. Particles or agglomeration can impair dosing of micropumps.
Safety Measures	Medical applications require a high level of safety. Therefore, products usually include safety measures such as pressure and temperature sensors for failure detection.	The same need for failure detection applies. However, integration into the dosing unit can be challenging for the lack of space. Failure modes can differ largely depending on the actuation and therefore development of individual safety measures is necessary.
Flow Requirements in Microdosing		
Flow Range	The required flow range depends strongly on the application.	Some applications, such as drug delivery, can require extremely small flow rates. Examples are the use of highly concentrated drugs, or animal trials with small rodents.
Dosing Accuracy and Precision	Requirements are not uniform. An example is diabetes therapy, where most insulin pump suppliers judge $\pm 5\%$ deviation acceptable [33].	Even if the dosed volume is small, percentage deviation should not increase. Hence, accurate measurement and control systems are required.
Dosing Stability	Changing environmental conditions should not influence the dosing accuracy significantly to allow for safe use at all times.	Depending on the actuation type, different surrounding conditions, such as backpressure and temperature, potentially have a large influence on the microdosing unit.
Dosing Flexibility	In many applications there is a need to adapt the flow rate to the patients' need (e.g., bolus and basal rate).	Depending on the actuation method, the range of applicable flow rates can be limited.

System-Specific Requirements		
Size and Weight	Limits for size and weight vary strongly with the application.	The miniaturization of the fluidic actuation unit offers the possibility to develop microsystems for size and weight critical applications such as implants, patch pumps, or dosing units for animal trials. However, even with miniaturized actuation, limitations can stay challenging.
Power Consumption	Depending on the application, power supply via a battery over a long period can be necessary.	Especially for implantable applications with limited energy supply, low power consumption or wireless supply are necessary, limiting the choice in actuation methods.
Lifetime	Lifetime requirements can vary from some minutes to many years.	There is less knowledge about the lifetime of microdosing systems compared to current macroscopic actuators.
Cost	Cost is especially critical for disposable products. For many dosing units, such as durable pumps, the actuation mechanism is reusable.	The microdosing device is often in direct contact with the dosed fluid, limiting it to mostly disposable or partly disposable use. Cost is therefore a key factor for industrialization.
Production	Reliable and cost-efficient processes are important to be competitive.	For microsystems, production strongly depends on the pump type, e.g., MEMS processes or extreme miniaturization of macroscopic mechanical production processes.

As **safety relevant aspects** we describe basic requirements that a pump has to fulfil to guarantee safe use for the patient. For clearer presentation and due to their key function, flow requirements, such as [precision](#) and accuracy, are discussed separately, even though they are highly relevant for a safe use.

The prevention of so called “[freeflow](#)” constitutes a basic safety measure within [microfluidic](#) actuation. For many pumps, an overpressure at the inlet (e.g., hydrostatic pressure or compression of a reservoir) can cause an uncontrolled fluid flow. To prevent [freeflow](#) can be specifically challenging, since countermeasures have to function at both low and high overpressure at the inlet [34, 35]. Contrary to macroscopic devices with enough space for additional valves, integration can be complex and innovative solutions with minimal space requirements are needed.

Not only fluid movement in flow direction caused by an overpressure at the inlet is problematic, but also backflow and leakage, especially while the pump is turned off. Often the required flow is not constant and sometimes the pump is turned off. If the outlet pressure exceeds the reservoir pressure, such as in hydraulic implants or in the case of drug delivery as safety measure, fluid can be pushed back and cause problems. For instance, if body fluid flows into the injection set, it impairs the drug delivery and can cause clogging. Therefore, as little leakage as possible is an important property of a [microfluidic](#)

dosing unit. Similar to [freeflow](#), leakage is strongly pressure dependent. Especially for passive flap valves, which usually show an initial gap [29], low pressure can cause higher leakage than higher backpressure that pushes the valves towards their valve seat. For energy-efficiency and safety, a normally closed or self-blocking setup (a pump that blocks the fluid path when turned off), can be beneficial. In addition to leakage, diffusion can cause unwanted drug release or movement of body fluid towards the reservoir.

To deliver the required flow securely, a dosing unit in medical applications has to be able to overcome a certain pressure level. For instance, drug delivery requires the pump to build up more pressure than the physiologic backpressure of the target tissue. This pressure is in the range of some hundred Pa to some tens kPa [36]. However, several additional effects add up to the real backpressure Δp the pump has to overcome: hydraulic pressure caused by height differences, fluidic resistance of channels, enlarged fluidic resistance due to clogging as well as capillary forces of small bubbles in the dosed liquid. For instance, the combination of a pump with microneedles for transdermal delivery requires high backpressure capacity of the pump due to the small channels [37]. For hydraulic implants, pressure levels can be even higher with some implants requiring more than 100 kPa [38].

Together with delivered medium, small bubbles get transported into the micro-pump. Those bubbles can be caused by incomplete priming of the reservoir, accumulation in corners, transmission through gas transparent tubing/bags, increase of environmental temperature or pressure differences causing degassing of saturated media, or accidental injection during a reservoir refill [39–41]. In some pumps, gas bubbles can be caused by cavitation, a condition where the fluid inside the pump chamber degasses or evaporates due to negative pressure during the pump supply mode [42]. Air is compressible and acts as a fluidic capacitance, effectively creating a fluidic low pass filter and dampening high frequency pressure pulses. Furthermore, surface tension becomes relevant in small dimensions. Bubbles therefore cause capillary pressure and possibly accumulate and block channels [43, 44], as they enter narrow structures such as check valves or filter pores.

Since it is impossible to consequently avoid bubbles, the dosing unit has to be [bubble-tolerant](#), even with applied backpressure. Many [microfluidic](#) actuators do not fulfil this criterion. All micropumps that exploit a fluid property for the actuation, such as osmotic pumps, electro-hydrodynamic pumps or magneto-hydrodynamic pumps, fail if a sufficiently large bubble enters the actuation chamber, as the fluid (that is needed for actuation) is replaced by air. These actuation mechanisms are therefore not discussed in this work, even though these pumps can be used successfully, when they are primed carefully and protected against bubbles during their life cycle.

Another relevant issue, especially for drug delivery or analysis systems, is the interaction of the pump with the transported media. In [microfluidic](#) systems, the pumped fluid often moves through the pump itself. While shear forces alone are shown to be less problematic [45], the combination of shear forces in small fluidic channels with surface interaction can cause protein denaturation [46]. Many studies show aggregation caused by solid/liquid interfaces and evaluate the influence of material as well as topography [47–49]. Additionally, a gas/liquid interface due to bubbles or cavitation can cause damage to proteins [50, 51]. A more severe interaction than seen in large scale dosing units is imaginable due to a large surface to volume ratio. Small and sometimes sharp moving parts, such as flap valves or microgears, are in contact with the medium and can cause

additional damage. The interaction of drug with the **microdosing** unit can impair the therapeutic effect [48]. However, damage on the pump caused by the dosed medium is also imaginable. Protein denaturation can cause adhesion of small agglomerates within the fluidic path that lead to a partial or total occlusion. Additionally, it is possible, that the transported liquid is impure and contains particles, or even cells and debris. For a reliable use in automated cell culture or miniaturized analysis systems, the particle tolerance of the pump is thus highly relevant. Nevertheless, up to date, scarce information is available on pump-medium interaction.

Even devices offering robust **dosing stability** in most environmental conditions can fail, which makes error detection indispensable. This is eminently important when the pump is used within a high-risk medical product, e.g., insulin patch pump. It is advantageous if failure detection can be included directly into, or closely to the micropump, since additional sensors to fulfil this task need additional space and production effort – decreasing the advantages of **microdosing**. Some examples of possible failure detection are discussed in Chapter 1.3.1.

Flow requirements in **microdosing** include, in addition to an adapted range of flow rates, dosing flexibility, dosing accuracy, **dosing precision** and **dosing stability**. Malfunctioning can have severe consequences and can even cause a patient's death [52], making the flow requirements a key specification in biomedical application.

Dosing flexibility is the ability to adapt the flow to what is needed, e.g., for the actuation of hydraulic implants, or for basal and bolus delivery. Commonly, the dosing unit needs to be capable of delivering fluids with variable flow rates and the possibility to program the flow is required.

Dosing accuracy describes how close the mean dosed volume is to the target volume. Large deviations between several dosing steps can still lead to accurate dosing, if the mean corresponds to the target flow. **Dosing precision** describes high repeatability and therefore only minimal deviations between several dosing steps. At high **precision**, the mean dosed volume can differ from the target volume. Biomedical application often requires both accurate and precise, to guarantee reliable use.

Dosing stability addresses how the mean flow rate and the standard deviation change with environmental parameters, such as temperature, backpressure, or humidity. For example, a highly variable backpressure, as can be caused by occlusion, or by changing environmental parameters, can distort the total dosed volume. In addition to the described need for a sufficiently high **blockingpressure**, a pressure independent dosing within the normal limits of application is highly favourable. Similar accounts for the temperature: expected deviations in surrounding temperature should not lead to a large deviation in flow creating the need for temperature independent **microfluidic** actuation. It is thus crucial to know and maybe observe occurring environmental conditions and adapt the **microdosing** unit to this range in a way that the needed flow accuracy and **precision** is assured at all times.

Based on the exact application, there are many more, **system-specific requirements**, a dosing unit has to meet. Those depend strongly on the use case, the exact setup, as well as the environment in which the micropump is used.

Microdosing units are often single use products, thus cost is critical. Obviously, each specific application as well as different countries and health care systems imply different cost limitations. However, estimated production costs give an interesting insight to the feasibility of a technology within a product. For larger scale devices it is a common approach to reuse the driving unit. In **microdosing** units, the transported medium often

passes through the pump itself, which makes a safe reuse of the actuator challenging. Since cost considerations are complex and only a distinct improvement justifies a large increase in cost, it is crucial to consider inexpensive production [53].

There are various production processes used for micropumps. Some pumps are based on standard MEMS processes with low costs for high production volumes [54]. Those processes allow for precise and repeatable production of small geometries and minimize sample to sample variation. Production is cost efficient for high numbers; however, industrialization and the production of small numbers generate high initial costs. Furthermore, the choice in materials is limited, restricting considerations of surface interactions, biocompatibility, or hermetic sealing slightly [55]. Other pump types scale down known macroscopic actuation mechanisms to the microscopic world and require cost and effort during production. Small mechanical parts, such as microgears, have to be produced with extremely low tolerances coming down to the order of magnitude of surface roughness [56]. Without utmost precision, assembly of the parts can be challenging and smooth sliding is not guaranteed.

The required lifetime of a micropump also strongly depends on the use case. While an implant can be used for extremely long periods, a disposable for short time use does not require long lifetime. This topic has to be addressed for each pump type individually, as each actuation method and pump geometry poses different challenges. In miniaturized systems, small scale of moving parts can cause problematic wear with a larger impact on the functionality [56], e.g., the abrasion caused on gears in a microgear pump. For micro diaphragm pumps, the lifetime of the actuator, the pump diaphragm as well as the adhesive connection of both components need to be considered in addition to the fluidic path.

Even though microfluidics imply small actuation principles, size remains a great issue for many systems, since space or weight can be extremely limited. A field with challenging weight and size restrictions is the pharmaceutical testing on small rodents. Not only for animal welfare, but also to minimize the influence on test results, it is crucial to have a precise, reliable dosing unit that limits animal strain [57]. Especially the weight of the device should be limited to prevent avoidable suffering. In the case of mice, the whole dosing system including electric power supply and a drug reservoir can only weigh some grams.

Size and weight restrictions demand for energy-efficient dosing units. Especially with implants designed for long term use, the units' power supply is often limited to a battery. To develop small systems, the energy consumption needs to be as little as possible in order to be provided by a small battery for the time of implantation or between recharge. Not only the energy source, but also the driving electronics need to be optimized in size, signal accuracy, and energy consumption. It is evident that the accuracy of the electronic signal has to be higher than the desired dosing accuracy not to impair the pump performance.

1.2. Experimental Evaluation of Microfluidic Dosing Accuracy

To compare various microfluidic dosing systems, a standardized evaluation is necessary. Currently, experimental methods differ for independent research works, which impacts the flow results. Differences in the measuring method, as well as fluidic surroundings, e.g., tubing length and diameter, or the fluidic resistance of sensors, can significantly change performance parameters such as maximal pressure built up or maximal

flow rate. Especially for extremely small flow rates, it is delicate to avoid a strong impact of the experimental setup. When comparing different micropump solutions, it is important to keep the difference in experimental evaluation in mind.

There is no test norm that describes the evaluation of **microfluidic** actuators. However, in the case of drug delivery, micropump based dosing units have to be tested following the international standard procedure: The norm IEC 60601-2-24 [58] describes the assessment of **dosing accuracy** as well as obstruction detection of commercially available infusion systems *in vitro* and also accounts for patch pumps. It proposes a gravimetric measurement and results are to be presented in a trumpet curve. Pleus et al. [59] point out that a trumpet curve is easily misunderstood, since contrary to intuitive interpretation, it does not show an evolution over time. Furthermore, only extreme values are displayed, which might not be representative for average flow variations. In addition, the long run-in period indicated in the norm (time to half empty the reservoir, though 24 h at the most) does not reflect the clinical application, where **dosing accuracy** matters from the start of the pump on [33, 59]. And indeed, diabetes patients sometimes report variations in their glycaemic control connected to the change of their pump [60].

In the case of insulin dosing, a lot of research has been conducted towards comparable dosing investigations, which offers a general insight to the evaluation of **dosing accuracy** of small amounts. Many studies evaluate the average deviation within a given observation window or the percentage of single doses within a specific range of **accuracy** in addition to or instead of the trumpet curve [8, 10, 33, 60–62]. For gravimetric methods, the influence of evaporation and condensation needs to be minimized either by covering the surface in the reservoir with oil [9, 33, 61] or by installing an evaporation trap [63]. To avoid any influence of hydrostatic pressure, the meniscus of liquid in the reservoir and the pump's outlet need to be levelled [33]. Further, the drift before and after dosing steps has to be measured to consider drift corrected data. Additionally, the capillary immersed to the reservoir on the balance causes inaccuracy. Changing volume in the reservoir evokes a linear change in mass caused by Archimedes force [63]. With a large enough reservoir and small tubing, this effect can be minimized. Capillary effects around the needle show to have a significant influence [63], since the microscopic roughness of the tubing changes the vertical surface forces when the meniscus is rising or falling. The effect of capillary effects can be minimized by using extremely smooth glass capillaries and reduce the surface tension of the dosed liquid by adding surfactant in the reservoir [63].

Another method to evaluate small delivery volumes is the optical observation of a meniscus in a precise measuring pipette [62]. With this method, it is crucial to have a tight connection between the pump and the pipette to avoid air bubbles and volume losses. Because of the limited size and resolution of the pipettes, the dosed volume can only be evaluated in certain ranges and it might be necessary to calculate the mean and standard deviation of single doses by repetitive measurements of several doses [62].

Exact environmental temperature and its influence on **dosing accuracy** is often not tracked in micropump studies and authors commonly only state laboratory condition within a certain range. Though, for microdevices, temperature can have a crucial influence by changing the viscosity of the pumped medium, or the pump chamber height and actuator displacement in the case of diaphragm pumps. Controlled temperature would therefore be an important addition to above methods.

To assess and compare the **bubble tolerance** of micropumps requires equal test conditions for each experiment. Bubbles need to be of similar and especially known size. A possible experimental setup is to fill the pump with water and then inject a defined

amount of air, e.g., with a syringe pump. Alternate pulling of air and water accumulates a desired number and size of bubbles in the inlet tubing [64]. This setup allows to test **bubble tolerance** and detect the air volume a pump cannot transport anymore. It is important to note that data points can scatter broadly, since the exact position of a bubble in the chamber influences the forces needed to move it.

Accurate flow measurement is difficult even within a laboratory environment. The additional miniaturization necessary for the integration into a microdevice poses a large challenge. However, closed loop control systems can require such accurate flow measurements. Two types of in-line sensors that can be miniaturized are calorimetric sensors and differential pressure sensors. Jenke et al. [65] describe the difficulty of measuring the pulsed flow of a micro diaphragm pump. Within their setup the authors reach an **accuracy** of 5% with the differential pressure element and 6.5% with calorimetric measurements [65].

1.3. State of the Art of Microfluidic Actuators

Many possibilities to categorize the various driving principles exist, however “mechanical” and “non-mechanical” emerged as a very common classification [21, 22, 28, 29, 66, 67]. Figure 1.1 gives an overview of common mechanical types of **microfluidic actuators** that this overview focuses on, since non-mechanical systems are often not **bubble-tolerant** or do not offer the possibility of continuous, adjustable dosing.

A widespread approach to dose small amounts of fluids are reciprocating **micro diaphragm pumps** (Figure 1.1 A-G). Dosing bases on a diaphragm that is moved actively up and down. This increase and decrease of the chamber volume and the resulting pressure gradient lead, in combination with mechanical or non-mechanical flow rectifiers, to directed flow. The former may be active or passive valves, e.g., flap valves, whilst the latter are commonly diffuser/nozzle setups. When neglecting flow influencing effects such as liquid damping effects or bubbles, the moved volume is proportional to the numbers of strokes conducted [68, 69]. This allows for adjustable flow and precise dosing. The **stroke volume** can be minimized by variations of the actuation signal, though has a lower limit that is determined by many parameters, such as the opening pressure of the valves, the signal form, and the minimal achievable diaphragm displacement. The pumping mechanism applied by diaphragm pumps inevitably causes pulsatile flow, since the suction and pumping phases are consecutive. Smoothing elements such as fluidic capacitances can average the flow and reduce pressure peaks.

A major asset of diaphragm pumps is the possibility for extreme miniaturization. For example the so far smallest piezoelectric pump with only $3.5 \times 3.5 \times 0.6 \text{ mm}^3$ is manufactured using **MEMS** processes [70]. The combination of such large volume production processes and the comparatively easy setup that often includes only a few layers, suggests economical production.

Diaphragm pumps can work with a single chamber as well as with several chambers in series making peristaltic, and therefore bidirectional actuation possible. There are various types of diaphragm actuation:

The most common actuation is the indirect *piezoelectric effect*, causing a piezoelectric ceramic to contract and expand when an altering electric field is applied [71]. A diaphragm with glued on piezoelectric actuator therefore bends up- and downwards under an altering voltage [72]. The popularity of this actuation bases on its easy use, its high

attained forces as well as its energy-efficiency [73]. Piezoelectric actuation allows for high actuation frequencies [73] and precise control. However, the achievable stroke is limited and requires high voltages of often several hundred Volts [74–76].

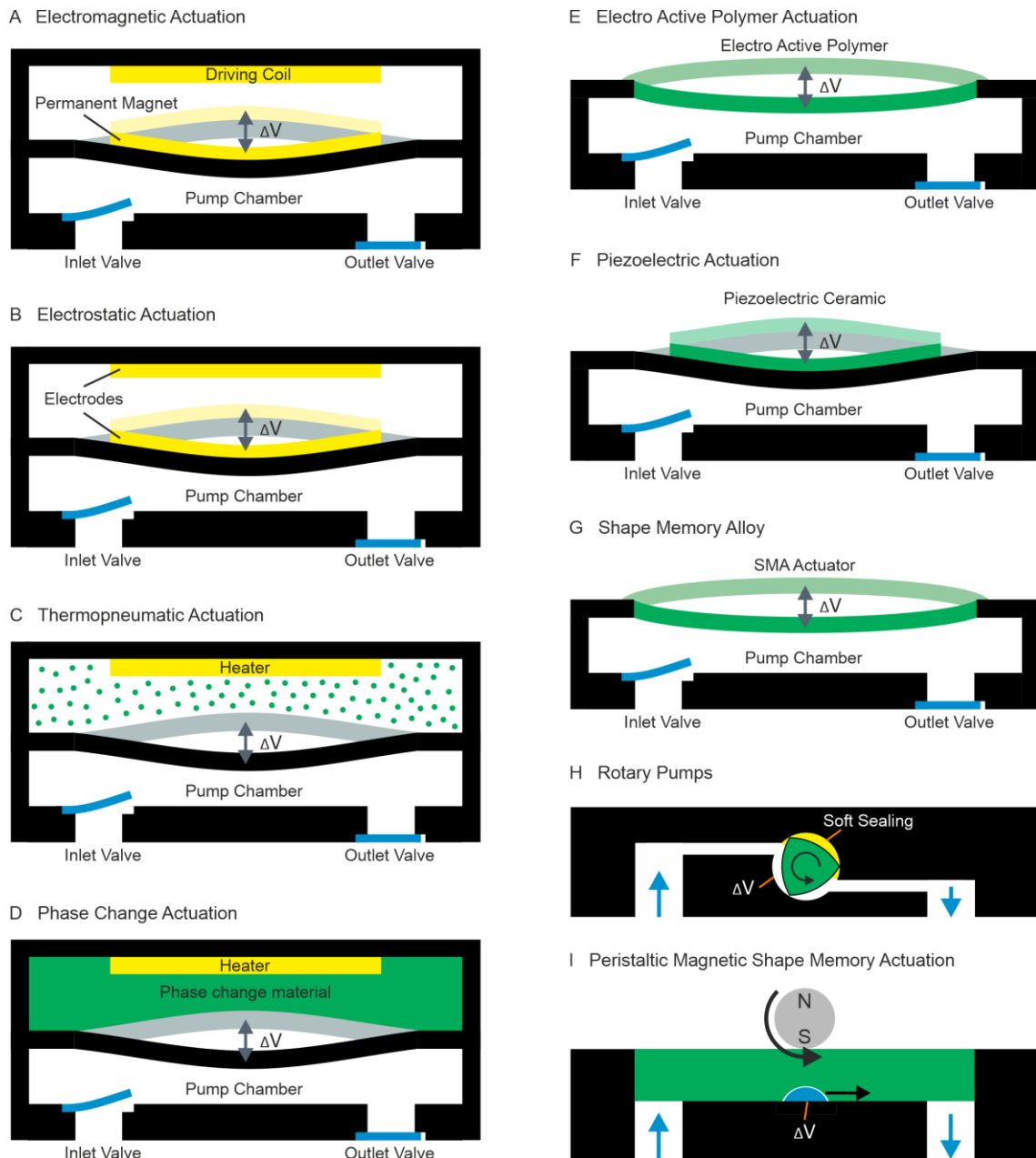


Figure 1.1 Overview of mechanical pump systems. A to G: In the case of micro diaphragm pumps, a periodic movement of the diaphragm increases and decreases the volume in the pump chamber and leads in combination with flow restricting elements to directed fluid transport. Common actuation principles base on electromagnetic forces (A), electrostatic forces (B), thermal volume expansion (C) or the volume increase of a material due to phase change (D), the conformational change of electroactive polymers (E), the indirect piezoelectric effect (F) and the thermal shape memory effect (G). H: Exemplary depiction of a rotary micropump that transports fluid due to a turning motion of its actuated part (green). In this example directed flow is achieved with a flexible soft sealing preventing backwards transport (yellow). I: Peristaltic micropumps actuated with a magnetic shape memory alloy transport liquid via local deformation due to changing magnetic fields.

The first micropump based *thermal shape memory alloy* actuation was developed by Benard et al. [77, 78] in 1997/1998. Thermal shape memory materials recover their

original shape upon heating [79] and can therefore be used to oscillate a diaphragm. Materials show either a two way or a one way shape memory behaviour and both are used for micropump actuation [80]. The two-way shape memory effect describes a transformation between two different states, while the one-way material only shows the return to its engraved state when heated but no shape change upon cooling. Hence, the one way effect requires a restoring force to push the actuator back to its zero position after deformation [77, 78]. The technology is known for its high achievable displacement as well as low operating voltages; drawbacks are low operating frequencies, a limited control of the exact deformation, and a high power consumption [73].

For *electromagnetic* actuation, a magnet fixed to the diaphragm, e.g., a permanent magnet, is actuated by an alternating magnetic field. This field is induced by an oscillating electrical current through a coil (power inductor) situated in proximity to the diaphragm, which leads to alternating magnetic attraction and repulsion of the permanent magnet [81]. Electromagnetic actuation enables energy-efficient fluid transport with some pumps using only 1.2 kJ/L when pumping water without backpressure [82]. However, actuation requires high current as well as high magnetic fields.

The diaphragm can also be actuated via *electrostatic* forces. Two electrodes, one on a diaphragm and one on a fixed counterpart, are drawn together when a voltage is applied and the diaphragm returns to its original position by mechanical counterforces when the voltage is removed [83]. Depending on the direction of mechanical movement compared to the electric field, we distinguish lateral and normal actuation. The first pump with normal actuation was presented by Zengerle et al. [83] in 1992. The first lateral actuation was presented more than 25 years later by Uhlig et al. [84]. Manufacturing often uses standard MEMS processes without additional steps such as gluing [83]. Further miniaturization, which is limited for other actuation mechanisms by the minimal size of their actuators, appears possible.

Progress in materials research enabled another type of actuator: *electro active polymer* (EAP) actuation for micropumps was first mentioned in the early 2000s [85]. Actuation bases on the change in size or shape of certain polymers caused by an electric stimulus with a high elastic energy density [86]. The electric actuation mechanism allows to differentiate two major groups of EAPs: ionic and field-activated materials. Ionic electroactive polymers (*iEAP*) base on diffusion of ions. When applying an electric field, ions that are normally well distributed are pulled to one of the electrodes, also carrying the solvent present in the material. The latter causes deformation of the polymer membrane and therefore transforms electrical into mechanical energy [87]. Specific types of *iEAPs* are ionic polymer-metal composite (IPMC) and conjugated polymers (CPs). CPs consist of a semiconducting polymer doped with donor or acceptor ions [87]. The most common materials today are polypyrrole (PPy) and polyaniline (PANI) [88]. Advantages are a large bending displacement at low actuation voltages of only few volts, easy and low cost production, and the possibility of bidirectional actuator movement [89]. A disadvantage is the relatively slow response (fraction of a second) due to slow ion drift [89]. Using an electrolyte also leads to some difficulties, such as electrolysis or production of a consistent material. The electrolyte must be in wet environment, only few self-encapsulating implementations are known [89].

The second category of EAPs are field-activated ones. We distinguish ferroelectric polymers that react due to intrinsic field-induced molecular conformational changes to the elastomer, and dielectric elastomers mainly responding to extrinsic electronic

charge attraction-repulsion at the surface electrodes [89]. The latter are basically capacitors that change their capacitance due to an applied electric field, essentially squeezing the polymer in thickness and hence expanding it laterally. Both mechanisms are inherent to all field-activated polymers, however usually one is clearly dominant. Advantages of field-activated **EAPs** are rapid response times (milliseconds), high durability, and a high mechanical energy density [89]. Under constant electric fields, the material holds the strain without need for power. A large disadvantage is the high necessary driving voltage with electric fields of dozens of V/ μm , which is close to material breakdown [89]. Furthermore, only monopolar actuation is possible due to electrostriction [89].

Another researched actuation mechanism is *thermal* actuation including thermo-pneumatic systems and phase change actuation. Thermo-pneumatic actuation bases on the expansion of volume due to heating, which pressurizes the diaphragm and deflects it [90]. Phase change micropumps use the volume expansion certain materials undergo during a phase change to move the diaphragm [91]. Thermal actuation enables large forces and hence high backpressure capability of the actuator. The actuation voltage is low in the range of some volts to some tens volts [92, 93]. However, the energy consumption to heat and cool the actuator is high leading to smaller efficiency compared to other driving mechanisms [94]. The example of Bodén et al. [91] shows a power consumption of approximately 400 mW resulting in roughly 90 kJ/L for transport without backpressure (compared to 1.2 kJ/L for electromagnetic pumps and less than 1 kJ/L for some piezoelectric pumps). The actuation frequency is often limited by the cooling cycle and restricts the achievable flow. A common actuator material is paraffin due to its large volume change, high pressure capability, adjustable melting temperature as well as low cost [91, 94].

Peristaltic actuation, which is for most actuation methods realized using several bending actuators, can also be achieved with *magnetic shape memory (MSM)* actuation [95] that was so far demonstrated by two research groups. The setup and functionality of **MSM** pumps differ from diaphragm pumps (Figure 1.1 J). The pump chamber with a high aspect ratio comprises an in- and outlet on the far ends and is covered by a **MSM** layer that is locally deformed by a strong magnetic field [95]. This local cavity moves along the actuator with changing magnetic field and transports liquid in a peristaltic manner. **MSM** pumps work bidirectionally and operation is contact free, though the driving magnetic field is high in the range of some hundred mT [95].

Another principle of **microfluidic** actuation are **rotational micropumps** that transport fluid with a turning motion of their actuated parts. One example are *microgear pumps*, where the turning motion of gears moves a fluid volume from an inlet towards the outlet (Figure 1.1 H). The rotating motion can also be used to squeeze liquid within a tube from an inlet to an outlet as within a miniature *peristaltic pump*. Typically, rotational micropumps enable continuous flow as well as stepless adjustment of the flow rate. The energy transfer from mechanical (revolution speed) to fluid (flow velocity) is efficient and in comparably small space, and most pumps show a good flow direction control due to a continuous pressure gradient that enables valveless configurations. However, manufacturing requires high **precision**, since the gap between rotors and pump chamber must be small to reduce leakage and backflow. Rotor configurations can cause high shear forces in the fluid and the surface-to-volume-ratio is high, which might prompt interaction with the dosed medium. Compared with diaphragm pumps, this pump type is usually large. Nevertheless, based on improved manufacturing methods, such as micro injection moulding [96–98], miniaturization is pushed.

A more detailed overview of micropumps, categorized regarding their driving mechanism as well as their valves and pump chamber, can be found in the work of Mohith et al. [67]. Laser and Santiago also provide a detailed description [27]. Functionality of many driving mechanisms is well depicted by Ashraf et al. [66] and Wang and Fu [21] give a summary of recent developments. Ogden et al. [94] present a comparison of energy density as well as achievable flow rate and backpressure for selected driving mechanisms. Micropumps based on electroactive polymers are described in the review of Bar-Cohen and Anderson [89] as well as the one of Annabestani et al. [88]. Yunas et al. [99] describe electromagnetic polymer actuators for biomedical applications.

1.3.1. Micropump Research for Biomedical Application

Despite specific challenges, the obvious possibility of improvement has prompted research towards reliable micropumps for biomedical application. A comprehensive overview of micropumps sorted by their actuation principle, including a detailed description of industrial pumps, i.e., the JewelPump, the Omni Pod, Sensile Medical's pump and the iPrecio system, can be found in the review article by Bußmann et al. [100]. This chapter provides a summary of micropump research for medical application, as well as more detailed information on the piezoelectric diaphragm pumps developed at the Fraunhofer EMFT Research Institution for Microsystems and Solid State Technologies ([Fraunhofer EMFT](#)). Table 1.2 summarises the fluidic performance of selected micropumps. The data does not necessarily reflect the maximal fluidic properties achievable with each actuation mechanism, since pumps presented in research are often not fully optimized in every geometric and electromechanical parameter. Furthermore, presented pumps are selected not only for fluidic performance, but also suitability for medical application.

Table 1.2 Overview of micropumps cited in this thesis; Pumped media are A- air, I- insulin, L-liquid, W-water and ^a saline solution, ^b methanol, ^c blood mimicking fluid, ^d sodium salicylate, ^e glycerol solution; Evaluation: 0 - not fulfilled, 1- partially fulfilled, 2- fulfilled

	Q_{max} in $\mu\text{L}/\text{min}$	Fluid	Voltage in V	Frequency in Hz	P_{max} in kPa	Freeflow Stop	Backflow Stop	Bubble Tolerance	Dosing Precision in μL	Size in mm^3	Power in kJ/L	Life Time in cycles
Piezoelectric Actuation												
[37]	3000	W/I	36	200	22	0	2	-	0.062	$\text{\O}15 \times 8$	-	-
[101]	3.5	W	24	1	3.2	1	1	1	-	$30 \times 10 \text{ mm}^2$	0.9	-
[102]	25	W	-	500	600	2	2	2	0.088	$7 \times 7 \times 1$	-	-
[76]	240	W	230	75	36	1	1	2	-	$23 \times 23 \times 2.2$	-	-
[103]	1.7×10^4	W	110	10	40	0	2	2	-	$20 \times 20 \times 6$	-	-
[104]	196	W ^c	140	25	6.4	0	2	2	-	$50 \times 50 \times 12$	-	-
[70]	1400	A	145	2000	40	0	2	-	-	$3.5 \times 3.5 \times 0.6$	-	-
[105]	150	W	140	20	180	2	2	-	-	-	-	-
[106]	4698	W	200	15	-	0	0	-	-	$65 \times 40 \times 12$	-	-
[75]	4800	W	300	125	1.8	0	0	0	-	-	-	-

Biomedical Application of Piezoelectric Micro Diaphragm Pumps

[107]	200	W	200	40	40	1	1	-	-	30×11 mm ²	-	-
[108]	70000	W	380	30	-	0	2	-	-	d 20×1.5	-	-
[74]	1.3×10 ⁵	W	240	400	10.8	0	2	-	-	-	-	-
[109]	1.8×10 ⁶	W	210	120	44	0	2	1	-	-	-	-
[110]	4.4×10 ³	A	140	1600	15.4	0	2	2	-	5×5×0.6	0.5	-
Shape Memory Alloy												
[77]	50	W	0.6	0.9	-	0	2	-	-	-	648	-
[78]	50	W	-	0.9	-	0	2	1	-	15×9.1 mm ²	756	-
[111]	235	W	-	80	-	0	0	-	-	8×8×1.8	-	2×10 ⁶
Electromagnetic												
[81]	66	W	1.5	9	0.98	-	0	0	-	-	43.6	-
[112]	400	W	-	12	1.2	0	0	0	-	36×22×3	-	-
[82]	1623	-	30	7	0.36	0	0	0	-	55×35×10	1.2	-
[113]	9.3	W	2	1.6	41	0	2	1	-	-	-	-
[114]	13.2	D	-	1.3	-	0	1	0	-	5×9 mm ²	-	-
Electrostatic Actuation												
[83]	70	W	170	25	2.5	0	2	0	0.01	7×7×2	-	-
Electroactive Polymer												
[115]	22	a	1.2	-	-	0	1	-	-	30×20×6	5.5	5 days
[116]	25	b	5680	63	0.35	0	0	-	-	-	-	-
[85]	550	A	-	1000	-	-	-	-	-	-	-	-
[117]	2	L	2.8	-	3000	-	-	-	-	Ø8×1	-	>10 ⁶
Phase Change Actuation												
[118]	0.1	W	-	0.083	-	2	2	-	0.011	7×13×1	11	26×10 ⁶
[91]	0.07	W	1	0.5	-	1	1	-	-	12×6×2	135	-
[93]	0.6	W	1.5	0.6	1.3×10 ⁴	1	1	-	-	-	34.4	-
[92]	0.1	W/d	3.7	0.33	5	1	1	1	1.2×10 ⁻³	8×8×3	-	20 min
Thermopneumatic Actuation												
[119]	9.2	W	5	1.5	0.5	1	1	1	-	16×18×5.5	-	-
Magnetic Shape Memory Alloy												
[120]	2000	L/A	-	320	1000	2	1	2	0.105	11×3.1×2.3	7.6	-
[121]	-	L	-	-	-	-	-	-	-	20×16×59	-	-
[95]	252	L	-	-	-	-	-	-	0.26	25×10×2.5	-	-
[122]	1800	W/f	-	270	150	2	1	-	0.110	18×10×5	700 0	>10 ⁶
Rotary Pump												
[56]	-	-	-	-	-	-	-	-	-	Ø3.2 mm	-	-
[123]	150	W	-	30	-	1	1	-	-	10×12×1.3	-	-
[124]	-	I	3.7	-	-	1	1	-	1	Ø 5.5×2	-	>3×10 ³
[34]	2050	L	1.5	14	82	2	2	1	-	30×15×14	-	-
[125]	275	W	5	180	40	2	2	2	-	Ø 24×40	-	-

Electrolysis actuation												
[126]	-	W	-	-	-	0	2	-	-	20×15×10	-	30 days
[127]	520	W	-	-	-	-	-	-	-	3.9×2.1×2	57.7	-
Commercial												
Jewel-Pump	360	W/I	400	3	-	2	2	2	0.2	6×10 mm ²	-	2.6×10 ⁶
Omni Pod	15	I	-	30	-	2	2	-	0.5	40×60×18	-	-
Sensile Medical	2.5×10 ⁴	L	-	20	400	2	2	2	0.25	-	-	-
iPrecio 310R	0.16	L	-	-	-	2	2	2	-	-	-	67 days
iPrecio 200	0.5	L	-	-	-	2	2	2	-	-	-	86 days
IP2000V	2.1	L	-	-	-	-	2	-	-	Ø78×14	-	20 years

Many of the challenges and requirements summarised in Chapter 1.1 are discussed in micropump research, while, up to date, there is little information concerning others. Many dosing properties do not only depend on the fluidic actuator itself, but also on the overall system, fluidic boundary conditions and especially the valve technology. The implementation of closed loop control increases the reliability of the dosing unit and enables error detection. Furthermore, weight and size constraints have to be evaluated on system level, since driving electronics, power supply as well as a reservoir can be large parts to consider. Other challenges can be solved within the micropump itself for example by design adaptations that allow for space efficient solutions. Resourceful technical adaptations are summarized in Figure 1.2 and described here below.

Freeflow, diffusion, and backflow can be prevented using active valves [76], however, those pumps do not block the flow path when turned off. Such a normally closed state is achieved with phase change actuation based on gallium [118], since it shrinks when melted and therefore opens the fluid path when actuated. A passive **freeflow** stop for micro diaphragm pumps is presented by Richter et al. [102] with a passive safety valve that blocks the fluid path when the inlet pressure exceeds the outlet pressure. Maillefer et al. [35] prevent **freeflow** as well as leakage with a valve pretension of the passive flap valves of 10 kPa. Additionally, a specific actuation signal reduces errors by uncontrolled leakage through the inlet or the outlet valve during pump operation [128]. In general, rotary pumps show little leakage, **freeflow**, and backflow due to geometric constraints. An example is presented by Pankhurst and Abdollahi [34] with only one moving part and a spring design **freeflow** stop. The iPRECIO pumps [129–134] are miniaturized peristaltic pumps. A micro stepper motor drives an eccentric disc cam that compresses the soft tubing transporting the dosed medium. Due to this peristaltic setup, these pumps prevent backflow, **freeflow**, and diffusion also in turned off state.

Bubbles, that are usually unproblematic for rotational micropumps, remain a huge challenge for diaphragm pumps. Their **bubble tolerance** strongly depends on their **compression ratio** ε [32, 135]. This ratio indicates how much volume is displaced compared to the dead volume of the pump. It is calculated with

$$\varepsilon = \Delta V / V_0 \quad (1.1)$$

with the displaced volume ΔV and the dead volume V_0 .

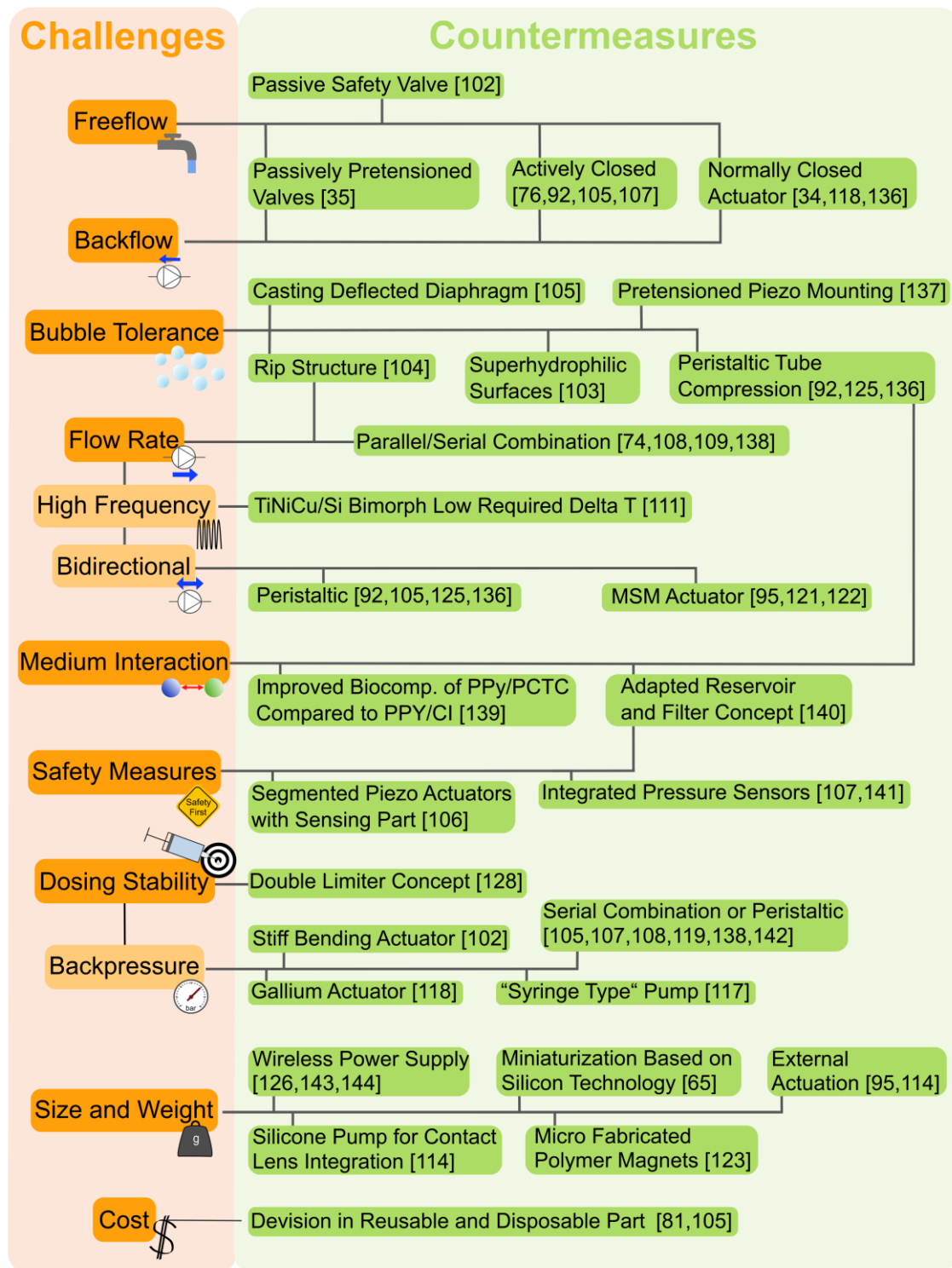


Figure 1.2 Overview of technical improvements with respect to challenges in biomedical application. Depicted on the left (orange) are the specific challenges for *microdosing* in medical applications as summarised in Table 1.1. On the right (green) we present possible countermeasures to overcome these challenges and meet specific requirements that are described in this review. The selected examples are presented by or implemented in Pankhurst & Abdollahi [34]; Maillefer et al. [35]; Jenke et al. [65]; Zhang et al. [74]; Pečar et al. [76]; Rusli et al. [81]; Forouzandeh et al. [92]; Ullakko et al. [95]; Richter et al. [102]; Wang et al. [103]; Ma et al. [104]; Trenkle et al. [105]; Zhang et al. [106]; Fuchs et al. [107]; Grünerbel et al. [108]; Peng et al. [109]; Zhang et al. [111]; Wang and Park [114]; Yan et al. [115]; Hiraoka et al. [117]; Johnson & Borkholder [118]; Yang and Liao [119]; Barker et al. [121]; Smith et al. [122]; Waldschik et al. [123]; Vinayakumar et al. [125]; Cobo et al. [126]; Khalil et al. [127]; Chappel et al. [128]; the iPRE-CIO pumps [136]; Herz et al. [137]; Huang et al. [138]; Yan et al. [139]; the JewelPump [140]; Chappel et al. [141]; Geipel et al. [142]; Liu et al. [143]; and Chee et al. [144]

The **compression ratio** has to be large enough to compress a bubble that, in the worst case, fills the whole pump chamber, further than the total backpressure Δp to transport the air through the chamber [32]. Capillary forces of an air-liquid interface also add to the total backpressure. Herz et al. [137] achieve a high **compression ratio** with their **pretension technique**. By applying a positive voltage to the actuator disc during glue hardening, the authors drastically increase their pumps **compression ratio**. Trenkle et al. [105] increase the **compression ratio** of their device by casting the deflected membrane to manufacture the pump chamber. Furthermore, **bubble tolerance** can be increased when reducing the force needed to transport a bubble out of the pump chamber, as done by Wang et al. [103] with a super hydrophilic surface of the pump chamber and by Ma et al. [104] with a rib structure in the chamber, which guides the fluid flow. Furthermore, a surfactant added to the transported medium decreases the surface tension and facilitates bubble transport [64]. Additionally, the performance of a micro diaphragm pump strongly depends on its valves. While flap valves increase **bubble tolerance**, minimize leakage, and increase forward flow, they are sensitive to particles [135]. Diffuser/nozzle valves are less susceptible to particles, but **bubble tolerance** is limited. A bubble in the inlet is pushed back and forth instead of moved towards the outlet, since the dynamic viscosity of air is 50 times smaller than the one of water in the outlet. Nevertheless, there are examples of **bubble-tolerant** pumps that employ diffuser/nozzle valves [145].

Not many authors investigated the interaction with the transported medium and clogging. In most cases, micropump evaluations are conducted with surrogate fluids, to facilitate handling and limit costs. However, the medium can damage the pump over time and the pump might impact the transported medium, e.g., damage the analyte, or impair the drug's functionality. Especially miniaturized pumps, with a high surface to volume ratio and sharp edges in small fluidic channels, might cause damage. To prevent interaction, Forouzandeh et al. [92] and Vinayakumar et al. [125] limit the contact of the medium to biocompatible tubing, through which medium is transported peristaltically. The same accounts for the iPRECIO systems. This approach enables easy fluidic connection without sharp edges and there are no sharp moving parts, such as flap valves, in the fluid path. The subject is also discussed in the research of the Swiss company DeBiotech. Their JewelPump, a piezoelectrically actuated micro diaphragm pump, utilises a specific drug reservoir in combination with a special filter to prevent insulin aggregation [140].

Often, safety measures are indispensable for medical application and space efficient integration is an advantage. For piezoelectric diaphragm pumps, the segmentation of the actuator ceramic into an active part and a sensing part, as shown by Zhang et al. [106], allows to detect any changes in the pump chamber and can be used to monitor transport, the occurrence of bubbles or a change in backpressure, e.g., caused by clogging. For the same purpose, Fuchs et al. [107] integrate a pressure sensor into their peristaltic pump system. To ensure stable dosing, Benard et al. [78] include an in-line filter to prevent particles and bubbles from entering the pump chamber. A similar filter concept is employed in the JewelPump [140]. Additionally, the system comprises two pressure sensors, one in the pump chamber and one after the outlet valve, for precise control and error detection. Therewith, correct priming, reservoir overpressure, reservoir emptying, presence of air bubbles, occlusion (within one stroke) [141], and leakage can be detected with the pressure profile [141, 146].

In addition to safety relevant aspects, flow properties are highly relevant for **microdosing** units. To improve the maximal flow rate without increasing the pump's size is

an important aim. Geometric adaptations that lower the fluidic resistance, such as the rib structure presented by Ma et al. [104], allow for higher flow rates. Furthermore, higher actuator displacement can improve maximal flow, which Zhu et al. [147] achieve with ring electrodes leading to actuator buckling instead of bending, and Yamataha et al. [112] by a soft silicone diaphragm. However, the soft diaphragm decreases the bending actuator's stiffness and therefore the maximal achievable pressure.

Not only high flow rates, but also the flexibility of bidirectional actuation can be advantageous. For instance, peristaltic actuation [92, 105, 125, 142] or the implementation of active valves [113] enable bidirectional flow. Additionally, the peristaltic actuation using magnetic shape memory actuators can move fluid in both directions [95, 121, 122]. Iacovacci et al. [124] developed a bidirectional microgear pump for a very small drug delivery systems.

Dosing accuracy and precision are extremely relevant in microfluidic setups. Many authors state the single stroke volume of their pump as limit of resolution. However, little information is available on the repeatability of single strokes and few authors present results on dosing variation at varying environmental conditions. It is necessary that pump evaluations include repeatable and reproducible measurements to develop reliable systems and enable market entry. Evaluation of dosing accuracy and precision are only available for industrial dosing units or systems close to the market [7–10, 59–61].

To ensure stable dosing at varying environmental conditions, the JewelPump comprises a double limiter concept that prevents diaphragm movement outside of fixed boundaries [128]. Therefore, the pump doses independently of the driving frequency (up to 3 Hz), pressure (± 10 kPa at inlet or outlet), temperature, aging, and medium's viscosity (up to 10 mPas)[35, 148, 149].

A diaphragm pump's flow often depends on the applied backpressure. Many authors describe a linear decrease in flow with increasing pressure applied at the pump's outlet [67, 75, 101, 102]. More stable dosing against varying pressure is achieved with peristaltic pump systems [105, 107, 119, 142] or the serial combination of several pumps [108, 138]. Richter et al. [102] present an extremely stiff bending actuator that shows a stroke decrease of less than 0.1% per kPa and a corresponding flow rate decrease of only 0.025 $\mu\text{L}/\text{min}$ per kPa backpressure increase. Pumps based on phase change actuation and magnetic shape memory actuation are generally less susceptible to changes caused by backpressure and can built up extremely high pressure [118, 120].

Especially for implantable, but also for patch pump application or hand-held analysis systems, size and weight constraints are an important requirement. Wireless power supply [126, 127, 143, 144] obviates the need of a battery and therefore enables systems that are small and light enough even for implantation into small rodents. Such systems omit the need to restrain the animal for electric contact during pump use. Specific manufacturing techniques, such as MEMS processes or 3D printing of miniaturized systems allows for extremely small pumps as shown by Richter et al. [70] ($3.5 \times 3.5 \times 0.6$ mm³ piezoelectrically driven pump) and Moussi et al. [127, 150] ($3.9 \times 2.1 \times 2$ mm³ electrolysis actuated pump). Xia et al. [116] present an extremely miniaturized dielectric polymer actuator of only 2.2×2.2 mm². The pump by Wang and Park [114] is small enough to be integrated into a contact lens. Furthermore, research pushes towards miniaturization of generally larger microgear pumps. Waldschik et al. [123] use polymer magnets with alternating axial magnetization manufactured using micro fabrication technologies to achieve a pump of only $10 \times 12 \times 1.3$ mm³.

1.3.2. Piezoelectric Micro Diaphragm Pumps developed at Fraunhofer EMFT

The department of [microdosing](#) at [Fraunhofer EMFT](#) researches on piezoelectric micro diaphragm pumps and microvalves and implemented silicon and steel devices (Table 1.3).

Table 1.3 Dimensioning and performance of selected micropumps developed at [Fraunhofer EMFT](#)

	P32009	P32010	P33001	μP015	μP029	μP027
Weight in mg	3850	4100	8350	70	30	12
Size in mm³	Ø20×1.7	Ø20×2	Ø29×2	7×7×1	5×5×0.6	3.5×3.5×0.6
Positive Actuation Voltage in V	300	450	300	240	100	70
Negative Actuation Voltage in V	-80	-120	-80	-76	-20	-20
Stroke Volume in nl	7,000	6,000	25,000	80	65	20
Backpressure (Air) in kPa	30	30	20	90	15	40
Maximal Flow Rate (Air) in μL/min	100,000	80,000	200,000	400	4,500	100
Blockingpressure (Water) in kPa	75	170	30	380	55	100
Maximal Flow Rate (Water) in μL/min	12,000	8,000	20,000	90	450	45

The smaller silicon micropumps can dose small amounts of fluid precisely and are able to overcome a high backpressure. For large numbers, production becomes very economic due to large-scale silicon production processes. Furthermore, standard [MEMS](#) production processes are extremely accurate and allow for the precise manufacturing of tiny structures. Therefore, extreme miniaturisation is possible. Today's smallest piezoelectric diaphragm pump is [EMFT](#)'s 3.5×3.5×0.6 mm³ pump (Table 1.3) [70]. Analytical modelling shows, that this size is the physical limit for piezoelectric actuation. Further miniaturization poses geometric constraints that make sufficient stroke impossible. To overcome this limitation, [Fraunhofer EMFT](#) researches on an alternative actuation principle: electrostatic actuation.

The steel micropump platform was developed in 2013 [151]. The devices are larger and achieve higher maximal flow rates. Manufacturing costs cannot be reduced as much as for the silicon micropump, however, smaller numbers are required for a profitable production. Furthermore, hermetic sealing is easier, since a metal cover can be added by laser welding.

Both types of micropumps, metal and silicon pumps, are [bubble-tolerant](#), even though air transport is specifically challenging for piezoelectrically actuated pumps: The piezoelectric elongation is comparably small, which is why the [stroke height](#) of the bending actuator is limited. Additionally, actuation towards negative fields is restricted [152], thus the largest proportion of movement is downwards. Hence, it is difficult to reach an optimal compression. At [Fraunhofer EMFT](#), a better [compression ratio](#) is achieved with the use of a specific manufacturing technique [137]: During the adhesion process of the

piezoelectric disc actuator, the ceramic is exposed to a defined electric field. Hence, bonding takes place while the ceramic is contracted. After curing, the voltage is removed and the actuator expands whereby it bulges out the pump chamber [137]. This specific mounting enables pump designs with very high **compression ratio** and therefore leads to self-priming and **bubble-tolerant** pumps. It is applied for all piezoelectric devices manufactured at **EMFT**. For instance, Richter et al. [102] introduce a $7 \times 7 \times 1$ mm³ small silicon pump that achieves an air backpressure of 90 kPa and is therefore capable of transporting bubbles even against backpressure.

A crucial pump feature is the prevention of **freeflow** caused by an overpressure at the inlet. For their silicon micropumps, Richter et al. [102] implement a **freeflow** stop realized as a flexible membrane covering the pump's outlet. The other side of the membrane is connected to the fluidic inlet. If the inlet pressure is higher than the outlet pressure, the membrane blocks the outlet [153]. An outstanding asset of this valve is its flat shape and placement right under the pump chip, enabling an overall system with the same footprint (7×7 mm²) and negligible additional system height. This passive component prevents **freeflow** even in turned-off state. The adaptation of the system for the steel platform is currently researched and part of the thesis of Claudia Durasiewicz.

In general, an adaptation of the fluidic properties for a specific application is possible and necessary. For instance, Richter et al. [102] reduce the pressure dependence of their micropump's flow rate with an extremely stiff bending actuator. The maximal flow rate of 25.8 μ L/min only decreases by 0.1 % per kPa backpressure. Linear extrapolation of the flow decrease measured up to 150 kPa indicates a maximal backpressure of 600 kPa.

In a comprehensive study, Jenke et al. [68] investigated influences on the flow characteristics of **EMFT**'s micropumps, such as viscous squeeze film damping, leakage effects on the valves, or the influence of air. He developed analytical models to estimate the effective flow rate including disturbances. According to analytical, as well as experimental data, the occurrence of cavitation in the pump chamber during the suction stroke is likely for fast actuator movements. These findings are specifically interesting for the transport of protein or cell solution, since the resulting air liquid interface can damage the transported medium.

2. Thesis Outline

Micropumps offer great potential for the improvement of biomedical applications. Not only do they enable the miniaturization of existing dosing units, but also the development of totally new concepts that allow medical treatment unimaginable up to date. However, biomedical application implies challenging requirements (v.s., Chapter 1.1). Even though in the last decades dedicated research has led to tremendous innovations as described in Chapter 1.3, many challenges are not yet solved and industrialization is pending. It is the aim of this thesis to advance towards the medical use of micropumps. The research proposal for this undertaking, and a summary of the achieved results are described in the following chapter.

2.1. Research Proposal

A great number of biomedical devices, setups, and processes involve the transport of fluids. Especially if the available space and power supply are limited, micropumps are an appealing solution for the active transport of small quantities of fluid. However, the **microfluidic** environment and high expectations in terms of fluidic performance and reliability pose significant challenges. To meet all requirements, extensive research is conducted to optimize different **microfluidic** actuation methods that come with specific advantages and disadvantages. However, the detailed literature review presented in Chapter 1 shows that most micropumps are not fully optimized devices, hence industrialisation is still pending.

In addition to general requirements that also apply for macroscopic fluid transport, many specific challenges arise when scaling down to the microscale. Targeted research has come up with many improvements and solutions to **microfluidic** tasks (v.i., Chapter 1.3). For example, it is by now possible to achieve flexible fluid transport with a **bubble-tolerant**, low-power and extremely miniaturized micropump. Inventive safety systems, or specific sensors to detect malfunctioning, have increased the reliability of dosing units. However, other requirements have not yet been evaluated in detail.

Dosing **precision** and **accuracy** are crucial properties for many biomedical applications. Nevertheless, for most micropumps presented in research, dosing variations are not evaluated. The single **stroke volume** that many authors state as the limit of resolution of their device can scatter significantly, leading to large dosing variations. Furthermore, additional deviations arise due to changing environmental parameters, such as varying backpressure, temperature or humidity.

The dosing **precision** can also be influenced by the transported medium. For instance, the transport of particles, protein solution, or cells can cause agglomeration within the pump chamber or the valve geometries. Such agglomerations can limit the actuator movement, cause occlusion, prevent the valve opening, or increase leakage, all of which cause a considerable decrease in pump performance. Though, not only damage caused by the transported medium to the pump is relevant, but also the impact of the pump on delicate substances, e.g., cell or protein solution. Even though interaction can be relevant, most studies are conducted with surrogate fluids, e.g., deionised water, since the target fluids are often expensive or complicated to handle and store.

Fraunhofer EMFT conducts research on piezoelectric micro diaphragm pumps and has implemented small silicon-based micropumps, and larger stainless-steel micropumps. As described in Chapter 1.3.2, many of the biomedical challenges have already been addressed in EMFT's research. However, there are still open questions that need to be addressed, before an industrialization for biomedical applications of Fraunhofer EMFT's pumps is possible.

The aim of this thesis is to investigate the properties of piezoelectric micro diaphragm pumps in detail, including the analysis of electromechanical and fluidic performance, dosing precision, and medium interaction. Based on this examination, the suitability of the pumps for biomedical applications is evaluated and the devices as well as actuation are improved for specific use cases.

The performance of a piezoelectrically actuated pump strongly depends on the properties of its disc actuator. It is therefore crucial to investigate the piezoelectric ceramic under relevant conditions. The high actuation voltage of the pumps requires knowledge of the large-signal behaviour of the piezoelectric material. Unfortunately, there is little information available from either the manufacturer or the literature. In particular, no studies concerning overdriving and long-term behaviour are available. Part of this thesis aims to enable a better understanding of the piezoelectric disc actuator. Therefore, the experimental evaluation of the large-signal piezoelectric elongation of the bare actuator disc is desirable. The characterisation of the piezoelectric coefficient enables better comprehension of depolarisation effects, a comparison of different ceramic materials and layer structures, and the improvement of the analytical pump design. The analysis of the bare disc actuator is the foundation for further evaluation of the bending actuator that includes a metal or silicon diaphragm with glued-on piezoelectric disc actuator. It is specifically interesting to investigate the negative actuation voltage amplitude that causes depolarisation, since due to the nonlinearity of the piezoelectric hysteresis, a possible increase of the negative voltage amplitude leads to an overproportional increase in performance. Especially for applications requiring large safety margins, such as medical devices, the achievable increase in performance is relevant.

As mentioned above, there is little to no statistically relevant data available that describes the dosing precision of piezoelectric micro diaphragm pumps. However, biomedical applications often require extremely accurate dosing units. High accuracy in combination with high safety requirements can often only be achieved by closed-loop control. A requirement for a well-functioning closed-loop control system is the reproducible dosing of small volume packages, especially if the target volume is close to the single stroke volume of the pump. The precision of a micropump can be influenced by the dosed medium, since additional disturbances can occur. To introduce drug solution into the pump can lead to agglomeration. Additionally, a change in viscosity can impair dosing. It is therefore of high relevance to evaluate the repeatability of package dosing not only with surrogate fluid, but also with drug solution itself. Within this thesis, the potential applicability of silicon diaphragm pumps for insulin delivery is evaluated based on the precision of package dosing with water as well as insulin solution. The change of the dosed medium allows to detect changes in precision caused by an interaction between the pump and the dosed medium. The improvement of dosing precision especially with the target medium can enable the development of space and energy-efficient delivery systems for extracorporeal or implantable applications.

For implants that require higher flow rates, e.g., different drugs or hydraulic implants, Fraunhofer EMFT's larger stainless-steel micropumps are better suited than small

silicon devices. Advantages are the biocompatibility of all wetted surfaces, and the easy solution for hermetic sealing by laser welding a cover to the pump's electronics. Unfortunately, stainless-steel can cause artefacts in medical imaging, limiting the implantable application of this pump technology. Also in literature, there is no fully biocompatible, hermetically sealable pump system that does not cause artefacts in imaging. Part of this thesis is thus to transfer the stainless-steel micropump technology to a titanium-based technology platform and therewith enable the flexible and cost-efficient development of biocompatible, imaging-compatible implants.

Biomedical applications usually require the transport of medium other than deionised water. Thus, additional disturbances can occur. For instance, the transport of particles can lead to agglomerations in the pump chamber or the area of the valves and therefore impair the functionality of the fluidic actuator. Even if the transported liquid is mostly particle-free solution, such as in the case of a hydraulic implant, it is impossible to prevent all contaminations. It is therefore highly relevant for safety reasons to understand the particle tolerance of the pump and develop systems that are resistant to such disturbances. Furthermore, some of the transported solutions are delicate and can be damaged by moving parts in the fluid path, e.g., flap or spring valves. This is the case for the transport of sensitive drug solution or cells. The evaluation of the interaction between the pump and the dosed medium is therefore of high interest. Hence, it is one of this thesis' objectives to provide both an understanding of the pump's reliability when dosing solutions other than water as well as an understanding of the pump's impact on transported living cells.

The detailed experimental evaluation of the fluidic properties, the design improvement towards a better performance, and the technological developments towards implants that do not cause imaging artefacts are the key objectives of this thesis. It therewith advances micropump technology towards its industrialisation and make a widespread use in the biomedical field possible.

2.2. Research Results

The technical developments and investigations conducted during this thesis have resulted in several journal and conference papers that are summarized below for a better overview. A detailed attribution of the author's contribution is available in the Appendix of the examination copy whereas the thematic contribution for each individual chapter is stated briefly in the summaries here below. The remainder of this thesis is structured as follows: Chapters 3 and 4 describe the evaluation of the piezoelectric bending actuator; its [large-signal behaviour](#) as well as the limits of the actuation signal for optimal performance without causing depolarisation of the piezoelectric ceramic are assessed. With these findings, an optimized 5×5 mm² silicon pump for drug delivery is developed and presented in Chapter 5. Furthermore, a titanium-based technology platform to forward the development of automated implants is presented in Chapter 6. It includes three individual components, two active valves and a micropump. This pump is larger compared to the discussed silicon pumps and thus potentially suited for the transport of cells. This possibility is investigated in Chapter 7 and Chapter 8. Furthermore, the reliability of the pump when transporting medium other than deionised water is assessed on the example of particle-laden fluids. The results of this research are not yet published and summarized in Chapter 9.

Chapter 3: Optical Evaluation of the Large-Signal Behaviour of Piezoelectric Disc Actuators to Increase the Precision of Micro Diaphragm Pumps

Agnes Bußmann, Phillipp Korzer, Christian Wald

Conference Paper, Actuator 2021, proceedings pages 97-100

This conference paper describes the experimental evaluation of the [large-signal behaviour](#) of the piezoelectric disc actuator used to manufacture EMFT's micro diaphragm pumps. The piezoelectric elongation of the upright actuator is measured optically using a white light profilometer. With this experimental setup, we evaluate the exact elongation of the disc caused by the voltage amplitude used for the pump actuation. Based on this measurement, the analytical modelling of the bending actuator can be improved, since calculations up to date rely mostly on the small signal data provided by the manufacturer. Furthermore, the full butterfly curve of the piezoelectric actuator is detected. Therewith, we measure the [coercive field](#) at which the polarisation of the ceramic material changes its direction. With the exact knowledge of this field, the pump's actuation voltage can be optimized towards higher negative amplitudes. Such higher negative fields increase the fluidic performance overproportionally due to the nonlinearity of the piezoelectric hysteresis. The impact on the pump's long-term stability is evaluated in Chapter 4.

This study was initiated, planned and conducted by myself with support by Phillip Korzer during the experimental work and Christian Wald for the manuscript review.

Chapter 4: Increasing Piezo Micro Diaphragm Pump Performance by Optimizing Piezo Actuation

Agnes Bußmann, Lorenz Grünerbel

Conference paper, Smart Systems Integration 2019, proceedings pages 305-308

Chapter 4 evaluates the influence of a higher negative actuation voltage on the fluidic performance of the pump, as well as its long-term reliability. Due to the nonlinearity of the piezoelectric elongation, the negative actuation voltage has a disproportionately high influence on the pump's performance. However, actuation fields close to the ceramic's [coercive field](#) E_c can cause depolarisation and therefore damage the bending actuator irreversibly. Chapter 4 evaluates the potential performance increase of both silicon and stainless-steel micropumps, as well as the long-term stability of the [actuator stroke](#) when pumps are actuated with a high negative field. An increase of the actuation amplitude of 15 % towards the negative voltage range leads to an increase in stroke of nearly 20%. This improvement translates directly to an increase of flow rate, since the single [stroke volume](#) depends linearly on the [actuator stroke](#). However, the performance increase is even more relevant when the pump needs to transport fluid against backpressure: at 30 kPa backpressure, the flow rate increases by approximately 150 %. The increased negative actuation voltage is thus extremely relevant as a safety measure when backpressure varies. In the long-term evaluation of up to one million strokes, neither stainless-steel nor silicon micropumps show depolarisation. The achieved performance increase based on higher negative actuation voltage allows the development of a small silicon micropump for drug delivery applications that is presented in Chapter 5.

The large-signal evaluation of the piezoelectric disc actuator was my effort. The study was supported by Lorenz Grünerbel with an investigation of the power-consumption when increasing the negative actuation field.

Chapter 5: Piezoelectric Silicon Micropump for Drug Delivery Applications

Agnes Bußmann, Henry Leistner, Doris Zhou, Martin Wackerle, Yücel Congar, Martin Richter, Jürgen Hubbuch

MDPI Applied Science, Special Issue Development of Microfluidic Devices for Medical Application, 2021, Volume 11(17), 8008

Drug delivery applications requires reliable, precise dosing of extremely small volumes. Chapter 5 introduces a specifically developed silicon micro diaphragm pump. It is adequate for drug delivery due to a change of the valve unit to minimize the risk of sticking and facilitate the transport of bubbles. The pump chamber is high compared to former pump designs to enable sufficient flow even with fluids of higher viscosity. The fluidic performance of the pump is sufficient for drug dosing, since the actuation voltage is increased based on the findings presented in Chapter 4. The dosing **precision** of the introduced $5 \times 5 \times 0.6 \text{ mm}^3$ silicon micropump when dosing packages between 0.05 and 5 mg is evaluated with both deionised water and insulin solution. This comparison reveals additional challenges caused by the change of medium: The transport of bubbles is more difficult, since insulin solution exhibits a higher surface tension than water and increases the capillary forces, impeding undisturbed transport. Nevertheless, the presented pump proves extremely precise compared to currently available commercial dosing units, even when dosing insulin. These results are extremely promising to evaluate the combination of the pump with higher concentrated drug solution.

This topic of the thesis was initiated, planned and conducted by myself with the support of the listed co-authors during the planning, experimental work, analysis and the making of manuscript as listed in the detailed authors' contributions un the Appendix.

Chapter 6: Piezoelectric Titanium-Based Microfluidic Pump and Valves for Implantable Medical Applications

Agnes Bußmann*, Claudia Durasiewicz*, Sebastian Kibler, Christian Wald

* contributed equally

Sensors and Actuators A: Physical, 2021, Volume 232, 112649

The high effort necessary to introduce a completely new technology into a medical application hinders the widespread use of **microfluidic** actuators, regardless of their many advantages compared to conventional medical dosing units. To reduce the effort of a new development, we therefore develop a titanium-based **microfluidic** technology platform that includes a pump for active transport as well as two active valves to regulate fluid flow. This platform allows the development of several **microfluidic** medical devices in parallel and therefore permits to reduce the high initial financial and time effort for each individual development. Since the devices are fully made of medical grade titanium – the only exception being the piezoelectric disc actuator – they are biocompatible, offer easy hermetic sealing by laser welding covers and do not cause artefacts in medical imaging. They are thus perfectly suited for the development of medical implants. The effort in this work, shared between my colleague Claudia Durasiewicz and myself, is divided into the development of the individual components: The development of the active valves is part of her dissertation, while I focused on the improvement of the diaphragm pump. The applicability of these pumps for further biomedical transport tasks, such as cell transport, is discussed in Chapters 7, 8, and 9.

This research was a shared effort between my colleague Claudia Durasiewicz and myself. The investigation of the active microvalves was led and conducted by Claudia Durasiewicz, whereas the work on the titanium micro diaphragm pump was initiated, planned and realized by myself.

Chapter 7: Cell Transport Using Piezoelectric Micro Diaphragm Pumps

Agnes Bußmann, Thomas Thalhoffer, Leopold Daum, Martin Richter, Oliver Hayden
Conference paper, MikroSystemeTechnik Kongress 2021, proceedings pages 290 - 293

In many biomedical applications the transport of living cells is necessary, either for the automatization of cell culture research, increased functionality of [microfluidic](#) experimental setups, or even the transport of cells for 3D printing. Micropumps offer an economic, space and energy-efficient solution that can be integrated into a disposable product. However, living cells are fragile and the pump is likely to impair the viability of transported cells. To enable the development of pumps capable of cell transport, a better understanding of the interaction between the pump and the cell solution is necessary. Therefore, the viability of K562 leukaemia cells is investigated after transport with two types of silicon micro diaphragm pumps, as well as stainless-steel pumps that are introduced in Chapter 5 and Chapter 6 respectively. The experiments confirm the expected large impact of a rectangular pump actuation, while sinusoidal actuation evokes only a small decrease in viability. Furthermore, the larger metal micropumps have a smaller impact on cells. Therefore, this pump type is used for a more detailed experimental evaluation described in Chapter 8.

This preliminary study on the transport of cells was initiated and conducted by myself. Experiments were conducted in the laboratories of Oliver Hayden with the support of Leopold Daum and Thomas Thalhoffer.

Chapter 8: Microfluidic Cell Transport with Piezoelectric Micro Diaphragm Pump

Agnes Bußmann, Thomas Thalhoffer, Sophie Hoffmann, Leopold Daum, Nivedha Surendran, Martin Richter, Jürgen Hubbuch, Oliver Hayden
MDPI Micromachines, 2021, Volume 12(12), 1459

Based on the preliminary experiments described in Chapter 7, the transport of cells is evaluated on a statistically relevant number of pumps and transported samples. The aim of this study is to determine the main reasons for damage on the cells, and limit the pump's impact by an improvement of the actuation signal. As shown in the preliminary experiments, sinusoidal actuation is less harmful. However, rectangular actuation is more efficient in terms of fluidic performance of the pump and therefore the desired actuation. The possibility to alternatively use a rectangular wave with sinusoidal flanks is evaluated by an investigation of the single [stroke volume](#) transported with sinusoidal, rectangular and mixed signals (rectangular with sinusoidal flanks). The single [stroke volume](#) and therewith the achievable fluidic performance, plateau with a flank steepness of 30 to 60 Hz depending on the voltage pulse frequency. Therefore, the cell solution in this study is transported with sinusoidal and rectangular actuation as well as with a rectangular actuation with 60 Hz sinusoidal flanks. The mixed signal shows the same impact on the cell solution as the sinusoidal actuation. An improved transport with a good fluidical performance as well as reduced impact on the transported medium is hence possible.

This study is based on the preliminary experiments presented in Chapter 7 and preceding research on the single stroke volume of micropumps by Thomas Thalhofer. The work was initiated and conducted by myself with the support of the co-authors as stated in the author's contribution in the Appendix.

Chapter 9: Particle Tolerance of Metal Micro Diaphragm Pumps

Not published

In Chapter 8, the impact of the [microfluidic](#) transport on cells in solution is evaluated. Additionally, the transport of fluids that contain cells, particles or fibres can impair the fluidic performance of the pump. An extensive evaluation is necessary to guarantee a safe use of the system. This chapter discusses a first experimental investigation of the particle tolerance of metal micropumps. As a reproducible model for particle-laden fluids, we use polystyrene particles of different sizes. The investigation shows that even small particles of 1 μm diameter impair the pump's functionality after a short transport period of 10 min. Nevertheless, the pumps do not fail completely and are even able to pump fluid after 48 h of continuous operation.

The experimental work of this study was supported by Nivedha Surendran and Sophie Hoffmann.

3. Optical Evaluation of the Large-Signal Behaviour of Piezoelectric Disc Actuators to Increase the Precision of Micro Diaphragm Pumps

Bußmann, Agnes^{a,b,*}; Korzer, Philipp^a; Wald, Christian^a

^aFraunhofer EMFT Research Institution for Microsystems and Solid State Technologies, Hansastrasse 27d, 80686 Munich, Germany

^bKIT, MAB - Biomolecular Separation Engineering, Fritz-Haber-Weg 2, 76131 Karlsruhe, Germany

*Correspondence: agnes.bussmann@emft.fraunhofer.de; Tel.: +49 89 54759-416

Abstract

The piezoelectric actuator and its electromechanical coupling largely influence the performance of a piezoelectric micro diaphragm pump. Therefore, it is crucial to investigate this property to understand and improve the pump. In this study, we introduce an experimental setup to investigate the **large-signal behaviour** of piezoelectric disc actuators optically using a white light profilometer. Obtained results are reproducible with an error of 5 % and in good agreement with comparative measurements using strain gauges. The comparison of singlelayer and multilayer actuators shows less elongation for the multilayer at same electric fields. However, the multilayer material does not saturate and reaches similar elongation at roughly half the voltage the singlelayer ceramic needs. The introduced setup is well adapted to evaluate actuators prior to piezo mounting to a pump and enables targeted lifetime evaluations.

3.1. Introduction

With their variable flow rate and high backpressure capability, piezoelectric micro diaphragm pumps are a possible solution for many micro fluidic questions. Often **dosing accuracy** plays a crucial role. To minimize variations from one sample to another, it is important to understand all parts of the system, including the piezoelectric disc actuator. The voltage dependant elongation of the ceramic at high electric fields has two main influences on the pump's performance. First, pumping bases on the indirect piezoelectric effect that causes a mechanical deformation when the piezoelectric ceramic is exposed to electrical actuation [154]. Hence, applying an alternating high voltage signal results in an alternating vertical diaphragm deflection that compresses and expands the pump chamber. The two passive flap valves direct the volume displacement and create an effective fluid flow (Figure 3.1). A difference in piezoelectric deformation changes the total stroke and consequently the achieved flow rate and pressure [155].

Second, the piezo electric coupling coefficient changes the zero position of the diaphragm. The piezo is glued to the membrane, while a voltage is applied, putting it to its contracted state (**pretension principle** – Figure 3.2). The actuator's increase in diameter when the voltage is disconnected after curing, leads to an upwards movement of the diaphragm and forms the pump chamber (Figure 3.2). That way, the actuator can expel most of the volume in the pump chamber during the compression stroke, which increases the **compression ratio** of the device significantly. Therefore, this mounting method is crucial

to produce pumps with little dead volume, capable of achieving high pressure with compressible medium such as gases or air bubbles in liquids [32, 137].

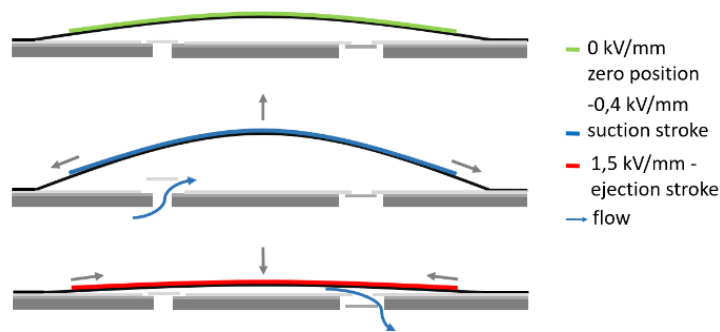


Figure 3.1 Working principle of the piezoelectric micro diaphragm pump

The position of the diaphragm changes the pump chamber height, which strongly influences the fluidic performance. A low chamber with little dead volume enables large backpressure with air. However, the maximal flow rate, especially with water, decreases, since a low chamber has a higher fluidic resistance than a high chamber.

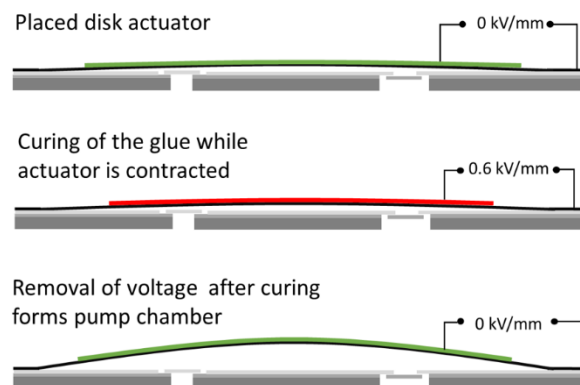


Figure 3.2 Piezo mounting using the *pretension* principle

Both, pump actuation as well as voltage during *pretension*, are in the *large-signal* range of the actuation, since the whole actuator displacement is necessary for efficient fluid displacement. The characteristics of a piezo ceramic actuator under high voltage can differ strongly from commonly measured properties at small electric fields. Hence, the exact knowledge of *large-signal* piezoelectric characteristics is crucial to design and manufacture well-adapted pumps for each application. To evaluate the influence of the piezoelectric elongation on the pump performance experimentally, a setup that does not influence the disc actuator is needed. That allows to characterize the piezoelectric ceramic prior to piezo mounting in order to correlate different elongation to varying pump performance. Therefore, the use of DMS is not possible.

There is no established, non-destructive experimental setup for the disc actuator geometry used in EMFT's micropumps up to now. Therefore, we established a setup to investigate the electro mechanical coupling coefficient in a non-destructive measurement. With this setup, we are able to investigate soft lead zirconate titanate (PZT) disc actuators

before piezo mounting to the pump to understand the influence of each piezo characteristic. In addition, fatigue testing of the disc actuator is possible, allowing better understanding of one of the pump's failure mechanisms.

3.2. Materials and Methods

We investigate standing disc actuators using a white light profilometer (Fries Research and Technology; 300 nm sensor). Two rubber bands hold the ceramic, which is clamped between two contact pins, down (Figure 3.3). The rubber bands are necessary to prevent the piezo from moving upwards. This would lead to a situation where it is held only by the electric spring contacts and does not touch the ground. In this case, the detected elongation is only of the upper part of the ceramic, as the lower part expands towards the bottom. Therefore, a measuring error of 20 % would occur, making it crucial to hold the ceramic down in all cases.

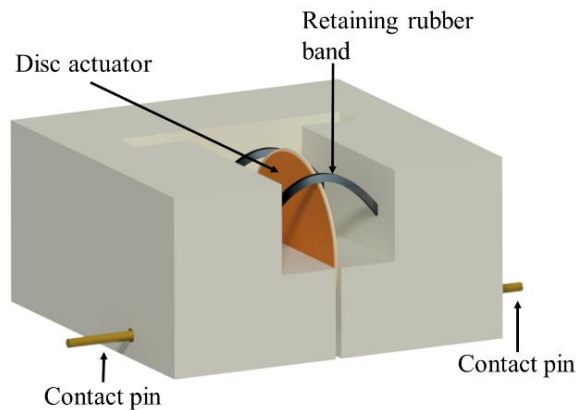


Figure 3.3 Measuring setup for the optical evaluation of the radial piezoelectric elongation

We mount a ceramic in the fixation and carefully align the sensor, choosing the highest point for the measurement. Since the roughness of the ceramic ($R_a \approx 5 \mu\text{m}$) is in the same order of magnitude as the elongation, it is important not to mistake roughness for elongation. Hence, we perform a line scan of the whole width of the sample for each voltage step and calculate the average height. Each voltage is applied for several seconds, making the investigation quasi-static and minimizing the influence of piezo electric time effects.

In this study, we investigate two types of disc actuators: singlelayer PIC 151 ($\text{Ø } 16 \text{ mm}$; $t = 200 \mu\text{m}$; six samples) and multilayer PIC252 with five active layers ($\text{Ø } 16 \text{ mm}$; $t = 315 \mu\text{m}$, two samples). Applied electric fields range from -3 kV/mm to 6 kV/mm .

To evaluate the setups accuracy, strain gauge (KYOWA; $R = 120 \Omega$) measurements are conducted on singlelayer piezo ceramics. The gauges are fixed central on the ceramics using two-component epoxy glue (EPO-TEK 353 ND).

3.3. Results and Discussion

In a first step, it is crucial to evaluate the variance of the new experimental setup. Thus, we conduct repeated measurements of the same ceramic, removing it from the holder after each measurement. The mean elongation of seven individual measurements is

$18.7 \pm 1 \mu\text{m}$. The error is not caused by the profilometer (the used sensor offers a resolution in the nm range) but rather from positioning errors and an inclination of the ceramic. The maximal tilt is limited to 10° by the mounting's gap width and height, causing an error of up to 2 %. In addition, a measurement apart from the top point of the disk is possible. Nevertheless, even a deviation of 1 mm, which is unrealistically high as the position is well adjustable, would only cause an error of 0.4 %.

To assess the setup's accuracy, we compare the results of six samples to strain gauge measurements (Figure 3.4). The restriction of movement caused by the strain gauge is minimal and the elongation before and after strain gauge adhesion shows no difference. In addition, the elongation does not differ whether the sample is mounted or hanging freely (held by the strain gauge's connecting cables), showing that the rubber bands do not restrict the ceramic's movement significantly. Experiments show no significant difference amongst strain gauge and optical measurements with an average deviation of $1.0 \pm 0.9 \mu\text{m}$. Hence, the optical setup is sufficiently accurate to characterize ceramics prior to mounting.

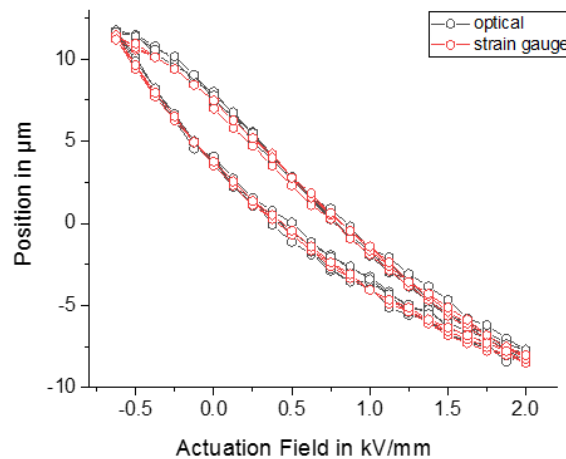


Figure 3.4 Exemplary radial elongation of one disk actuator measured optically and with strain gauges. Results are in good accordance

Using the introduced setup makes it possible to detect the full hysteresis of a piezoelectric disc actuator (Figure 3.5). This measurement helps to compare different materials and gain knowledge on the limits of use of an actuator. The **coercive field** is visible at roughly 0.9 kV/mm.

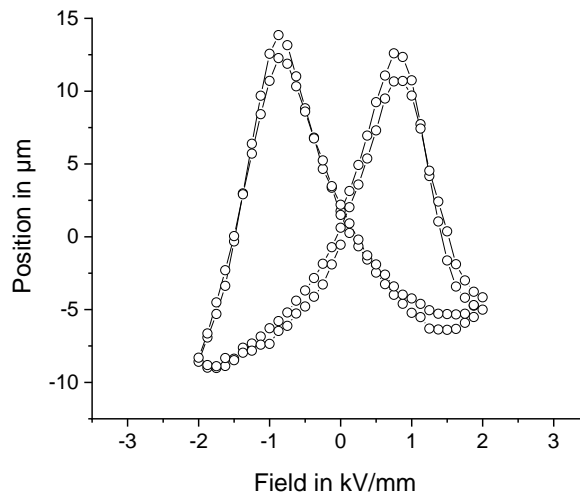


Figure 3.5 Piezo electric hysteresis of a singlelayer sample

The **coercive field** is especially interesting, since actuators are not supposed to be used with more than 30 % of their negative **coercive field**. However, the negative part of the actuation provokes a larger increase in the micro pumps stroke and hence in maximal flow and pressure capacitance, due to the nonlinear elongation of the ceramic. Consequently, it can be beneficial for some applications to extend the negative amplitude further towards the **coercive field**. The exact knowledge of the latter makes it possible to improve actuation towards optimized pumping properties. However, lifetime has to be considered, since it most probably depends on the actuation signal.

The investigated singlelayer actuator is the standard actuator used for our metal micro pumps [151]. Even though the material is well adapted to most applications, it shows one important disadvantage: the voltage levels needed to drive the micropump are comparatively high (up to 300 V or even higher for thicker piezo actuators). Multilayer actuators are a possible solution for this issue, since they reduce the voltage needed for actuation significantly. The multilayer actuator investigated within this study has five active layers of 45 μm each. Hence, the thickness of active material is roughly 25 μm larger compared with the singlelayer actuator. However, the material used is slightly different and shows a smaller piezoelectric coefficient d_{31} than the PIC151 material (-180 nm/kV compared to -210 nm/kV at low electric fields). Furthermore, isolating layers are necessary, adding 90 μm of passive material to the active layers of the actuator. Therefore, we expect a decreased stroke for similar electric fields. Figure 3.6 shows the comparison of elongation measured on a singlelayer sample and measured on a multilayer sample. For clarity, only one sample each is shown. However, all samples exhibit similar behaviour in the measurement.

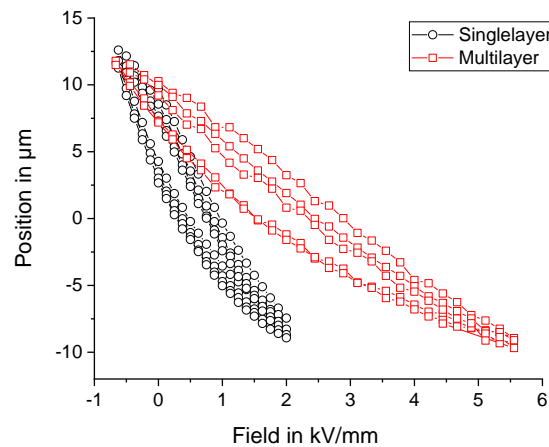


Figure 3.6 Elongation comparison of a single- and multilayer sample

The expected decrease in stroke is clearly visible in Figure 3.6. The multilayer actuator only reaches the same elongation as the singlelayer actuator at 5 kV/mm. It is interesting to notice that the ceramic does not reach saturation until this point. A further increase of the electric field therefore increases the elongation and consequently the pumps stroke and achievable flow rate.

Depending on the application, not only electric field but also the corresponding voltage are crucial. The multilayer disc reaches the same elongation as the singlelayer at 5 kV/mm, which corresponds to just above 200 V. To apply a field of 2 kV/mm to the singlelayer requires 400 V. The multilayer can therefore be useful for applications with lower stroke requirements or lower voltage limitations. However, energy consumption

has to be considered. To reach the same elongation with the multilayer as with the single-layer, the energy consumption is higher.

3.4. Conclusion

The introduced non-destructive measurement enables the investigation of piezoelectric **large-signal** properties. The optical measurement is able to replicate the results achieved with strain gauge evaluations with an average deviation of $1.0 \pm 0.9 \mu\text{m}$. Its repeatability is high with an average elongation measured in independent measurements on the same sample of $18.7 \pm 1 \mu\text{m}$.

Since the method is non-destructive, it allows for piezo characterisation prior to piezo mounting without changes to the pump's setup such as an added strain gauge. It therefore enables us to investigate the influence of the exact piezo electric elongation on the pumps stroke as well as the diaphragms zero position further. The experiments will enable the refinement of theoretic pump models and enable more accurate pump design for specific applications.

In addition to the better understanding of all important influences, the setup allows for a specific material selection. The **large-signal behaviour** is not usually measured and given in standard data sheets. It is therefore of great interest to evaluate it in order to compare different materials to be used as potential disc actuators for the pump application.

Part of this evaluation is also lifetime testing, since the pump's long-term stability as well as long term precise dosing largely depends on the piezoelectric actuator. If the piezoelectric stroke decreases with the number of driving cycles, the flow rate of the pump will drift away from its set value. The maximal achievable flow decreases and a system that is not closed loop controlled will show an increasing error in the flow rate. However, fatigue of the piezo actuator is only one possible reason for a drift in the flow rate that can also be caused by changing valve quality, fatigue of the adhesive layers, etc. It is therefore of extreme interest to investigate the **large-signal** long-term stability of the actuator itself without other influencing effects.

Initial tests concerning long-term stability show that the setup is well suited for this type of experiment. A point measurement enables the monitoring of the dynamic stroke throughout the experiment and regular hysteresis measurements during the experiment give detailed information on changes.

In future measurements, we will develop a detailed picture of depolarization of the used disc actuators with differing electric actuation. The aim is to adapt the driving signal depending on the application. A long-term application with need for long stable piezoelectric elongation and strong need for secure function can use a different actuation than a short-term, high performance pumping, where depolarization after the duration of usage is unproblematic.

Acknowledgements

This work was partly founded by the VDI/VDE Technik GmbH within the project "ADOS – Piezoelektrische Metall-Mikropumpe für Flüssigkeiten und Gase", reference nr. ESB071/002.

4. Increasing Piezo Micro Diaphragm Pump Performance by Optimizing Piezoelectric Actuation

Bußmann, Agnes^{a,b*}; Grünerbel, Lorenz^{a,c}

^aFraunhofer EMFT Research Institution for Microsystems and Solid State Technologies, Hansastrasse 27d, 80686 Munich, Germany

^bKIT, MAB - Biomolecular Separation Engineering, Fritz-Haber-Weg 2, 76131 Karlsruhe, Germany

^cTUM, TEP - Chair of Physics of Electrotechnology, Theresienstrasse 90, 80333 Munich, Germany

*Correspondence: agnes.bussmann@emft.fraunhofer.de; Tel.: +49 89 54759-416

Abstract

Actuation of piezo ceramics applies only up to 30% of their negative **coercive field** strength E_c . This ample distance of the field where polarization reaches zero is necessary to avoid depolarization. This work examines the effect of further approaching E_c on micro diaphragm pumps. The higher negative actuation voltage increases two fundamental micro pump characteristics. First, would be an increase of maximal flow and second a better air backpressure capability. Sinusoidal actuation, applying higher negative voltages, while keeping the positive amplitude on a standard level, does not cause degradation within one million cycles.

4.1. Introduction

Piezoelectric micro diaphragm pumps are used in many technical and medical applications. **Fraunhofer EMFT**'s micro diaphragm pumps consist of either a silicon or steel body and diaphragm with a glued-on piezo ceramic actuator. Pumping bases on the indirect piezoelectric effect, causing a mechanical deformation when the piezoelectric ceramic is exposed to electrical actuation [154]. Hence, applying an alternating high voltage signal results in a vertical diaphragm deflection and fluid movement through two passive flap valves and creates an effective fluid flow (Figure 4.1).

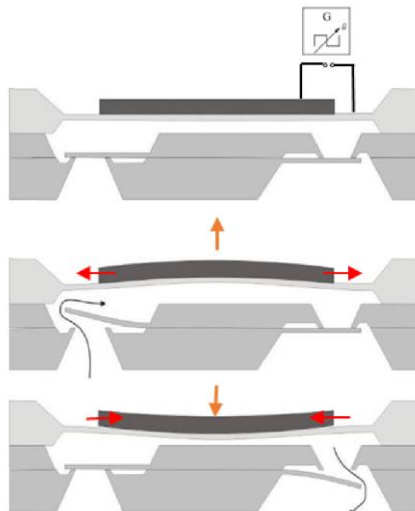


Figure 4.1 Setup and working principle of a piezoelectric micro diaphragm pump

Fraunhofer EMFT has developed micro pumps for the last 25 years, already achieving strong pumping performance [68, 156]. So far, the used actuation signals never

exceed 40% of the negative **coercive field** E_c . However, recent studies claim that symmetric actuation up to 95% of E_c does not cause damage within at least one million cycles [152]. This work examines the impact of applying higher negative fields on the pumping performance and long-term piezo stability.

4.2. Materials and Methods

For research on micro pump performance, several of EMFT's silicon and steel pumps are evaluated. In this study, the ceramic PIC151 from PI Ceramics ($E_c = \pm 1.0$ kV/mm [152]) is glued onto the pumps with epoxy glue (EPO-TEK 353ND). Depending on the pump type, the piezo actuators have a thickness between 50 μm and 200 μm . A common function generator with external amplifier generates the actuation signal for the measurements. The flow and backpressure measurements as well as the long-term stability evaluation are conducted with sinusoidal actuation using different amplitudes. Air flow rate measurements are conducted with Bronkhorst anemometers. Controlled pressure abuts at the micro pump's outlet during the investigation of its backpressure capability. A commercial confocal white light microscope from FRT enables stroke measurements, where the voltage induced movement of the actuator membrane is monitored optically. Both, dynamic and quasi-static measurements are possible. Stroke verification each 75000 cycles during continuous pumping enables observation of actuator fatigue. All measurements are conducted with air.

4.3. Results and Discussion

To investigate a performance increase by actuating the steel micro pump with a higher negative electrical field, the static **actuator stroke**, the maximal flow rate and the pumps backpressure capability are evaluated. The static stroke measurement shows an actuation from -0.7 kV/mm to 1.5 kV/mm increases the total stroke by nearly 20 % compared to the standard -0.4/+1.5 kV/mm actuation (Figure 4.2 a). This increase of the **stroke height** generates a theoretical increase of the **stroke volume** of 17 %, Therefore, we also anticipate a notable performance increase. The investigation of five samples shows an average increase of the maximal flow rate by 30 ± 16 % at sinusoidal actuation with 250 Hz and no applied backpressure (Figure 4.2 b). Thus, the flow rate increases nearly twice as much as the theoretical **stroke volume**.

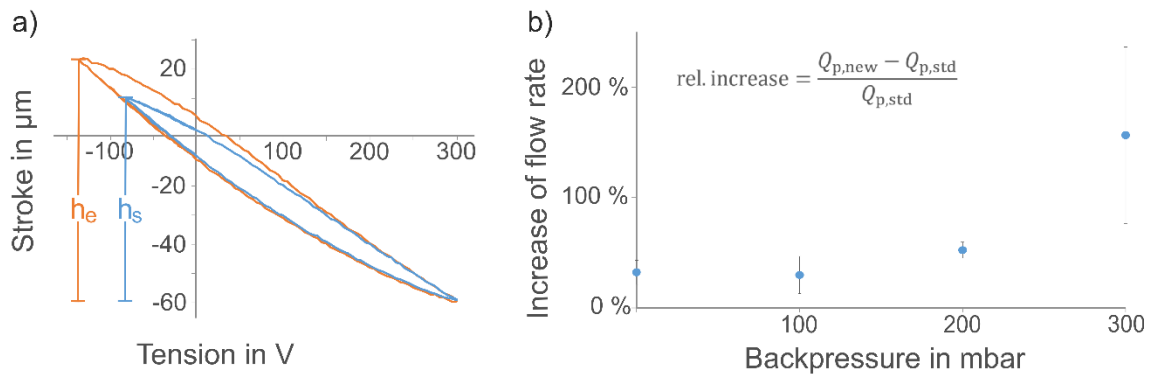


Figure 4.2 Increase of the pump's performance when actuated with a higher negative voltage amplitude. (a) Total stroke of a steel pump, blue: standard actuation (-0.4 to 1.5 kV/mm) with a total stroke of $h_s = 70 \mu\text{m}$ and orange: high negative amplitude (-0.7 kV/mm) with a total stroke of $h_e = 83 \mu\text{m}$. (b) Relative increase of the flow rate with high voltage actuation (-0.7 to 1.5 kV/mm) compared to the flow with

standard actuation for each applied backpressure; error bars indicate the standard deviation of the 5 pumps

Several other effects add to the increase of **stroke volume**. By applying a higher negative voltage, the actuator diaphragm is pulled further up, increasing the maximal pump chamber height and therefore decreasing the flow resistance, which enables a higher flow increase. Furthermore, there are imperfections within the valves and other periphery parameters, which are not considered when examining the single **stroke volume**. This theoretical parameter is the maximal volume that can be moved within one stroke, assuming perfectly closed and opened valves as well as no fluidic capacitances or any other counter forces. Nevertheless, the experimental setup measuring the flow rate obviously creates a certain fluidic backpressure and the valves in the pump need time to operate as well as they show leakage. Higher negative actuation voltage causes a higher and more rapid pressure pulse and therefore increases the flow rate additionally by quick valve movement and overcoming counter forces. The flow measurement with applied backpressure at the micro pump's outlet substantiates these findings. At 300 mbar backpressure, the flow rate increases by $155 \pm 80 \%$. The results show, that actuation with higher negative amplitudes is more advantageous when the pump needs to overcome backpressure.

One reason for the high variation in the measured performance can be the difference in valve quality. To investigate the benefits of higher negative fields, also samples with leaking valves are included in this study, making the variation within the samples bigger. Nevertheless, for all samples an increased flow rate is detected. It is important to underline, that all measurements are conducted with a 250 Hz sinusoidal actuation and the measured increase is only a first indicator of a better pump performance. There is still a need to investigate the micro pump behaviour with differing actuation signals and under various operating conditions.

After showing possible advantages of the actuation with higher negative voltage, it is important to investigate possible drawbacks. To start, the energy consumption of the micro diaphragm pump should be as small as possible, since many applications are mobile battery devices. A comparison of the power consumption of a silicon micro diaphragm pump driven with standard actuation and higher voltage signals shows no significant change in the energy consumption. The energy, which is necessary to achieve one micro-metre of stroke, provides a reasonable measure for comparison of power consumption during different operating conditions. Table 4.1 shows changes of less than $10 \mu\text{W}/\mu\text{m}$, which is within measuring inaccuracy.

Table 4.1 Power consumption per μm stroke depending on the actuation amplitude and frequency

Power Consumption in $\mu\text{W}/\mu\text{m}$		Frequency		
		100 Hz	200 Hz	300 Hz
Electrical Field in kV/mm	-0.4/1.5 kV/mm	224	275	216
	-0.5/1.5 kV/mm	221	274	216
	-0.9/1.5 kV/mm	219	283	223

Furthermore, long-term stability is examined using a 250 Hz sine wave actuation of different amplitudes. Three steel samples actuated with an electric field from 0.7 to 1.5 kV/mm after one million cycles still show in average 98% of their initial stroke (Figure 4.3 a). Further investigations are necessary to evaluate stability beyond one million cycles. In addition, different actuation amplitudes are tested on three silicon pumps: the standard actuation of -0.4/1.4 kV/mm; a higher voltage actuation of -0.9/1.4 kV/mm and even an actuation up to the negative **coercive field** of -1.0/1.4 kV/mm. None of which show signs of depolarization (Figure 4.3 b). The beginning of each measurement goes with a slight change in stroke, supposedly caused by piezo repolarization after storage. Aligned dipoles in the material can deviate slightly over time. The actuation signal with a positive amplitude of 1.4 kV/mm or more, regains the initial polarization.

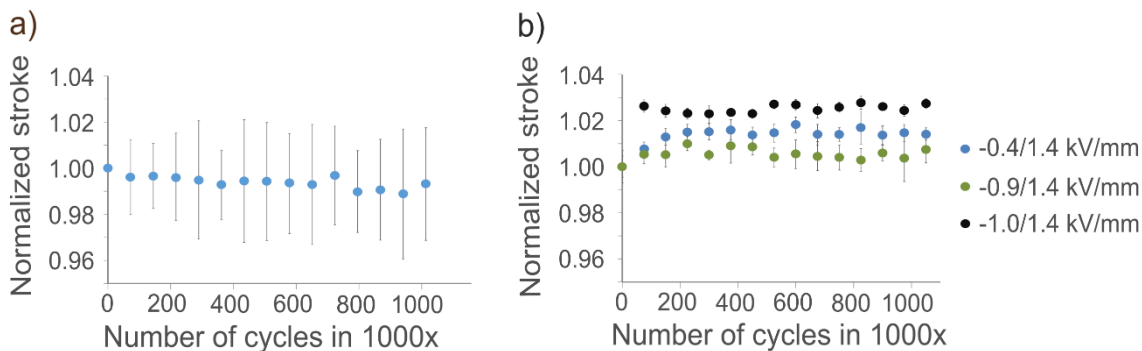


Figure 4.3 Long term stability of pumps actuated with higher negative voltage. (a) Stroke of three steel samples actuated with -0.7/1.5 kV/mm, normalized to their initial stroke; error bars indicate the standard deviation among the samples; (b) Stroke of individual silicon pumps normalized to their initial stroke, actuated with different amplitudes; error bars indicate the standard deviation of ten strokes

4.4. Conclusion

State-of-the-art limitations regarding negative actuation signals to piezoelectric ceramics restrict the maximal micro pump performance. First long-term tests show a stable operation when applying electrical fields of up to -1.0 kV/mm while applying a high positive amplitude (1.4 kV/mm). The non-symmetric positive actuation is likely compensating possible depolarization. The increase of flow rate is considerable, especially when pumping against backpressure.

EMFT's micro pumps, which already show a high backpressure capability due to their high **compression ratio**, can therefore achieve even higher pressure. These findings open the possibility of research on applications with more intense specifications or in need of a high margin of safety.

Acknowledgement

This work is part of the POSITION-II project funded by the ECSEL Joint Undertaking under grant number Ecsel-783132-Position-II-2017-IA. www.position-2.eu

5. Piezoelectric Silicon Micropump for Drug Delivery Applications

Bußmann, Agnes^{a,b,*}; Leistner, Henry^{a,c}; Zhou, Doris^a; Wackerle, Martin^a; Congar, Yücel^a; Richter, Martin^a; Hubbuch, Jürgen^b

^aFraunhofer EMFT Research Institution for Microsystems and Solid State Technologies, Hansastrasse 27d, 80686 Munich, Germany

^bKIT, MAB - Biomolecular Separation Engineering, Fritz-Haber-Weg 2, 76131 Karlsruhe, Germany

^cTUM Chair of Molecular Electronics, Theresienstr. 90, 80333 Munich, Germany

* Correspondence: agnes.bussmann@emft.fraunhofer.de; Tel.: +49 89 54759-416

Abstract

Subcutaneous injection is crucial for the treatment of many diseases. Especially for regular or continuous injections, automated dosing is beneficial. However, existing devices are large, uncomfortable, visible under clothing, or interfere with physical activity. Thus, the development of small, energy-efficient and reliable patch pumps or implantable systems is necessary and research on microelectromechanical system (MEMS) based drug delivery devices has gained increasing interest. However, the requirements of medical applications are challenging and especially the dosing precision and reliability of MEMS pumps are not yet sufficiently evaluated. To enable further miniaturization, we propose a precise 5×5 mm² silicon micropump. Detailed experimental evaluation of ten pumps proves a backpressure capability with air of 12.5 ± 0.8 kPa, which indicates the ability to transport bubbles. The maximal water flow rate is 74 ± 6 µL/min and the pumps' average blocking pressure is 51 kPa. The evaluation of the dosing precision for bolus deliveries with water and insulin shows a high repeatability of dosed package volumes. The pumps show a mean standard deviation of only 0.02 mg for 0.5 mg packages and therefore stay below the generally accepted 5% deviation, even for this extremely small amount. The high precision enables the combination with higher concentrated medication and is the foundation for the development of an extremely miniaturized patch pump.

5.1. Introduction

Medical care relies strongly on pharmaceuticals to treat diseases. Intravenous or subcutaneous injections are an easy and very common way of administration. However, manual injections can be uncomfortable, require regular attention, and do not offer the possibility of continuous dosing. Automated delivery can circumvent these disadvantages.

One well-known drug dosing application is the treatment of diabetes. The strict management of the blood glucose level is crucial for the patients' wellbeing [4]. It is known that continuous subcutaneous insulin delivery with a pump system improves patient's care significantly compared to multiple daily injections [5, 6, 157]. Currently, two pump types for subcutaneous drug delivery are available: durable pumps in combination with an infusion set, and patch pumps. The latter reduce the need for regular disconnection, for instance when practicing sports or showering, and therefore enable a constant insulin supply. Moreover, the elimination of tubing leads to more comfortable and less

visible use and therefore improves the patient's compliance. Consequently, patch pumps show to ameliorate the therapeutic success [3, 158]. Continuous drug delivery to specific tissues also leads to a better therapeutic result with limited side effects for specific cancer treatments and studies show that a delivery adapted to the circadian rhythm is beneficial [11, 12].

Even though research pushes towards automated, small dosing units for patch applications or implantation, there is still improvement necessary [100]: Existing patch pumps for insulin delivery are large enough to be visible under clothing. Furthermore, the **accuracy** of currently available pumps is lower compared to durable pumps [8, 9, 61, 159]. The improvement of the **dosing accuracy** as well as further miniaturization is therefore desirable.

The drug delivery application demands for well-adapted properties under challenging conditions [100]. The device needs to be utmost reliable with high **dosing accuracy** and **dosing stability**, even against backpressure. In addition to demanding fluidic requirements, patch pumps need to be cost-efficient, since they are often at least partly disposable and need to compete with the cost of conventional therapy.

Further miniaturization of delivery systems is possible based on micropumps that enable small and lightweight systems for energy-efficient delivery. Since the production is mostly based on standard, large scale processes, e.g. **MEMS** processes, costs are low if production numbers are sufficiently high. However, the use of micropumps implies new challenges. For instance, the transport of air bubbles that is usually unproblematic for macroscopic actuators, can lead to the failure of a micro diaphragm pump, since air is compressible and acts as a fluidic capacitance in the chamber of the displacement pump [32]. Additionally, surface tension becomes extremely relevant and the **microfluidic** actuator needs to be capable of moving the liquid meniscus through the system while overcoming resulting capillary forces [39–41]. **Bubble tolerance** of diaphragm pumps can be achieved with adapted designs towards a large **compression ratio**, the ratio between displaced volume and dead volume, that enables to overcome high air backpressure [32].

To enable the use of micropumps for drug delivery application, a sufficient **dosing accuracy** has to be guaranteed. However, up to date, micropumps presented in research are not tested extensively with respect to their dosing **precision** and reliability [100]. The only extensively tested, **MEMS** based patch pump system is the JewelPump developed by DeBiotech. The integration of a double limiter concept, several pressure sensors and the pretension of the passive flap valves enable stable dosing even at varying temperature, inlet and outlet pressure, or medium's viscosity as well as a quick error detection [35, 148, 149]. Borot et al. [61] confirm a high **dosing accuracy** compared to other insulin pump systems, and an exceptionally fast error detection.

To further evaluate the usability of micropump based delivery systems, a detailed experimental characterisation of the fluidic properties, as well as the dosing **precision** and robustness of the fluidic actuator are necessary. However, the little volume of dosed packages and the small measured flow rates make an experimental evaluation extremely challenging.

The norm IEC 60601-2-24 [58] regulates the assessment of **dosing accuracy** for drug dosing devices, also including patch pumps. Unfortunately, the proposed gravimetric measurement is not described in detail and data is to be presented in a trumpet curve, which is often criticised by the scientific community [59]. In addition, the norm allows for a run-in period of up to one day that does not reflect the clinical application where

accurate dosing is required at all times [33, 59]. Hence, several improvements to the experimental assessment of dosing accuracy are proposed to evaluate insulin delivery systems: It is common to depict the average deviation of the dosed volume within a given observation time, or the accuracy of single doses [8, 10, 33, 60–62]. While optical flow detection that evaluates the volume in an accurate capillary is also used [62], most studies rely on gravimetric measurements [9, 33, 61]. It is necessary to minimize the influence of evaporation and condensation. Both, to cover the surface of the reservoir with oil [9, 33, 61] as well as an evaporation trap are adequate methods [63]. Furthermore, hydrostatic pressure can influence the measurement, which is why the inlet and outlet reservoir should be levelled [33]. Even if drift is prevented with all means, drift correction is indispensable for accurate data analysis.

In this work, we use a gravimetric measurement based on the introduced studies to evaluate the dosing precision of our piezoelectric micropump. The $5 \times 5 \times 0.6 \text{ mm}^3$ small pump is specifically designed for the requirements of drug delivery, including fluidic performance such as flow and pressure capability, as well as the ability to transport bubbles. The precision of package dosing is investigated with water and insulin solution. Therewith, we evaluate the reproducibility of bolus dosing and investigate additional challenges caused by the change of the transported medium. This preliminary study is designed to investigate a general feasibility and reveal necessary improvements. The accuracy of an integrated pump in a closed-loop controlled dosing unit is the subject of subsequent studies.

5.2. Materials and Methods

All investigations in this work are conducted with Fraunhofer EMFT's $5 \times 5 \times 0.6 \text{ mm}^3$ micropumps (Figure 5.1) [110]. Compared to former versions of the pump, the chamber height is increased to $20 \text{ }\mu\text{m}$ and the valve seat circumference as well as flap area are increased. Therewith, the fluidic resistance is reduced, which enables higher flow rates and the transport of higher viscous fluids.

A set of ten pumps is used to establish statistical significance. All wetted surfaces are composed of silicon and respective native oxides. The pump consists of two valve layers and the actuator diaphragm with the glued on piezoelectric disc actuator (Figure 5.1). Fluid transport bases on the indirect piezoelectric effect: an alternating high voltage signal causes the piezoelectric ceramic to expand and contract and thus induces an oscillating upwards and downwards movement of the diaphragm. The resulting expansion and contraction of the pump chamber leads, in combination with the passive flap valves, to a directed fluid flow.

The pumps are manufactured based on standard silicon processes (Figure 5.2). For the valve structure, two n doped silicon (100) wafers are covered with a silicon dioxide/silicon nitride hard mask that is subsequently structured by a lithography and dry etching process step (1). After the first KOH wet etching (2), one wafer is flipped and the wafer are bonded to form the valve unit. After oxidation and bonding the valve wafer stack is finalized with a grind and polishing step (3). A third silicon wafer (100) with a pre-etched micropump chamber is bonded on top of the valve wafer stack (4) and a grind and a spin etching process step finalize the actuator diaphragm of the micropump (5). The piezoelectric disc actuator is glued on the actuator diaphragm using a two-component epoxy adhesive (6). Table A.1 (Appendix A) gives an overview of the used material.

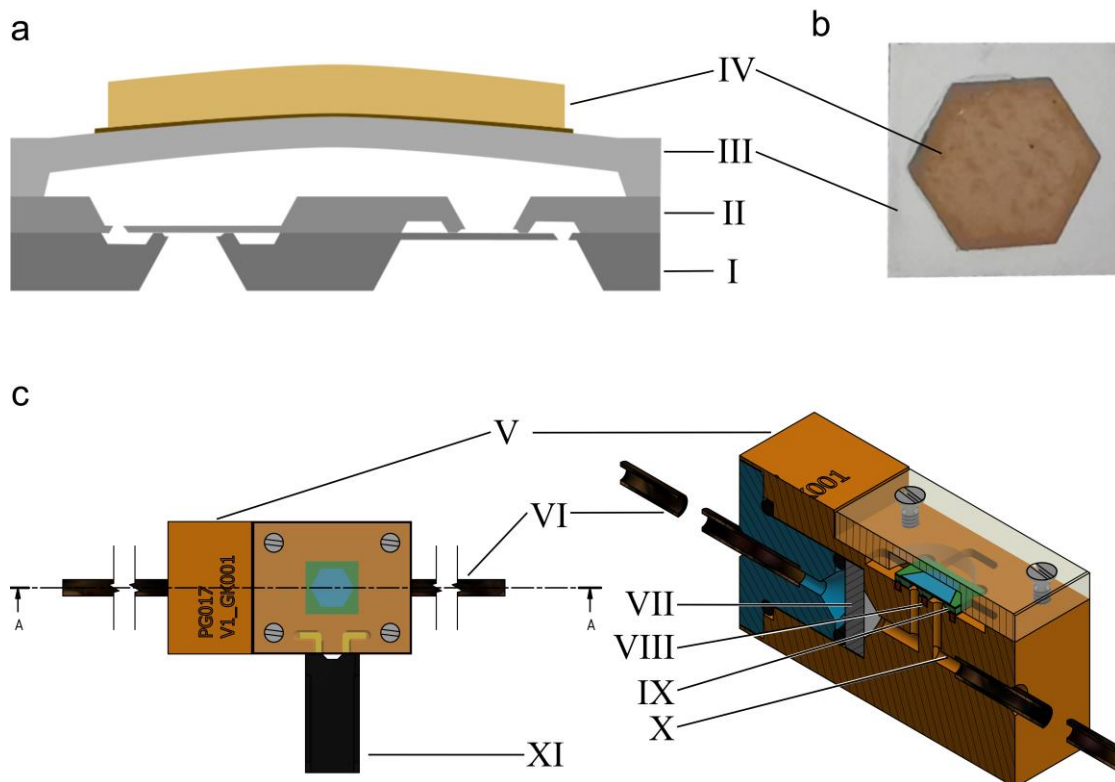


Figure 5.1 Schematic cross section (a) of a $5 \times 5 \times 0.6 \text{ mm}^3$ silicon micropump (b) with a 4.5 mm pump chamber diameter. The three grey layers represent the silicon pump body with the lower valve unit (I), the upper valve unit (II), and the actuator diaphragm (III) with the glued on piezoceramic (IV). For the fluidic characterization, the pumps (IX) are mounted into a test housing (c) that consists of a polyether ether ketone body (V) with drilled fluidic paths (X), inlet and outlet capillaries (VI), a stainless-steel filter (VII), and a soft sealing (VIII).

Bubble tolerance of the pumps is achieved with a specific adhesion process for the piezoelectric actuator [137]. During the curing phase, we apply an electric field that puts the ceramic in its contracted state. Once the glue is hardened, the voltage is disconnected and the ceramic expands and therewith bulges up the pump chamber. Due to this mounting technique, the **compression ratio** (ratio of displaced volume to dead volume in the chamber), is high, which is a condition for a high backpressure capability with compressive fluids as well as robust **bubble tolerance**. The **compression ratio** of the silicon micropump is estimated from its design: Due to exact silicon manufacturing techniques, the volume of the pump chamber can be calculated easily. The **stroke volume** is determined analytically and confirmed during the fluidic characterisation of the pumps. Based on the dead volume and the single **stroke volume**, we calculate the **compression ratio**.

The power consumption of the pump itself can be estimated considering the piezoelectric actuator as ideal capacitor. The used disc actuators have a capacitance of 2.45 nF. An actuation optimized for liquid transport (120 V_{pp} and 65 Hz) results in approximately 1.2 mW. To achieve maximal air flow, a higher voltage amplitude and a high frequency (150 V_{pp} and 1.6 kHz) are necessary, which requires approximately 440 mW, though an operation with a lower frequency is possible to limit the power consumption.

For the large-scale production of the pump, we intend both the entire manufacturing including piezo mounting, and the fluidic test of the pump to be realized on wafer-level. To this end we developed a wafer-level tester that allows to reduce costs significantly [156]. Assuming 200 wafer starts per week with an 8-inch process resulting in approximately 10 million pumps/year, we estimate 0.8 €/pump including front end, back

end and test costs. This price bases on a yield of 90 % and does not comprise any margin, or additional costs for medical devices and regulatory affairs.

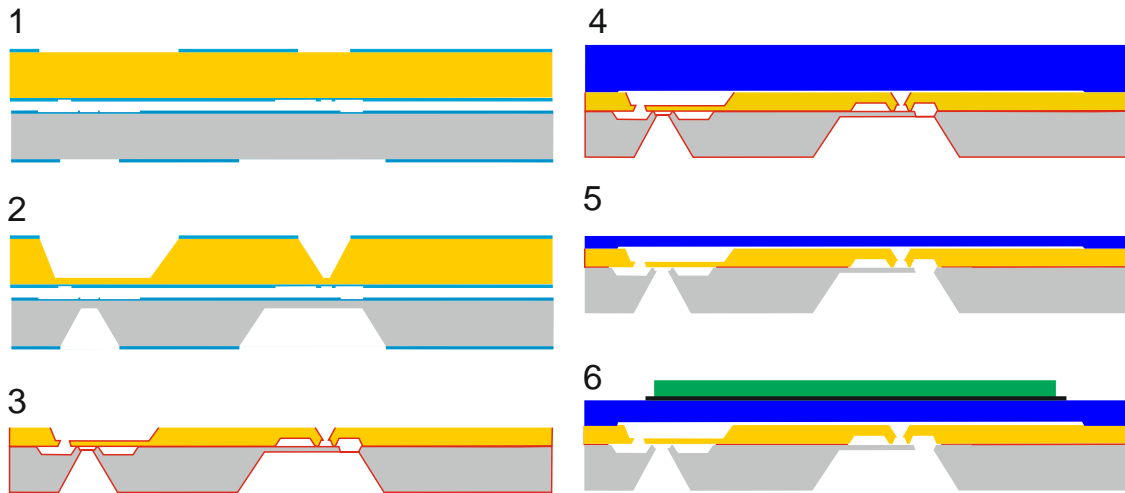


Figure 5.2 Schematic depiction of the process steps to manufacture the silicon micro diaphragm pump starting with the application of a structured hard mask (1) and subsequent KOH wet etching (2) of the two valve wafers. After oxidation, bonding, and a grind step (3) the actuator diaphragm with a pre-etched micropump chamber is bonded on top of the valve wafer stack (4). The diaphragm is finalized by a grind and spin etching process step (5) and the piezoelectric disc actuator is glued on the actuator diaphragm (6).

The ten pumps examined in this work are mounted into polyether ether ketone (PEEK) housings with glued in PEEK capillaries for fluidic connection (Figure 5.1). The pump chip is clamped onto a fluorine rubber sealing. At its inlet, the housing holds a stainless-steel filter unit with a pore size of 5 μm . The silicon pump chips remain in the housing for all conducted experiments.

5.2.1. Basic Characterization

The basic characterization of the micropumps includes optical **stroke** measurement, air flow characterization, and water flow characterization.

The **optical stroke measurement** evaluates the deflection of the actuator diaphragm due to a quasi-static voltage signal. The actuator position is detected with a white light profilometer (MicroProf 100 – CWL, FRT GmbH) including an optical sensor with a range of 300 μm and resolution of 100 nm. The quasi-static voltage signal in a range from -50 to 120 V is applied with a piezo amplifier (SVR 500–3, piezosystem jena GmbH). This voltage expands beyond the normal actuation voltage to enable the detection of mechanical contact between the actuator diaphragm and the chamber bottom shortly outside of the normal actuation range.

Part of the **characterization with air** are the maximal achievable flow rate as well as pressure capability of the actuated micropump. We detect the air mass flow with an EL-Flow prestige ($\pm 0.5\%$ accuracy, Bronkhorst) at the inlet of the fluid path. The back-pressure is measured with the pressure sensor 26PCCFA6D ($\pm 1\text{kPa}$ accuracy, Honeywell) at the outlet of the closed fluid path. The alternating voltage signal of -30 to 90 V is applied with an Agilent 33120A frequency generator and amplified with a piezo amplifier. To determine leakage rates, a controlled pressure (CPC3000, WIKA Mensor) is applied to the turned off pump's outlet and the resulting flow is detected (EL-Flow mass flow meter) at the pump's inlet.

The flow **characterization with water** includes the achieved mass flow at different backpressures from 0.2 to 40 kPa. It is performed with a purpose-built fluidic setup: The reservoir, sensors and pump are connected with steel capillaries. The inner diameter of the capillaries is sufficiently large and therefore has a neglectable influence on the detected flow rate. A worst-case estimation based on the Hagen-Poiseuille equation results in a pressure loss of only 0.04 %. Pressure is applied as a nitrogen head-pressure over the outlet reservoir with a pressure generator (Mensor CPC3000) and verified in the fluid path 30 cm away from the pump with a Transducer WU-15 (WIKA). The water mass flow is determined with a Liqui-Flow from Bronkhorst ($\pm 1\%$ accuracy). Amplification of the 15 Hz rectangular waveform with sinusoidal flanks (approximately 130 Hz) is achieved with an SVR 500/3 amplifier from Piezomechanik GmbH.

5.2.2. Bolus Characterization

The dosing **precision** of our silicon micropumps is determined with deionized water as well as insulin solution. A microgravimetric measuring method based on IEC 60601-2-24 and the setup proposed by Kamecke et al. [33] is used to determine the water bolus **precision**. A schematic of the experimental installation is shown in Figure 5.3.

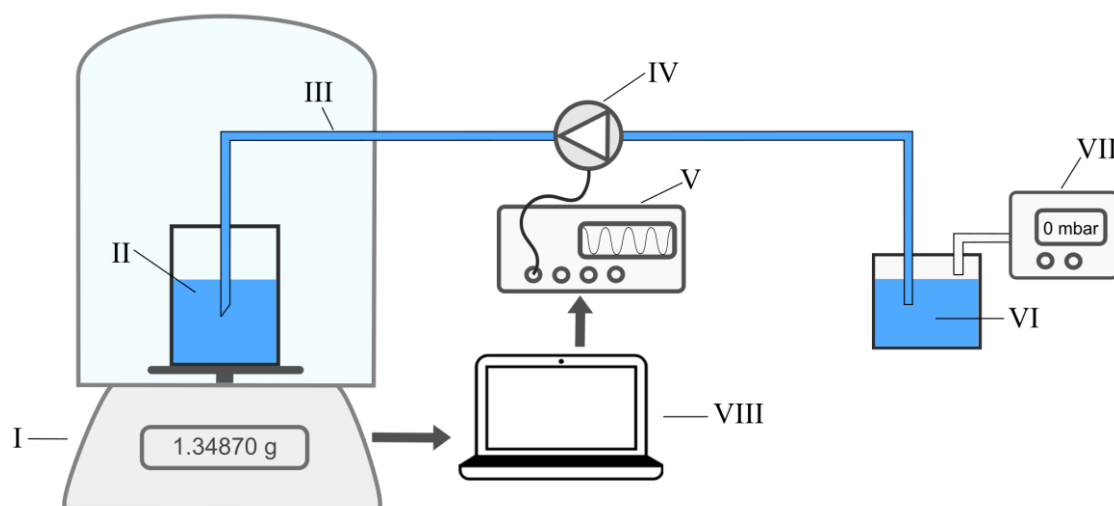


Figure 5.3 Experimental setup for the gravimetric measurement of package dosing. The pump (IV) transports liquid through PEEK capillaries (III) from the inlet reservoir (VI) toward the outlet reservoir (II) that is placed on a balance (I). The pump is actuated by a signal generator and amplifier (V) and controlled with a laptop (VIII) that collects the recorded weight data. For priming, the inlet is connected with a pressure controller (VII).

Experimental characterization of the package dosing with water is conducted with nine pumps. Purified DI water is pumped from an input reservoir to an output reservoir which is placed on the Sartorius 225S scale (0.025 mg reproducibility). The pump is installed outside the scale's measurement chamber in a casing. PEEK tubes (IDEX Health&Science 1538) are connected to the inlet and outlet tubes of the pump's casing and inserted into the water in the inlet and outlet reservoir. The used capillaries have an inner diameter of 1 mm. The distance to the inlet is approximately 20 cm and the capillary length to the outlet approximately 40 cm. Both input and output reservoir are filled with water such that the surfaces are levelled to avoid effects of hydrostatic pressure. A 2 mm thick layer of oil (thermo scientific E33 (12017/00043)) is dispensed onto the water in the output reservoir to prevent evaporation.

The used silicon pumps are self-priming. However, to rapidly prime the dead volume of the setup, the system is passively primed. After the pump is connected we apply a positive pressure of 200 mbar to the inlet reservoir (Mensor CPC4000 pressure controller) until no further air emerges from the outlet capillary. This priming procedure enables accurate measurements, since remaining bubbles in the fluid path and especially fluidic connectors are flushed out of the system. A Keysight 33500B waveform generator and a Piezomechanik SVR 500-1 amplifier are used to generate a rectangular waveform with sinusoidal flanks (100 Hz) with a voltage of -30/+90 V and a frequency to 65 Hz to operate the micropump.

The measurements are conducted for three bolus sizes of approximately 0.5025 mg, 5.025 mg, and 50.25 mg. For U100 insulin solution, these packages sizes correspond to 0.05 international units (U), 0.5 U, and 5 U of insulin. In this experiment, the pumps are not closed-loop controlled and the number of strokes needed for a given bolus size is calculated with the average [stroke volume](#) of this pump type. Variation of the pumps due to manufacturing tolerances can cause the average bolus volume to deviate. We therefore do not aim to evaluate [dosing accuracy](#), but rather the repeatability of package dosing, meaning the dosing [precision](#). A calibration on each individual pump's [stroke volume](#) or a closed-loop control can later be implemented to achieve sufficient [accuracy](#). For each bolus size and individual pump, we dose forty volume packages by repeating a sequence of four dosages (active pump) and one subsequent reference measurement without dosing (inactive pump) for ten times. During the reference measurement, the pump is not actuated, no fluid is transported, and the resulting dosed volume after drift correction should be zero. Hence, the reference measurement without pump actuation allows us to detect errors in the experimental setup. Based on the water characteristics for a pump frequency of 65 Hz, one [actuator stroke](#) delivers in average 62 μg of water. Thus, for the different bolus sizes, the required number of single strokes is computed to 8, 81, and 815 with a corresponding active time per dosage of 0.12 s, 1.25 s, and 12.54 s. The data is drift compensated based on approximately 33 s drift measurement conducted before each dosed bolus.

Insulin dosage is evaluated with U100 of NovoRapid® (trivial name: insulin aspart) from the company Novo Nordisk, where one millilitre of the solution contains 100 international units (3.5 mg) of insulin. The experimental setup and procedure remain the same as was used for the characterization of the dosing [precision](#) with water. The only adaptation is the inlet reservoir, where we used a smaller jar to account for the limited sample volume. Due to a limitation of the insulin volume, the dosage of large packages was only possible for nine out of ten pumps.

5.3. Results and Discussion

Drug delivery applications require very specific characteristics, which makes a detailed experimental analysis indispensable. The results presented in this work include the evaluation of ten individual micropumps of the same batch regarding the silicon micromachining (frontend), piezo mounting (backend) and assembly.

5.3.1. Standard Characterization

The characteristics and fluidic performance of the ten micropumps used for the evaluation of the dosing [precision](#) are summarized in Table 5.1.

The first indication for the functionality of a diaphragm pump is the achievable **actuator stroke**, since it directly determines the volume displaced within one pump cycle and, hence, achievable flow rates. Furthermore, the optical **actuator stroke** measurement allows to detect a touchdown, i.e., the mechanical blocking of further movement when the diaphragm reaches the chamber bottom. It causes a characteristic kink in the displacement curve and limits the **stroke volume**. None of the tested pumps shows a touchdown. The average stroke (Δz) of all ten microactuators achieved with -20 to 100 V quasi-static actuation is $\Delta z = 15.0 \pm 1.1 \mu\text{m}$ leading to an approximate **stroke volume** ($\Delta V = \pi \cdot R^2 / 3 \cdot \Delta z$) of $\Delta V = 79 \text{ nL}$. This volume corresponds well to the characterization of similar pumps by Leistner et al. [110].

Table 5.1 Average mechanical and fluidic characteristics of the ten evaluated piezoelectric silicon micro-pumps at a given actuation signal (amplitude; frequency).

Fluid	Characteristics	Actuation	Mean Value
-	Stroke Height	-20/+100 V; quasi-static	$15.0 \pm 1.1 \mu\text{m}$
Air	Flow Rate	-50/100 V; 1.6 kHz	$6.5 \pm 0.5 \text{ mL/min}$
Air	Backpressure	-30/90 V; 65 Hz	$0.26 \pm 0.07 \text{ mL/min}$
Air	Backpressure	-30/90 V; 65 Hz	$14.3 \pm 0.3 \text{ kPa}^1$
DI Water	Flow Rate at 0 kPa	-30/90 V; 15 Hz	$0.074 \pm 0.006 \text{ mL/min}$
DI Water	Blockingpressure	-30/90 V; 15 Hz	$51.2 \pm 0.9 \text{ kPa}^1$

¹ The air backpressure and water **blockingpressure** are calculated from a linear fit of the backpressure measurement as depicted in Figure 5.4

All pumps are characterized regarding their air transport, e.g., backpressure capability as well as frequency dependent air flow rate. The air flow achieved with an actuation frequency of 65 Hz and a peak to peak voltage of 120 V, which is the signal used for later bolus dosing, is $0.26 \pm 0.07 \text{ mL/min}$. With an actuation optimized for air transport (-50/100 V; 1.6 kHz), the pumps achieve higher flow rates of $6.5 \pm 0.5 \text{ mL/min}$.

The pressure capability when transporting air depends strongly on the **compression ratio**, which is approximately 0.15 for the $5 \times 5 \text{ mm}^2$ silicon pump and is sufficient for gas transport [32, 135]. Sufficient backpressure capability with air is a condition for **bubble tolerance** and therefore evaluated with the same actuation signal used for fluid transport, even though this actuation is not optimized for air transport. From a linear fit of the pressure dependent mean air flow of all samples we calculate a backpressure capability of $14.3 \pm 0.3 \text{ kPa}$ (Figure 5.4).

The water flow rate with and without applied backpressure is analysed for all pumps (Figure 5.4). Without additional backpressure, the mean water flow rate of the ten pumps is $Q_{\text{water},0\text{kPa}} = 74 \pm 6 \mu\text{L/min}$. With U100 insulin, this allows to deliver a bolus of 10 U in approximately 90 s and puts our micropump in the same range of delivery speed as currently available delivery systems [60].

A linear regression of the water flow rate at increasing backpressures allows to determine the **blockingpressure**, where the flow reaches zero. At 40 kPa the average achieved flow rate is $Q_{\text{water},40\text{kPa}} = 16 \pm 7 \mu\text{L/min}$ and the linear regression shows an extrapolated **blockingpressure** of $p_{\text{block}} = 51.2 \pm 0.9 \text{ kPa}$. The results are in good agreement with previous research [110]. The high achievable pressure is necessary to overcome counterforces in a delivery system. While the pressure of the tissue as well as the fluidic

backpressure of the channels are low for reasonable flow rates, clogging of the injection site might cause a high backpressure that the pump needs to overcome.

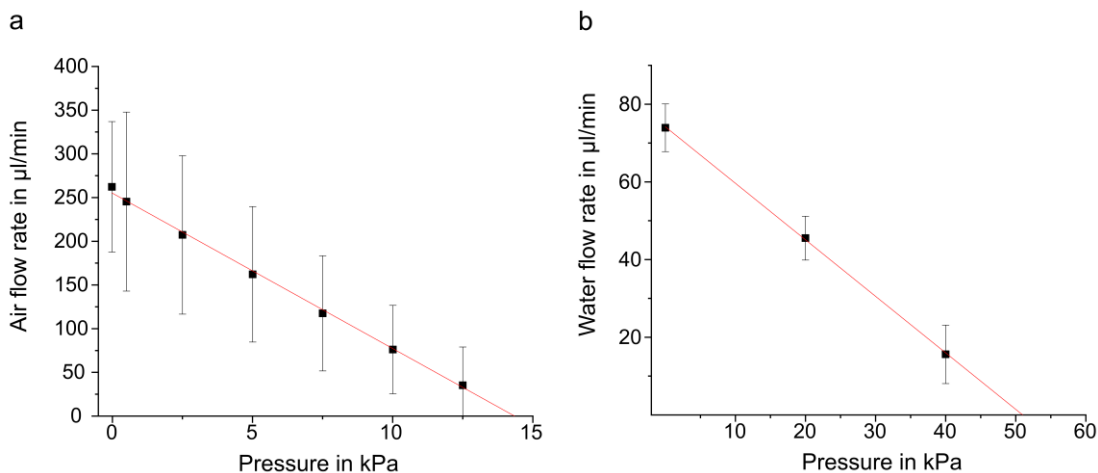


Figure 5.4 Flow characterization of the ten micropump samples. (a) Average air flow rate of the ten pumps at varying backpressure. The pumps are actuated with $-30/90$ V and 65 Hz. The extrapolated achievable backpressure is 14.3 kPa. The error bars depict the standard deviation. (b) Average water flow rate of the ten pumps at varying backpressure. The pumps are actuated with $-30/90$ V and 15 Hz rectangular waveform with sinusoidal flanks (approximately 130 Hz). The extrapolated blocking pressure is 51 kPa. The error bars depict the standard deviation.

5.3.2. Bolus Precision Investigation

The repeatable precise dosing of small volume packages is indispensable for bolus drug delivery. In this work, we aim to evaluate the repeatability of package dosing of our 5×5 mm² micropump without the influence of a control unit. Thus, we test in an experimental setup that is not closed-loop controlled. We dose a package size that is defined by the number of single strokes performed and aims at an approximate quantity. However, small variations between the pumps due to manufacturing tolerances cause the average package size to differ slightly for the pumps. This deviation can later be prevented based on individual calibration and closed-loop control. However, a precondition for a well working controlled dosing unit is a high reproducibility of dosed individual volume packages. We therefore present a detailed investigation of our pump's dosing precision.

In preliminary experiments we evaluate the package dosing with water. Figure 5.5 shows the precision of the tested pumps when dosing small, medium and large packages with approximately 0.5 mg, 5 mg, and 50 mg, respectively. These packages are the equivalent mass of insulin solution needed to deliver 0.05 U, 0.5 U and 5 U of insulin.

It is clearly visible that the dosage of extremely small packages is more challenging. The sample to sample variation between the forty individually dosed 0.5 mg packages is higher than for larger packages. However, the standard deviation also varies for the pumps and ranges from 2.5 % to 14.9 %. Five out of nine pumps show high dosing precision even for small packages with a standard deviation of less than 3 % and two pumps, μP_03 and μP_06 , show approximately 5 % deviation, which is generally considered acceptable by pump manufacturers [33]. Only two pumps μP_02 and μP_05 dose the forty volume packages with a standard deviation of over 10 %.

For larger packages, such as 5 mg and 50 mg the standard deviation tends to be smaller. For 5 mg packages it ranges from 0.2 % to 1.8 % with only one outlier, μP_06 , with a standard deviation of 4.8%. This higher deviation is likely caused by air in the fluid

path, since four consecutives out of forty packages deviate. This is likely the case if a bubble passes the pump and needs some strokes to be ejected before efficient fluid transport continues. The air can be entrapped in connectors, capillaries, or the edges of the test housing. Therefore, a geometric adaptation of the fluid path, e.g., reducing sharp edges, can facilitate priming and minimize the occurrence of bubbles that reduce the dosing **precision**. Such design recommendations also hold for fluid reservoirs and paths in the drug delivery application, since bubbles can also occur during drug dosing. Since it is impossible to reliably prevent bubbles at all times, the higher deviation detected for one sample is a relevant drawback. An increased **independence of bubbles** is therefore desirable for future improvements of the introduced pump.

Repeatability of water package dosing

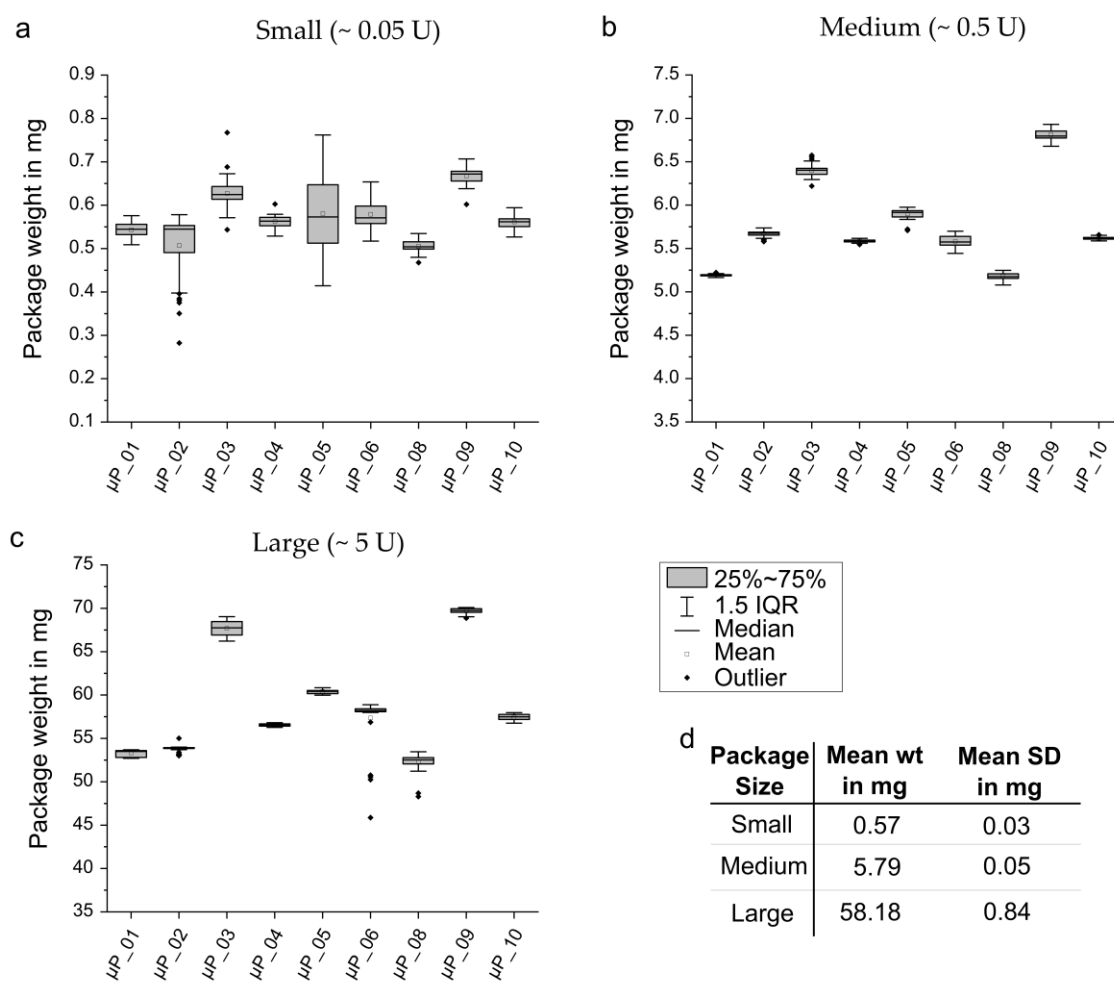


Figure 5.5 Repeatability of package dosing for each individual micropump (μP_{01} to μP_{10}) with water for small (a), medium (b) and large (c) packages of approximately 0.5 mg, 5 mg and 50 mg, respectively. The overview (d) of the mean dosed weight and the mean standard deviation of all tested pumps shows an overall high dosing **precision**.

Package dosing with insulin shows generally slightly higher standard deviation for all package sizes (Figure 5.6). Similar to water dosing, the small package size of 0.05 U is challenging, since it only contains eight pump strokes. Nevertheless, four out of ten pumps (μP_{3} , μP_{5} , μP_{6} , μP_{9}) show a standard deviation under 3 % and only μP_{7} and μP_{10} dose 0.5 mg with a standard deviation of over 10%.

For 0.5 U and 5 U packages, the standard deviation varies between 0.3 and 6.5%, however only two pumps, μP_6 and μP_{10} , show standard deviations over 5%. The slight decrease in **precision** for the insulin dosing compared to water dosing is probably due to poorer priming of the fluid path, e.g., fluidic connectors and filter chamber of the test housing. The sample volume was limited and less fluid could passively be pushed through the setup to flush all air from the system. Furthermore, a high surface tension causes the liquid-air interface to be more stable for the insulin solution compared to DI water. Thus, the transport of bubbles through the valves, the pump chamber or fluidic connectors requires more pressure and has an increased impact on the fluid transport. Hence, an optimization of the pump towards higher **bubble tolerance** and **bubble independent** dosing is even of higher relevance when changing the dosed medium from DI water to insulin solution.

Repeatability of insulin package dosing

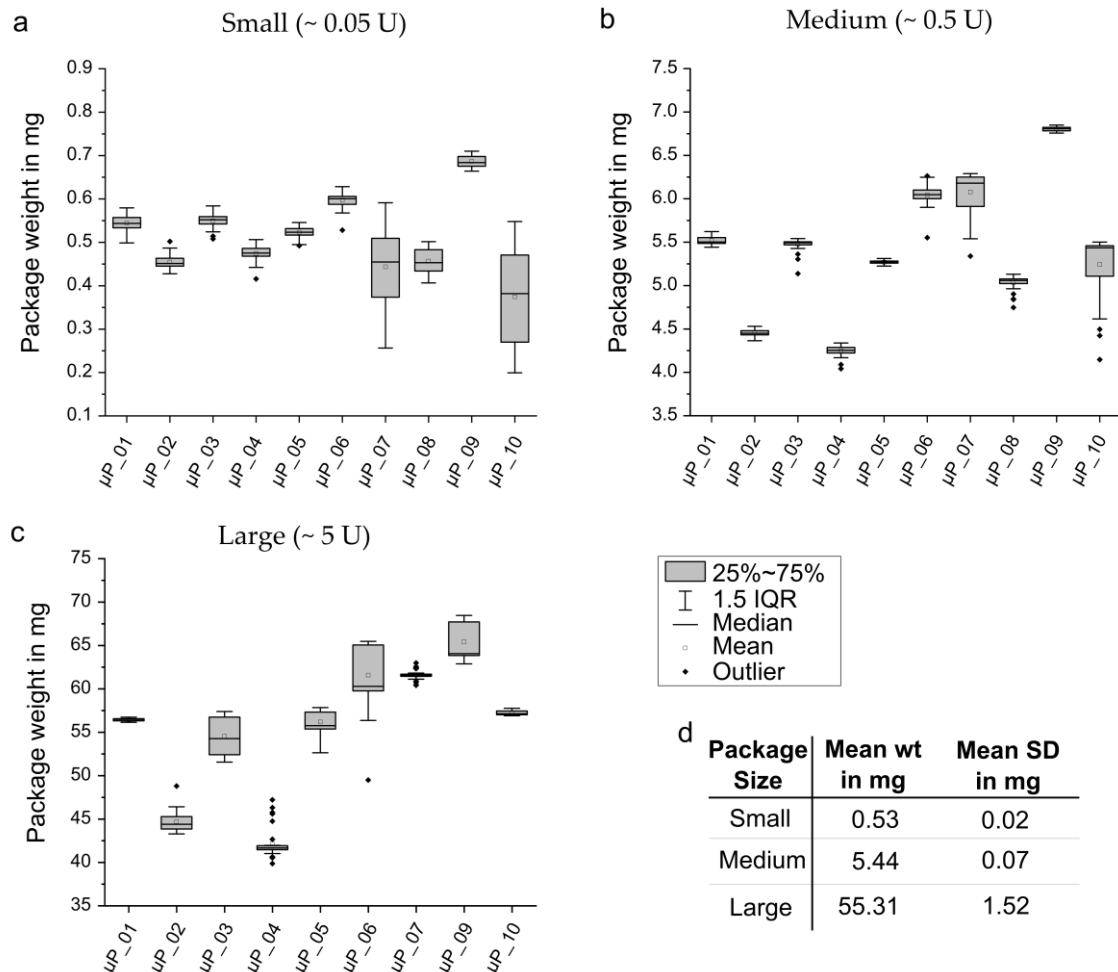


Figure 5.6 Repeatability of package dosing for each individual micropump (μP_{01} to μP_{10}) with NovoRapid U100 insulin injection solution for small (**a**), medium (**b**) and large (**c**) packages of approximately 0.05 U (~ 0.5 mg), 0.5 U (~ 5 mg) and 5 U (~ 50 mg), respectively. The mean dosed weight and the mean standard deviation (**d**) are similar to experiments conducted with water.

Overall, the experiments show a high dosing **precision** of the 5×5 mm² silicon pump. For 0.5 U and 5 U, only one pump shows a higher standard deviation than the generally required 5%. This high achieved **precision** stands out in comparison to insulin delivery units on the market. For example, Laubner et al. [8] analyse two commercially

available units and show that only 20% of 0.5 U bolus are delivered within $\pm 5\%$ accuracy [8]. The high **precision** possible with this piezoelectric micro diaphragm pump for 0.5 U (5 mg packages) can therefore enable a dosing unit with higher **precision** than current insulin delivery systems available on the market.

The smallest package size tested in this work is not commonly tested for insulin dosing systems and most studies start their experiments with 0.5 U or 1 U [8, 60]. Only Zisser et al. [62] consider small bolus sizes of 0.05 U, however, for accurate measurements, they calculate the **accuracy** from series of ten to twenty doses. The detection of outliers is therefore not possible.

The analysis of 0.05 U packages shows that most of the tested pumps are able to dose these small units precisely with seven out of ten pumps showing a standard deviation of 1.9 to 3.5%. Only two pumps dose packages with a standard deviation of more than 10%. For those pumps, a time dependent decrease in package size is visible. However, this decrease in performance is not permanent, since the pump regains the expected package size for the consecutive measurement of 0.5 and 5 U packages. The decrease can be caused by insufficient priming: enclosed air in the outlet capillary is transported to the outlet reservoir on the balance and impairs the correct detection of transported volume. Additionally, the introduced silicon pumps are **bubble-tolerant** due to their **compression ratio**. However, dosing is influenced by air bubbles passing through the pump chamber. That means that the pump is able to transport the liquid-air interfaces, but the dosed package volume decreases until the chamber is filled with liquid. To achieve high **accuracy** even with bubbles in the system therefore requires active control. Closed-loop control systems can detect undelivered strokes and trigger compensating strokes.

The high dosing **precision** that we achieve with the presented pump makes a combination with higher concentrated insulin imaginable. We were able to show a similar dosing **precision** for 0.05 U packages that pumps on the market have for 0.5 U. Thus, it is imaginable to deliver U 500 or U 1000 insulin. The comparatively high pump chamber of the micropump enables transport of more viscous solutions due to higher insulin concentration, which will be evaluated in subsequent studies. The combination of high concentrated insulin solution with this small **MEMS** pump allows the development of an extremely compact and energy-efficient dosing unit with only a small insulin reservoir.

5.4. Conclusions

In the presented preliminary experiments, the introduced piezoelectric micro diaphragm pump proves well adapted for drug delivery applications. Its relatively large **compression ratio** (compared to other state of the art **MEMS** pumps) enables self-priming as well as the transport of bubbles, though the dosing **precision** is not **independent of bubbles**. The fluidic performance meets the requirements of **microfluidic** drug delivery. The water flow rate of $74 \pm 6 \mu\text{L}/\text{min}$ allows the delivery of 10 U of insulin (0.1 mL drug solution) within 45 s, which is in the same range as macroscopic automated dosing units on the market [60]. The **blocking pressure** of 51 kPa of the pumps is high enough to overcome the physiological backpressure as well as additional flow restrictions due to clogging of the injection site.

The pumps show a high repeatability of package dosing. However, the **precision** decreases slightly with insulin compared to the transport of DI water. The higher surface tension of insulin solution increases the pressure necessary to transport air bubbles

through the chamber. The decrease of **precision** shows that a pump that doses more **independently of bubbles** is desirable for the transport of insulin solution. Such a fluidic actuator can be achieved with design modifications towards a further decrease of the valve's capillary pressure and a higher **compression ratio**. The increased **compression ratio** requires a smaller pump chamber to decrease the dead volume. In future design adaptations, the compatibility of such a pump with higher concentrated drugs and therefore liquids with a higher viscosity, needs to be evaluated carefully. In subsequent development steps, the integration of our pump with a miniaturized, capacitive volume control will enable closed-loop control of the dosing unit, which allows for higher **dosing accuracy** even with occurring disturbances. Nevertheless, the presented experimental results already show that even small packages of approximately 0.5 mg are dosed as precise as commercial pumps dose larger packages of 5 mg. Hence, the 5×5 mm² silicon micropump is suitable for a precise dosing of a U100 insulin. Furthermore, this high **precision** enables a combination with higher concentrated drugs, which limits the needed reservoir size as well as reduces the volume to be dosed. This enables a lower energy consumption and therefore smaller batteries. Hence, the overall size of the delivery device can be significantly reduced. The development of small and comfortable patch pumps or even implantable systems is therefore attainable.

Data Availability Statement

The **actuator stroke** and fluidic test data that support the findings of this study are available in Fordatis – Research Data Repository of Fraunhofer-Gesellschaft with the identifier <http://dx.doi.org/10.24406/fordatis/143>

Acknowledgments:

Many thanks to Dr. Werner Regittnig for his support during the study as well as the provision of the NovoRapid samples. We thank Dr. Axel Wille for his efforts during the funding acquisition.

This research is part of the Moore4Medical project, which has received funding within the Electronic Components and Systems for European Leadership Joint Undertaking (ECSEL JU) in collaboration with the European Union's H2020 Framework Program (H2020/2014-2020) and National Authorities, under grant agreement H2020-ECSEL-2019-IA-876190 www.moore4medical.eu

6. Piezoelectric Titanium-Based Microfluidic Pump and Valves for Implantable Medical Applications

Bußmann, Agnes^{a,b,*} and Durasiewicz, Claudia^{a,c,*}; Dr. Kibler, Sebastian^a; Wald, Christian^a

^aFraunhofer EMFT Research Institution for Microsystems and Solid State Technologies, Hansastrasse 27d, 80686 Munich, Germany

^bKIT, MAB - Biomolecular Separation Engineering, Fritz-Haber-Weg 2, 76131 Karlsruhe, Germany

^cTUM, TEP - Chair of Physics of Electrotechnology, Theresienstrasse 90, 80333 Munich, Germany

* A. Bußmann and C. Durasiewicz contributed equally; Correspondence: agnes.bussmann@emft.fraunhofer.de; Tel.: +49 89 54759-416 and claudia.patricia.durasiewicz@emft.fraunhofer.de, Tel.: +49 89 54759-497

Abstract

Medical devices often require precise movement of fluids. Automated implants with no need for manual handling improve patient care significantly. However, existing **microfluidic** devices do not fulfil the necessary specifications of size, safety, hermetic sealing, and artefact free medical imaging, as well as energy-efficiency combined with adapted fluidic properties. In this work we designed, manufactured, and experimentally evaluated three piezoelectric **microfluidic** devices for implant automation: a diaphragm pump, a normally closed valve, and a normally open valve. All devices are made of titanium, minimizing the risk of artefacts in medical imaging. They have similar form factors and use the same actuation method. For the later, a specific mounting process of the piezo actuator enables outstanding fluidic performance during experimental evaluations. The titanium micropumps show a maximal flow of 14.0 ± 2.2 mL/min and pressure build-up of 75 kPa. The normally closed valve's leakage rates are extremely low with less than 1 μ L/min. Detailed investigations further include the **actuator stroke**, a lifetime study for normally open valves, and a numerical and experimental evaluation of the normally closed valve's spring foil. The introduced titanium technology platform is ideally suited for system integration accounted for by the use of the same actuation principle and the similar form factor and a simple design. The development of small, smart, and energy-efficient implants for improved treatment is possible based on the introduced platform.

6.1. Introduction

The transport of liquids is a ubiquitous task in implantable medical applications. Examples are, among others, **microfluidic** systems to move body fluids, dose medication precisely, or hydraulic implants [1–3]. Prosthetic hands [160], extra-aortic balloon (**EAB**) pumps [161], as well as artificial sphincters base on hydraulic actuation. These implants can be realized using flexible, fluid-filled actuators, such as artificial fingers [160], or a cuff placed around a vessel or muscular tube, to facilitate a biological function. The actuators are operated using intra- or extracorporeal pumps and/or valves. Cuffs in **EAB** devices are dynamically pressurized by extracorporeal pumps to levels of 250 to 300 mmHg (333 to 400 mbar), providing cardiac support by increased blood flow for patients suffering from heart failure [161]. However, current systems are too large for implantation. Sphincter implants [162, 163], restore opening and closing functionalities in the rectal or urinary path. Current systems on the market are manual devices which the patient operates by hand. Furthermore, the physician sets the pressure to a fixed level that

is not adapted to the patient's activity, which can cause tissue damage. Even if specifications vary largely with the use case, a small, light, automated, and user-friendly device is desired for future developments of implants. Ever since the first studies on piezoelectric diaphragm pumps [164], many different kinds of micropumps have been developed to enable reliable, safe, and economic medical products [27, 67].

Micropumps in research achieve water flow rates of up to 9.1 mL/min or water pressures of up to 40 kPa, though fail to exhibit high flow and pressure simultaneously [21]. Additionally, the occurrence of bubbles due to degassing or cavitation [42] impacts the fluidic performance. For safety reasons, medical applications require **bubble tolerance**, even under backpressure. We therefore seek to develop a high performance micropump with **bubble tolerance** capabilities. This is ensured by an adapted design including a large **compression ratio** (ratio of displaced volume to dead volume in the pump chamber [32]). A high ratio can be achieved by a specific mounting procedure for the piezo ceramic: a voltage, applied during glue hardening, causes the actuator diaphragm to permanently bulge out, creating the pump chamber [137]. The achieved **compression ratio** leads to a high-pressure build-up with air and enables **bubble tolerance**.

Microvalves are an important additional component for implantable applications, for instance as a safety measure. Based on different actuation methods, e.g., piezoelectric, shape memory alloy, electrostatic, or magnetic, various types of microvalves have been developed [165, 166]. The two basic groups of valves are normally closed (**NC**) and normally open (**NO**) valves. **NC** valves block the fluidic path, only opening when actuated. By contrast, **NO** valves allow flow while not actuated and are actively closed. Both types offer adapted properties for different applications. Examples of piezoelectric valves are presented in research [167–169]. Water leakage rates as low as 0.013 $\mu\text{L}/\text{min}$ [170] and water free flow of up to 8.75 mL/min [171] are achieved. In contrast to existing microvalves, we want to combine low leakage of a soft sealing on a solid valve seat with a large free flow operating range. Valves are designed to benefit from the high force and fast response time abilities of piezoelectric actuation, which allows their usage in challenging flow conditions such as high differential pressure.

Fluidic conditions are not the only demanding aspect in **microfluidic** systems. The electrical system needs to be hermetically sealed from the fluid path to prevent damage. Use within the human body requires additional sealing, and every material in contact with tissue has to be biocompatible. Metal pumps, such as stainless steel pumps [172, 173], offer welding as possible hermetic sealing. However, stainless steel has a large disadvantage when it comes to long-term medical implants: this material causes artefacts in magnetic resonance imaging (**MRI**) scanning, as evaluations on different implants have shown [174–176]. A suitable material to solve this issue is titanium which offers numerous advantages for use in medical applications [177] in addition to its **MRI** compatibility: When exposed to air, its surface forms biocompatible and antibacterial titanium dioxide [178, 179]. Titanium components can be hermetically sealed from the human body, e.g., by welding titanium covers to them [180]. Since no different materials are bonded together, the risk of galvanic corrosion is minimized [181]. So far there are examples of micropumps and valves partly manufactured of titanium [37, 182–184].

In our work, we develop a titanium platform of micro fluidic devices for medical implants. It includes new designs of a **NO** valve and a **NC** valve, making use of the beneficial properties of titanium. In addition, we adapt the proven design of known steel micropumps [172] to titanium. The small and light devices are designed to allow easy

integration into efficient products. These automated solutions aim to increase patients' comfort.

6.2. Micropump and valve design

Hydraulic actuators usually rely on a combination of pumps and valves. For **microfluidic** implants, many combinations are imaginable and design strongly depends on the exact use case. Figure 6.1 depicts a generalized fluidic setup for hydraulic actuation. The pump actively transports fluid from P1 to P2 and builds up a pressure, while an active valve maintains or releases the pressure as needed. P1 and P2 are volumes that can either be the hydraulically actuated part or a fluid reservoir. In case of a malfunction such as the loss of power, the implant has to remain in a safe state, where any critical pressure is released to prevent risk of injury. Therefore, depending on the exact design, e.g., a pressurized or non-pressurized reservoir, the use of a **NO** or **NC** valve is required. A **NO** valve ensures pressure release in non-actuated state, for a hydraulically actuated volume at P2 where a permanently applied pressure can cause injury. Whereas if a constant pressure is unproblematic regarding safety aspects, a **NC** valve can be used to enable a more energy-efficient use.

In general, piezoelectric actuation allows for energy-efficient driving (v.i., “Experimental Results and Discussion”) [27]. Even a **NO** valve, operated to be closed most of the time, does not require excessive energy, since the piezoelectric ceramic acts as a capacitance and leakage currents are low. Hence, the applied voltage remains stable over long periods. Therefore, this titanium technology platform enables the development of space and energy-efficient products.

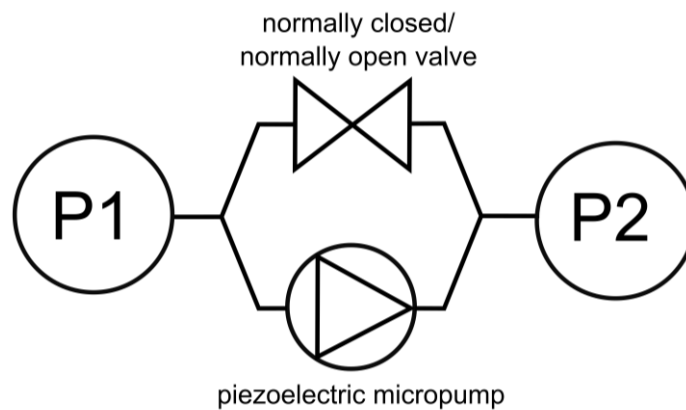


Figure 6.1 Fluidic setup of a hydraulic actuation unit. The pump transports fluid between a reservoir and the actuated part, which are depicted as P1 and P2 here. The valve can maintain and release the built-up pressure as required. Different working principles achieved with alternative circuit arrangements are possible. The decision for a normally closed or a normally open valve depends, among others, on safety aspects, since a pressure release of the actuated part in the case of power loss is often necessary.

For easy combination, we design the three devices to use the same actuation principle, be manufactured in similar processes, and be geometrically alike. Titanium and **FKM**, the wetted materials of the **microfluidic** devices developed, were sourced in medical grade. Those materials exhibit beneficial traits and are already used in medical devices. However, a detailed biocompatibility testing is necessary and not yet part of this study, which focuses on the technical development. Since the hydraulic fluid system is a closed-circuit setup, contact to the body does not occur during orderly function. A critical

element is the piezoelectric actuator. The lead content as well as the electric contact makes hermetic sealing and electric isolation indispensable. The devices are designed to allow such sealing, e.g., by laser welding.

6.2.1. Titanium pump

The design of the titanium micro diaphragm pump (Figure 6.2 a) is similar to our steel pumps [172]. The pump includes a titanium body in combination with a glued on piezoelectric disc actuator (PIC 151, $d = 16 \text{ nm/C}$; $200 \mu\text{m}$) (Figure 6.2 c). The body consists of a base plate and three titanium foils: two valve foils and one actuator foil. All metal parts are laser welded to form the impermeable pump chamber. The current device has a diameter of 20 mm and a height of 1.5 mm.

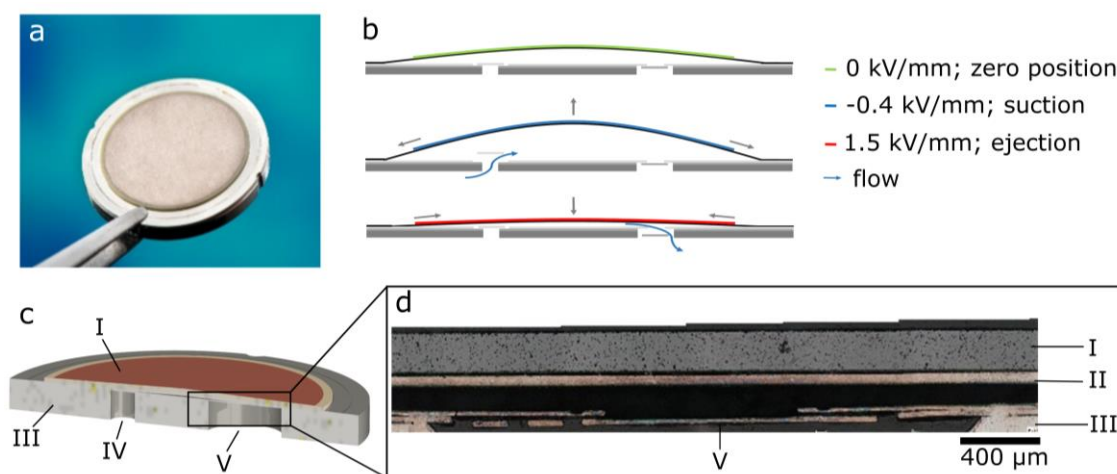


Figure 6.2 (a) Picture of a piezoelectric titanium micropump; (b) working principle. Due to the indirect piezoelectric effect, an alternating high voltage causes an oscillating movement of diaphragm. In combination with two passive spring valves, this leads to an effective flow; (c) model of the pump showing the piezo actuator (I), the pump body (III), the inlet (IV) and outlet (V). d section of the outlet valve (V) welded to the pump body (III) with piezo ceramic (I) glued to the actuator diaphragm (II).

Pumping bases on the indirect piezoelectric effect, causing a mechanical deformation when the piezoelectric ceramic is exposed to electrical actuation. Hence, applying an alternating high voltage signal results in an oscillating vertical diaphragm deflection and creates a fluid movement through two passive spring valves (Figure 6.2 b).

The **pretension technique** [137] for piezo mounting promotes a high pumping performance. The ceramic is exposed to a defined electric field while curing the glue. Therefore, bonding takes place in a contracted state of the piezo. After curing, the voltage is removed and the expansion of the ceramic bulges out the pump chamber. This specific mounting establishes a large **compression ratio** (displaced volume / dead volume) and therefore leads to self-priming and **bubble-tolerant** pumps up to at least 30 kPa.

6.2.2. Normally open valve

The design of the titanium **NO** valve is similar to the titanium pumps, though the passive check valves are omitted (Figure 6.3 a). The bending actuator is a $100 \mu\text{m}$ titanium foil with a glued on piezo ceramic (PIC 151, $d = 16 \text{ nm/C}$; $200 \mu\text{m}$). It is laser welded to the valve body, which includes two drilled openings for valve inlet and outlet. An O-ring soft sealing (medical grade **FKM**, nominal thickness of $500 \mu\text{m}$), integrated into the

valve body before laser welding, enables low leakage rates. The current device has a diameter of 20 mm and a height of 2.6 mm.

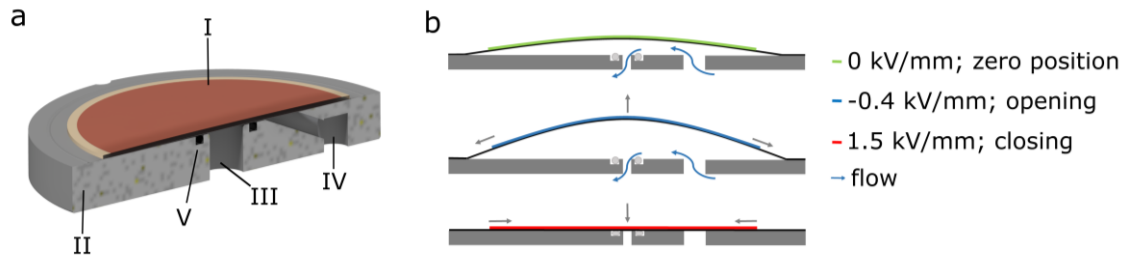


Figure 6.3 (a) Model of a normally open valve showing the bending actuator (I), the valve body (II), the outlet (III) and inlet (IV) as well as the FKM sealing (V). (b) working principle. In the non-actuated state, the diaphragm hovers over the sealing, allowing for fluid flow. Using the indirect piezoelectric effect, the valve can be actively opened, further decreasing its fluidic resistance, or actively closed, using a high positive voltage to compress the sealing.

During non-actuated mode, fluid can pass through the clearance between the soft sealing and actuator membrane of the NO valve (Figure 6.3). Exposure of the piezo ceramic to an electrical field causes a deflection towards the valve chamber bottom. Eventually, the diaphragm compresses the O-ring and blocks fluid movement (Figure 6.3 b). The pretension technique for piezo mounting is the driving factor for the valves' fluidic performance in its open state. It adjusts the chamber height and therefore determines the valve's fluidic resistance. Blocking is ensured as long as the actuator's force is greater than the force introduced to the membrane by fluid pressure. The NO valves use the same bending actuator as the titanium pumps and therefore overcome a minimal pressure of 80 kPa.

6.2.3. Normally closed valve

While the overall setup of the normally closed valve is more complex (Figure 6.4 a and b), its bending actuator is the same as for the pumps and NO valves. The NC valve includes an O-ring (medical grade FKM, nominal thickness of 500 μm) that is integrated into the valve's body. The soft sealing is compressed by a plunger, suspended by a 50 μm thin spring foil that pulls it upwards. The current device has a diameter of 20 mm and a height of 3.6 mm.

For manufacturing, the plunger is inserted in the valve body from beneath, bringing it into contact with the soft sealing. The spring foil is welded to the plunger and subsequently to the valve body. A difference in height of the two weld planes causes the initial pre-displacement of the spring foil, which pulls the plunger upwards and compresses the soft sealing. The pre-displacement is designed to be 100 μm , adding up the difference in height of the plunger and the valve body, and the soft sealing's elevation. The valve body, the plunger, and the spring foil form the impermeable valve chamber. Finally, the actuator foil is laser welded to the valve body.

Blocking of the flow in non-actuated mode is ensured due to the spring foil's restoring force (Figure 6.4 c). Moreover, a pressure acting on either the spring foil or the plunger induces an additional closing force. Therefore, a fluidic pressure applied on either the valve's inlet or outlet increases sealing of the double normally closed valve. A high voltage on the bending actuator causes the diaphragm, and therefore the plunger, to move downwards. The plunger loses contact to the soft sealing and opens the fluid path (Figure

6.4 c). Opening takes place as long as the actuator's force is greater than the restoring force of the spring foil.

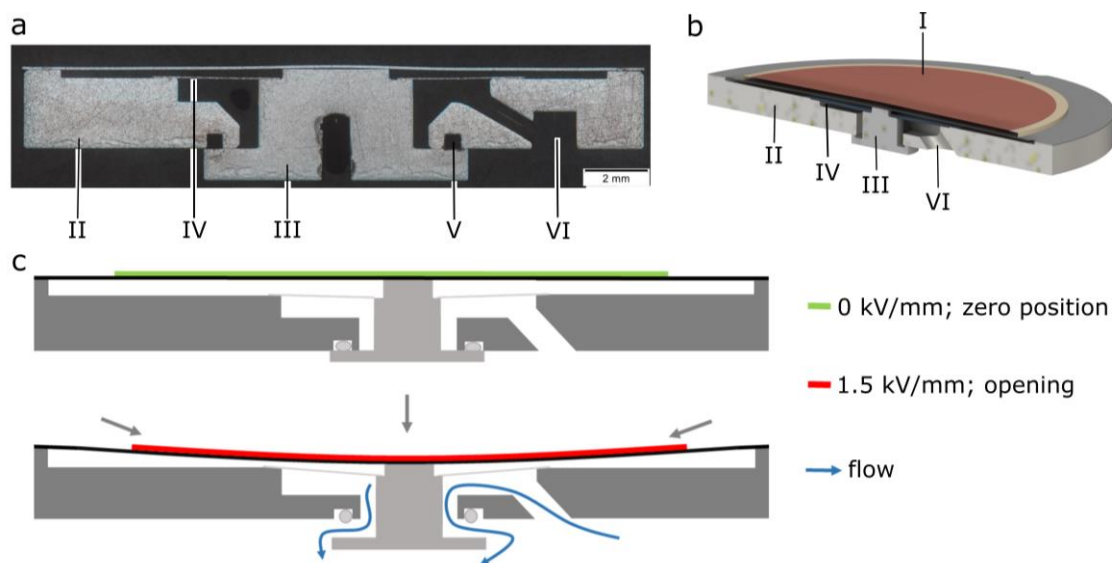


Figure 6.4 (a) Section of a normally closed valve showing the valve body (II), the plunger (III), the sealing notch (V) as well as the inlet of the valve (IV). The plunger (III) is welded to a spring foil (IV) and compresses a FKM sealing in the notch (V). (b) model of the valve including the glued on piezo actuator (I). (c) working principle. In non-actuated state, the spring foil pulls the plunger up, closing the valve's outlet. The indirect piezoelectric effect causes the actuator diaphragm to move downwards when a high voltage is applied, which opens the fluid path.

The initial spring force displacement is crucial for a functioning device, since it determines the balance of sufficient opening in actuated state and low leakage in closed mode. Therefore, the elastic behaviour of the spring foil is investigated experimentally and with finite-element-modelling (FEM) simulation. By variation of the initial spring displacement its effect on the spring force is determined.

6.3. Materials and methods

For assembly of the novel micropump and valves, we use solely titanium, since it offers high resistance to plastic deformation and is commonly used in medical applications[185]. Rigid parts, such as the pump/valve body, or the plunger of the NC valve, are manufactured using high precision milling. The structured foil components are etched from cold-rolled titanium sheet material of different thicknesses (from 25 μm to 100 μm). Inspecting the topologies of all components ensures flatness of foils, surface smoothness of milled parts, and compliance with geometric requirements. For assembly, foil components are welded to the pump/valve bodies using a fibre laser. The parts are aligned with dowel pins and firmly pressed together to ensure a high-strength bond resulting in hermetic sealing of the devices' chambers. After laser welding, piezo ceramics are mounted using a two-component epoxy glue.

6.3.1. Stroke measurements

The stroke measurement describes the optical detection of the diaphragm displacement using a quasi-static voltage (amplifier SVR 500-3, piezosystem jena GmbH). Exact movement is determined with a white light profilometer (Fries Research and Technology). The optical sensor has a range of 3 mm and a maximal resolution of 30 nm. The

applied voltage passes through the whole range of interest several times to detect the hysteresis as well as initial repolarization of the ceramic. The measurement automation ensures that the time between two recorded voltages is kept constant, minimizing piezoelectric time effects as sources of error. The measurement accuracy of the total **actuator stroke** is 2 μm , as evaluated from repetitive measurements of several samples.

Furthermore, displacement measurements investigate the **NC** valve's initial spring tension and elastic behaviour. We manufactured four samples specifically for this measurement. The plunger of the valve is not covered with an actuator membrane and can therefore be accessed directly by an applied pressure. A pressure controller (Mensor CPC3000: range -0.5 bar to 2 bar, accuracy: ± 0.5 mbar) applies an increasing pressure to the top side of the spring foil, thus forcing a movement of the plunger that is detected optically.

6.3.2. Fluidic test

We conduct fluidic characterization for each manufactured sample using DI water at room temperature. The sensors used are: Coriflow sensors of different ranges (Bronkhorst MINI CORI-FLOW M14: range 0.5 mL/min to 167 mL/min, accuracy: $\pm 0.2\%$ and ML120V00: range 0.8 $\mu\text{L}/\text{min}$ to 500 $\mu\text{L}/\text{min}$, accuracy: $\pm 0.2\%$); a pressure controller (Mensor CPC3000; v.s.) and two piezoresistive pressure sensors (EPCOS Gauge pressure transducers AKR 1.000 C40: range 0.0 bar to 1.0 bar, accuracy: ± 6 mbar). The latter are placed in the flow path to evaluate the pressure drop over the sample. It is important to notice that the use of coriflow sensors depicts an additional flow resistance in the fluidic path and therefore diminishes the achievable flow rate. Thus, the presented results are the minimal achievable performance.

Micropumps are fluidically characterized by their frequency-dependent flow rate at zero backpressure, their pressure dependent flow, and leakage. For evaluations of the frequency-dependent flow rate, the pump is actuated with a sinusoidal actuation of -0.4 kV/mm to 1.5 kV/mm. A frequency sweep from 5 Hz to 80 Hz is conducted and the resulting flow recorded after stabilization. All experiments are realized using the same setup, since any changes in the periphery can cause large differences in fluidic performance. Furthermore, pressure dependent flow with 30 Hz sinusoidal actuation is measured. A linear extrapolation of the data enables calculation of the theoretical blocking pressure. We shorten measurement time of the large number of samples by omitting experimental investigations of the **blockingpressure**. In addition to active flow, we evaluate leakage through the passive check valves with pressure up to 40 kPa.

Fluidic testing of microvalves includes testing of the actuated and non-actuated mode. In our experiments, valves are actuated using a sinusoidal signal with a frequency of $f = 0.01$ Hz and electric fields of -0.4 kV/mm to 2.0 kV/mm. We evaluate the pressure dependent characteristics of an actuated valve for closing and opening lead times. For both actuated and non-actuated valve testing, an applied head pressure is varied using a pressure controller. During open valve testing, the fluid pressure allows a flow through the valve and the flow rate dependent on the electrical field is measured. For closed valve testing, the pressure dependent leakage through the valve is tested.

6.3.3. Simulation

For investigation of mechanical tension within the foil components of titanium devices, ANSYS workbench 2019 R1 is used for **FEM** analysis. Nonlinear analysis of

large-deformation loads on thin foils is conducted for evaluation of pressure-induced deformations in the elastic regime. This data is compared to mechanical evaluation and crucial for further valve development.

6.3.4. Data Statement

The **actuator stroke**, fluidic test, and simulation data that support the findings of this study are available in Fordatis – Research Data Repository of Fraunhofer-Gesellschaft with the identifier [<http://dx.doi.org/10.24406/fordatis/74>] [186].

6.4. Experimental results and discussion

Medical applications, such as hydraulic implants, require very specific fluidic characteristics. A detailed experimental evaluation is necessary to adapt devices to those requirements and improve the pump and valves further. Table 1 provides an overview of the introduced devices and their fluidic characteristics described hereafter.

Table 6.1 Overview of design parameters and experimental results of the introduced devices

	Titanium Pump	Stainless Steel Pump	Normally Open Valve	Normally Closed Valve
Number of tested samples	24	24	24	3
Size in mm ³	Ø 20×1.5	Ø 20×1.5	Ø 20×2.6	Ø 20×3.6
Driving Voltage in V	-80 to 300	-80 to 300	-80 to 500	-80 to 400
Frequency in Hz	up to 80	up to 80	not applicable	not applicable
Stroke height in µm	79.2 ± 4.3	79.8 ± 2.9	57.3 ± 6.3	39.9 ± 4.0
Energy consumption in J/L (linear regime)	330	330	not applicable	not applicable
Energy consumption in J/L (maximal flow rate)	420	440	not applicable	not applicable
Maximal flow rate in mL/min	14.2 ± 2.5	12.2 ± 2.2	not applicable	not applicable
Extrapolated block-ingpressure in kPa	75	75	not applicable	not applicable
Leakage at 5 kPa back-pressure in µL/min	50 ± 40	40 ± 10	3.4 ± 6.3	2.6 ± 1.9
Open state flow at 20 kPa in mL/min	not applicable	not applicable	27.5 ± 5.3	9.0 ± 9.5
Leakage at 20 kPa in µL/min	not applicable	not applicable	10.9 ± 28.1	0.36 ± 0.15

6.4.1. Titanium pump

To assess the titanium pumps' performance, we manufactured a batch of our known steel pumps in parallel to titanium samples and compare the obtained results.

The **actuator stroke** of a micro diaphragm pump determines the displaced volume per actuation cycle. Optical **stroke** measurements serve as initial function tests and enable the detection of a touchdown of the diaphragm to the pump chamber bottom, caused by

deviations during the piezo mounting process. Figure 6.5 a displays an example of a titanium pump *stroke* measurement. The quasi-static actuation is applied from -0.4 kV/mm to 2 kV/mm, covering the operating range as well as an additional positive voltage range for potential touchdown detection. The piezoelectric hysteresis is clearly visible.

The *stroke* of 24 titanium samples is $79.2 \pm 4.3 \mu\text{m}$. It is compared to 24 steel pumps' average *stroke* of $79.8 \pm 2.9 \mu\text{m}$ (Figure 6.5 b). None of the overall 48 samples exhibit a touchdown. Titanium and steel actuator foils have a thickness of $100 \mu\text{m}$. Since titanium is more flexible than steel (Young's modulus of $E_{\text{Ti-foil}} = 112 \text{ GPa}$ compared to $E_{\text{Steel-foil}} = 195 \text{ GPa}$ [187, 188]), one expects a higher *actuator stroke*. Using considerations of Herz et al. [155], we calculated the theoretic difference as approximately $7 \mu\text{m}$. Nevertheless, we cannot detect this difference. Other influences such as variations during laser welding, piezo mounting, and deviations in the raw material overlay the influence of the Young's modulus. For instance, incoming goods inspection of the used piezo lot reveals an average thickness of $202 \pm 2.8 \mu\text{m}$, capacitance of $21.9 \pm 0.6 \text{ nF}$ and weight of $314 \pm 4.4 \text{ mg}$. Comparison of each individual piezo characteristic and device performance reveals no direct dependence. This is due to the sample size of 48 devices, which does not allow to differentiate all influencing parameters.

Figure 6.5 c shows the measured flow rate of titanium and steel pumps. Both show an initial linear frequency dependence of the flow. Within the linear range, the average flow rate of titanium and steel pumps is alike and reaches up to 11 mL/min . Nonlinear behaviour starts at approximately 30 Hz , where the inertia of the fluid and passive check valves limits further linear increase and causes a decrease of flow for even faster actuation. The maximal flow is higher for titanium pumps with $14.2 \pm 2.5 \text{ mL/min}$ compared with $12.2 \pm 2.2 \text{ mL/min}$ for steel pumps. However, error bars of both groups overlap. The cause for the deviation in maximal flow rate without any difference in the linear regime is not yet solved conclusively. A hypothesis is that the increased elasticity of the spring valves due to the change in material can lead to higher flow rates as inertia effects are less pronounced. It is important to note that the maximal flow strongly depends on the fluidic periphery and pump comparison should always take place in the linear regime.

The flow rate of diaphragm pumps does not only depend on the actuation frequency but also on the applied backpressure. A fixed actuation with increasing backpressure shows a linear decrease in flow (Figure 6.5 d). Titanium and steel pumps behave very similarly. The extrapolated *blockingpressure* is approximately 75 kPa . An ideal pump's flow rate is backpressure independent, which can be achieved in further development steps, e.g., with design adaptations [128]. Here, the backpressure dependent flow gives additional information on the micropump's quality. While a pump with poor valves can show reasonable flow without any backpressure, its behaviour with pressure is usually deficient. Especially *bubble tolerance* can suffer, if valves are insufficiently closed. Leakage measurements give further insights on the valve quality. The titanium samples show an average leakage of $0.05 \pm 0.04 \text{ mL/min}$ with 5 kPa applied to the pumps' outlet. This is similar to the steel pumps' leakage of $0.04 \pm 0.01 \text{ mL/min}$.

Some characteristics of the individual devices show large variation. While the *actuator stroke* has a variance of 5%, the flow rate error reaches up to 20% (Figure 6.5) and the leakage shows a large scattering with a deviation of up to 80%. The *stroke* variation can be caused by deviations in raw material characteristics and geometry, such as the piezo characteristics mentioned above. The notably larger scattering of the flow rate is

likely due to differences in the valve quality. This hypothesis is substantiated by the extreme scattering of the leakage measurement. A deformed valve that causes large leakage rates allows backflow during the pump stroke and limits the fluidic performance. Such a deformation can be caused by the raw material quality as well as occur during the laser welding process due to heat effects. Not all crucial influences are fully understood yet. We aim to minimize the sample to sample variation in further development steps, considering each individual influence.

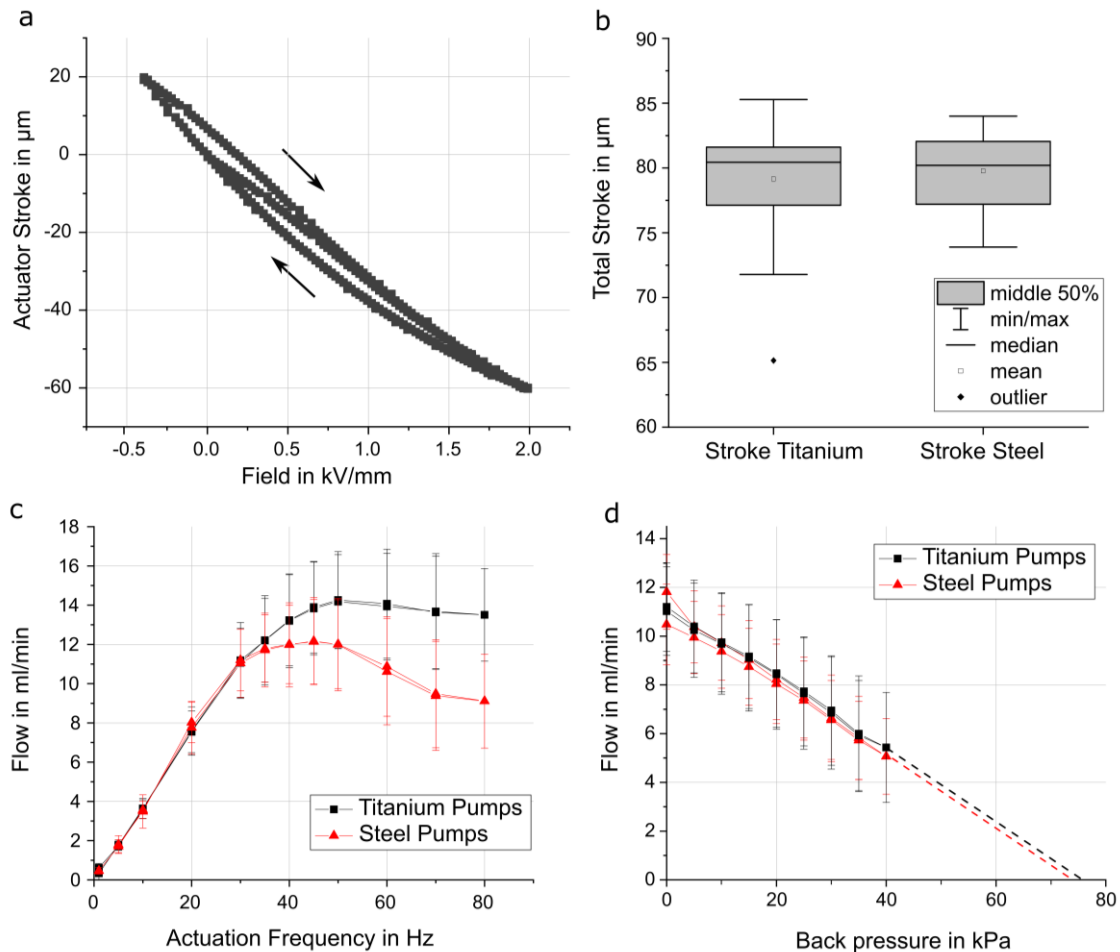


Figure 6.5 (a) Typical *stroke* measurement of a titanium pump. The piezoelectric hysteresis is visible and no touchdown to the pump chamber bottom is detected; (b) box-plot for *stroke* comparison. The change in material does not cause a change in *stroke*. (c) average frequency dependent flow rate with no backpressure and sinusoidal actuation of -0.4 to 1.5 kV/mm ($n_{\text{Titanium}} = 24$, $n_{\text{Steel}} = 24$). Both pump types show the same behaviour in the linear flow regime. Error bars depict the standard deviation; (d) backpressure capability ($n_{\text{Titanium}} = 24$, $n_{\text{Steel}} = 24$) with sinusoidal actuation of 30 Hz and -0.4 to $+1.5$ kV/mm . The extrapolated *blocking pressure* is 75 kPa and does not change with a change in material. Error bars depict the standard deviation.

The power consumption of the bending actuator is experimentally determined on the pump samples to be 2 mJ/stroke with no dependency on the frequency in the relevant range up to 100 Hz or backpressure conditions. Hence, the pumps' power consumption depends on the frequency and the power per displaced volume depends on the applied pressure. Without applied backpressure, titanium and steel pumps have an energy requirement in the linear regime of 330 J/L . The maximal flow in the nonlinear regime requires 420 J/L for titanium pumps and 440 J/L for steel pumps. The resulting power consump-

tion only includes the piezoelectric actuation, while the efficiency of the driving electronics needed to actuate the devices is not taken into account. In general, piezoelectric pumps are considered energy-efficient compared to other actuation types [94], however, few authors give exact information. The presented actuator proves to be energy-efficient compared to other piezoelectric pumps that require 900 J/L [101] or 1400 J/L [189]. The only pump that requires less energy per displaced volume known to the authors bases on electrostatic actuation and is designed for smaller flow rates and lower backpressure [190].

6.4.2. Normally open valve

Equivalent to micropump stroke testing, **NO** valves are tested with a quasi-static actuation from -0.4 kV/mm to 2 kV/mm. Piezoelectric hysteresis as well as the repolarization initial curve are visible (Figure 6.6 a). The overall stroke of 24 **NO** valves is $57.3 \pm 6.3 \mu\text{m}$. The mechanical blocking of the actuator diaphragm due to the O-ring is clearly visible at approx. 1.3 kV/mm (Figure 6.6 a). The variance of the stroke is larger for the NO-valves as for the pumps, since the mechanical blocking on the O-ring limits the actuator movement. Due to deviations in O-ring thickness, this actuator blocking occurs at lower or higher actuation voltage.

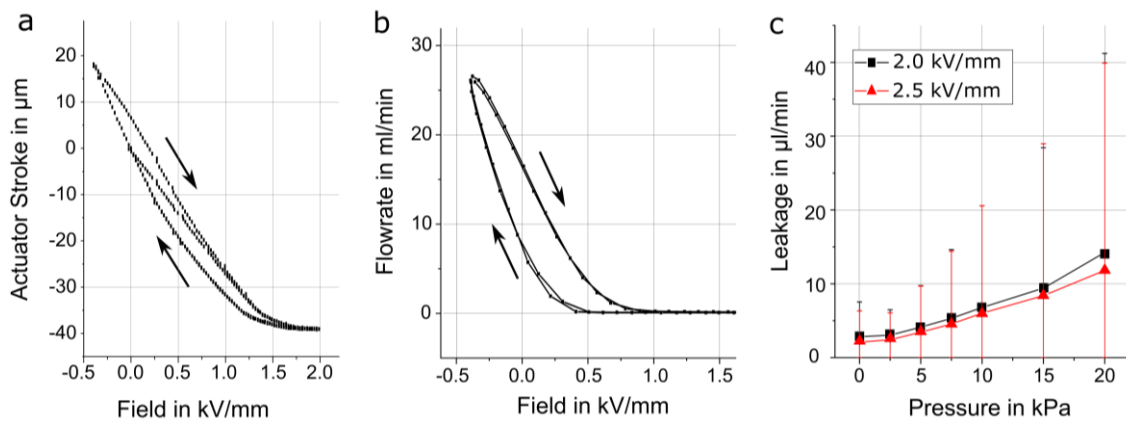


Figure 6.6 (a) Typical stroke measurement of a normally open valve. A change in slope is visible at approximately 1.3 kV/mm, when the actuator starts to compress the O-ring creating a large counter force; (b) typical flow characteristic of a normally open valve with 20 kPa head pressure showing complete blockage at approximately 1 kV/mm. Active opening (negative voltage applied) allows a flow of 26 mL/min; (c) average pressure dependent leakage rates of 24 actuated valves at 20 kPa head pressure. Error bars show the standard deviation.

Fluidic testing of the **NO** valve includes flow characterization with dynamic actuation (0.1 Hz, sinusoidal waveform) as well as leakage testing with a constant electric field. Figure 6.6 b shows the opening and closing characteristics of an exemplary **NO** valve during actuation with 20 kPa head pressure. A strong hysteresis of the passive flow through the valve occurs during actuated mode, which is caused by the piezoelectric hysteresis already observed in stroke measurements, as well as transient flow mechanisms causing fluidic hysteresis. When the electrical field starts to increase from a negative value, the valve is starting to close from its fully opened state. With a high velocity fluid flow being present at full opening, the dynamic pressure within the valve chamber is low during this flow phase. Compared to the opening operation of the valve with a decreasing electrical field, the pre-existing flow field exhibits low velocities and high dynamic pressures. Therefore, the dynamic pressures being present in the valve are different during

opening and closing operation, resulting in different flow rates at the same head pressure. The average maximum passive flow of 24 samples is 27.5 ± 5.3 mL/min.

During leakage characterization of **NO** valves, the actuation field further extends towards positive voltages up to 2.5 kV/mm. This additional field increases the compression of the O-ring by deflecting the diaphragm further. Figure 6.6 c shows the pressure dependent leakage rates of 24 samples at 2.0 kV/mm and 2.5 kV/mm. The leakages through the tested valves are less than 50 μ L/min in the tested pressure range of up to 20 kPa. With an electrical field of 2.0 kV/mm applied, the maximum leakage rate observed is 14.8 ± 27.4 μ L/min, while the maximum leakage at 2.5 kV/mm is 10.9 ± 28.1 μ L/min. The large sample to sample variation can be caused by geometric differences of the used O-ring. As later characterization shows, the thickness of the O-rings in the used batch varies strongly with 495 ± 33 μ m. To further improve leakage rates, the inspection of individual O-rings is planned in future development steps.

6.4.3. Lifetime investigation normally open valve

An investigation of the piezo lifetime was conducted for micropumps in previous studies [173]. Lifetime evaluations in this study include two devices (**NO** valve 1 and **NO** valve 2) to gain first insights whether a shorter lifetime of **NO** valves is to be expected due to additional mechanical stress (touchdown on the O-ring) compared to micropumps.

A failure due to piezo cracking is detected optically and electrically by measuring the samples' capacitance. A crack decreases the capacitance significantly, since only the electrically contacted part of the piezo is detected.

Prior to life time evaluations, the valves are characterized regarding actuation behaviour and leakage. All life time tests are conducted on samples filled with water, and without applied pressure, using sinusoidal actuation, with an electrical field of -0.2 kV/mm to 1.9 kV/mm. The valves are actuated at frequencies of [0.1; 1; 2; 10; 20; 50; 100; 275] Hz and 10^4 cycles are driven per frequency step. After each frequency, the capacitance is measured. Finally, the **NO** valves are driven at 100 Hz until a total amount of one million cycles. Piezo failure was not detected and capacitances remained constant at 14.9 ± 0.2 nF and 15.8 ± 0.3 nF (**NO** valve No. 1 and No. 2, respectively). Valve performance testing is repeated including stroke measurements, as well as actuation and leakage testing at 20 kPa head pressure. For **NO** valve No. 2, the change in performance is < 5% (total stroke, leakage rate at $p = 20$ kPa), whereas the stroke of **NO** valve No. 1 decreases by 30% and leakage at 20 kPa increases by 100% compared to results right after assembly. The different behaviour after lifetime testing is assumed to be under the influence of thickness variation among the O-rings used within the **NO** valves. For future studies, geometric characterization of the soft sealing in the valves is implemented in order to find correlations to the phenomena observed.

6.4.4. Normally closed valve

In initial testing, many of the manufactured **NC** valves showed to be non-functional, since even with high actuation voltages no open state was reached. During failure analysis, we examined the used O-rings regarding their thickness. Their mean thickness deviates significantly from the nominal value of 500 μ m and shows large sample-to-sample variation with an average of 585 ± 45.4 μ m. Moreover, slightly compensating the increased O-ring thickness, the corresponding sealing notch depth is 50 μ m larger as designed. The initial spring displacement is therefore higher than the targeted value of

100 μm , which causes an increase of the spring force and subsequently an imbalance of the forces in the mechanical system. Consequently, the piezoelectric actuator's force is too low to open many of the manufactured valves.

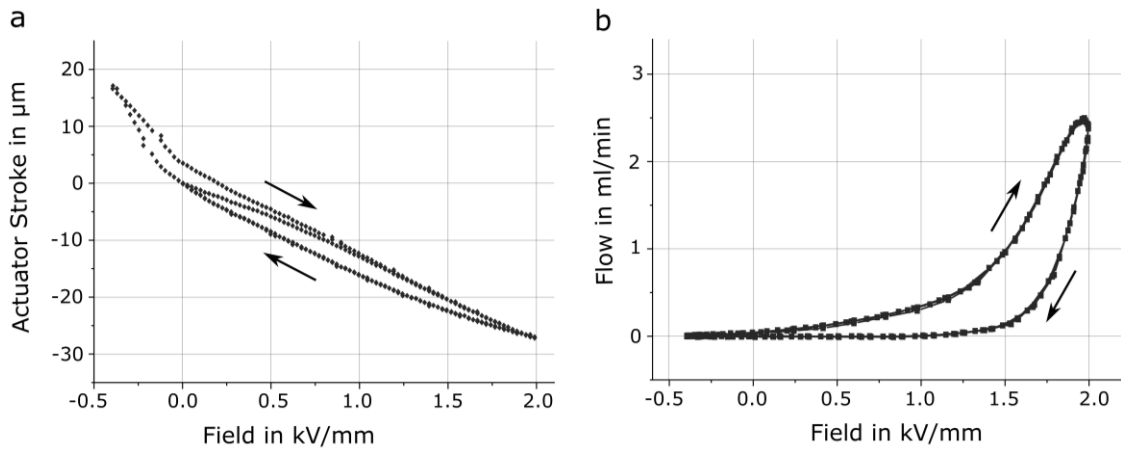


Figure 6.7 (a) Typical stroke measurement of a normally closed valve. A change in slope is visible at approximately -0.2 kV/mm, when the actuator diaphragm loses touch to the plunger; (b) typical flow characteristic of a normally closed valve at 20 kPa pressure difference showing a blockage of the fluid flow up to 0.25 kV/mm and a maximal flow in open state of 2.5 mL/min with 20 kPa pressure applied.

The three functional **NC** valves are tested for stroke and fluidic performance. Overall stroke of the three **NC** valves is 39.9 ± 4.0 μm with a quasi-static actuation of -0.4 kV/mm to 2 kV/mm. Figure 6.7 a shows a typical stroke measurement of one exemplary valve. The slope is steep for negative voltages, where the actuator diaphragm is not in contact with the plunger. This part of the curve characterizes the mechanical behaviour of the bending actuator. A change in slope occurs at the touchdown of the diaphragm to the plunger (Figure 6.7 a). The counter force of the spring foil attached to the plunger reduces possible movement.

Fluidic testing of the **NC** valve includes flow characterization with actuation as well as leakage testing during non-actuated mode at 20 kPa head pressure. Leakage through all three tested valves is less than 1 $\mu\text{L}/\text{min}$ with an average of 0.36 ± 0.15 $\mu\text{L}/\text{min}$. This is in good accordance with the designed high O-ring compression enabling a tight seal. Figure 6.7 b depicts the opening and closing characteristics of a **NC** valve in actuated mode. Same as for **NO** valves, a fluidic hysteresis occurs due to piezo hysteresis and dynamic pressure differences. The average maximum flow of three samples at 20 kPa head pressure is 9.0 ± 9.5 mL/min.

6.4.5. Spring foil investigation normally closed valve

The elastic deformation of the **NC** valve's spring foil is crucial for its functionality. Therefore, we conduct an experimental and numerical investigation. A comparison of the data enables targeted design changes to achieve desired opening and leakage behaviour.

A half model of the spring foil (thickness of 50 μm) is investigated and a fine, structured hexagonal mesh is implemented (Figure 6.8 a). A pressure load is applied to the inner area, which is the interface of the spring foil and the plunger (Figure 6.8 b). This inner area (C, yellow) that is welded to the plunger, can solely move in z direction, while movement in x or y direction is suppressed in order to comply with the physics of the

weld. The area of the outer weld line connecting the foil to the valve body is defined as a fixed support (A, blue). It is restrained in all six degrees of freedom. Boundary condition B (red) is the applied pressure load that leads to a displacement by elastic deformation of the structure. Figure 6.8 c shows the deformation in true scale, with z-displacement presented in false colour.

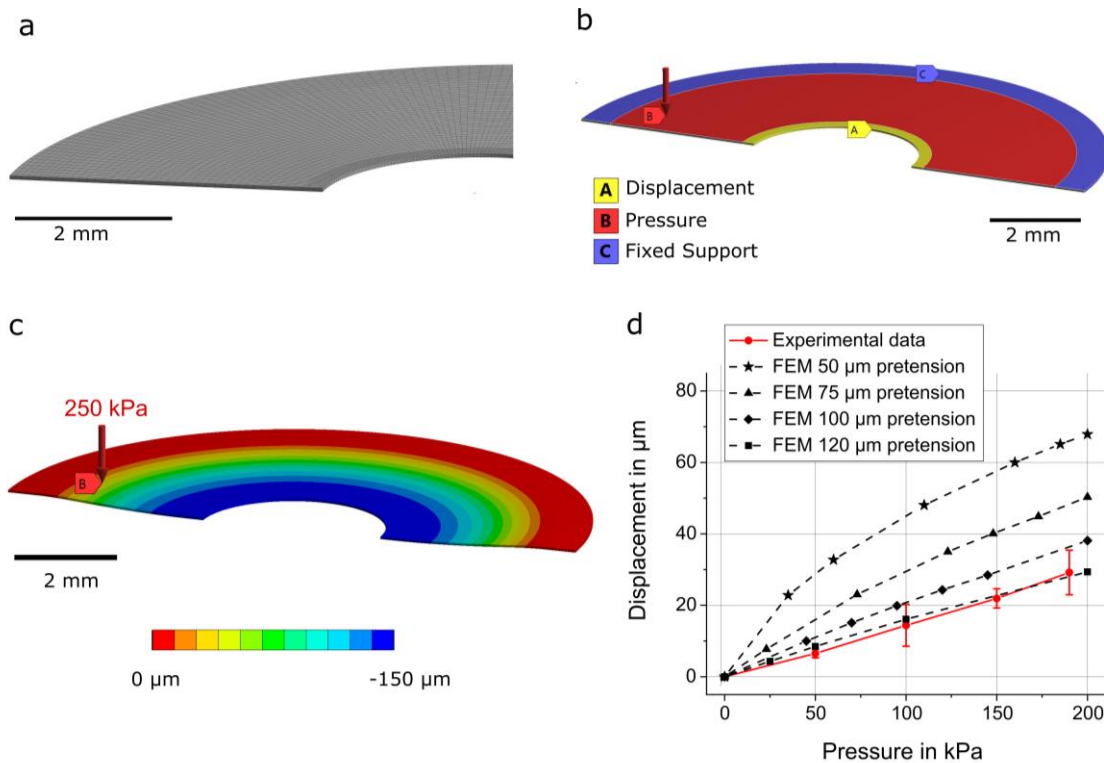


Figure 6.8 (a) Half model of the spring foil with structured mesh; (b) boundary conditions. The outer ring (C) is set as fixed support and the displacement of the inner ring (A) is evaluated with a given pressure applied to area B; (c) deformed model in true scale for a pressure of 250 kPa. (d) experimental and FEM results of the spring foil's displacement under pressure load. With 50 μm initial displacement, the numerical solution differs strongly from the experimental results, while a calculation using 120 μm pre-displacement shows fitting results.

We evaluate the spring foil deformation under pressure load with regard to an initial spring displacement (Figure 6.8 d). The dotted curves show the pressure dependent behaviour starting at a given displacement by forcing an inner ring position in order to imitate the initial displacement during manufacturing. The solid line depicts experimental results. It is evident from the FEM data that the displacement depends strongly on the initial spring displacement after laser welding. Higher initial displacement leads to stiffer behaviour of the foil.

Experimental data is in good agreement with the FEM data assuming a 120 μm initial spring displacement. The increased O-ring elevation of 35 μm can cause such a shift from the designed 100 μm initial displacement to 120 μm when assuming O-ring compression, which was not individually evaluated for each device in this study. The total stroke of the spring foil at 100 kPa pressure load is below 20 μm for a high initial spring displacement (120 μm) in numerical evaluations as well as for experimental results. Such a low displacement of the spring foil and the plunger leads to a low decompression of the O-ring, not opening the valve. Further improvement of the design and adaptation of O-rings is necessary. A displacement of 40 μm or more, which allows full opening, in the blocking pressure range of the piezoelectric actuator of roughly 80 kPa is possible for an

initial spring displacement of 50 μm . Therefore, design parameters need adaptation towards lower initial spring tension.

6.5. Conclusion

This work summarizes the development and evaluation of a titanium-based **microfluidic** platform for medical applications. The combination of the piezoelectric micro-pump, a **NC** as well as a **NO** microvalve offers many possibilities to develop small and energy-efficient implants with broad functionality and automated control instead of manual operation.

The titanium micropumps show promising results. With $79.2 \pm 4.3 \mu\text{m}$, their **stroke height** is similar to comparable steel pumps showing $79.8 \pm 2.9 \mu\text{m}$ of **stroke**. The flow characteristics of both pump types are alike, which matches their similar **stroke**. Within the linear regime, the novel titanium pumps reach an average flow of $11 \pm 2 \text{ mL/min}$. The average maximal flow of the 24 samples is $14.2 \pm 2.5 \text{ mL/min}$ and thereby 2 mL/min higher than the one of the steel samples. The backpressure capability is also very promising, showing an extrapolated **blockingpressure** of 75 kPa.

In this work, we also describe the development and evaluation of new titanium **NO** valves. Even though they use the same actuator, the valves show a smaller stroke of $57.3 \pm 6.3 \mu\text{m}$ as compared to the titanium pumps, since a touchdown to the O-ring blocks further membrane movement. Leakage rates of all 24 samples are in an acceptable range below $50 \mu\text{L/min}$. The sample-to-sample variation of leakage is rather high with an average of $10.9 \pm 28.1 \mu\text{L/min}$. Further improvement to minimize variations is necessary and possible. Nonetheless, already good closing behaviour is achieved and many samples exhibit low leakage, proofing the feasibility of this device. Free flow is evaluated for 20 kPa head pressure, which is a realistic pressure the pump easily provides. The high flow of $27.5 \pm 5.3 \text{ mL/min}$ displays a low flow resistance, which is important for efficient system architecture.

In the **NO** valve, premature failure can occur due to the touchdown of the actuator membrane on the O-ring, which causes a different strain distribution within the piezo ceramic compared to the pumps where the membrane can move freely. Preliminary lifetime tests on two samples showed no piezo failure within one million cycles. However, fluidic performance changed unreproducibly, making further design considerations and lifetime testing necessary.

Manufacturing of functional **NC** valves posed problems, since extremely low tolerances of all parts are necessary. The large deviation in O-ring thickness observed leads to a too high initial spring tension acting on the plunger and a resulting high spring force countering piezo-actuator movement. Therefore, only three out of thirty samples showed valve functionality, while all others stayed constantly closed. Comparison of measured O-ring thicknesses and **FEM** simulation are in good agreement and indicate that slight design changes can increase the yield of working valves tremendously. The three functioning samples show very promising results. Leakage in closed (non-actuated) mode is extremely low with $0.36 \pm 0.15 \mu\text{L/min}$.

The introduced titanium platform offers great possibilities for **microfluidic** applications, especially in the medical field. The presented pump combines high flow rates with high backpressure abilities. We designed and tested microvalves with low leakage rates and high free flow, making them suitable for reliable flow restrictors with low fluidic

resistance in open state. Additionally, we showed possibilities for further improvement. All devices consist only of titanium, FKM sealing, and a glued on piezo ceramic, achieving MRI-compatibility. In addition, compatibility with a large variety of fluids is given since all wetted surfaces are titanium or FKM. Especially for medical applications, energy-efficiency can be a crucial property. Piezoelectric actuation offers an energy-efficient as well as space saving actuation method for both pumps and valves. Furthermore, the similar form factor of the devices enables easy and space efficient combination. The choice between NC and NO valves makes it possible to design well-adapted systems with the lowest possible energy consumption. The introduced devices are the base of a micro-fluidic titanium-based technology platform. The aim of future research is to further develop existing devices and extend the functionality of the platform further.

Acknowledgements

This work was partly funded by the “Bayrische Forschungsstiftung” within the project “Aktive, theranostische Blasenschließmuskeltechnologie” (active, theranostatic bladder sphincter technology) as well as the Federal Ministry of Education and Research [project reference numbers 16FMD01K, 16FMD02, and 16FMD03].

7. Cell Transport Using Piezoelectric Micro Diaphragm Pumps

Bußmann, Agnes^{a,b,*}; Thalhoffer, Thomas^{a,c}; Daum, Leopold^c; Richter, Martin^a; Hayden, Oliver^c

^aFraunhofer EMFT Research Institution for Microsystems and Solid State Technologies, Hansastrasse 27d, 80686 Munich, Germany

^bKIT, MAB - Biomolecular Separation Engineering, Fritz-Haber-Weg 2, 76131 Karlsruhe, Germany

^cTUM LBE - Heinz-Nixdorf-Chair of Biomedical Electronics, Einsteinstrasse 25, 81675 Munich, Germany

* Correspondence: agnes.bussmann@emft.fraunhofer.de; Tel.: +49 89 54759-416

Abstract

New developments enable far-reaching cell culture research. However, many setups require manual fluid handling or bulky pump systems. The use of piezoelectric micropumps can enable further miniaturization and cost-efficient disposables, provided that cells are not damaged during transport. This work is first to investigate the impact of micropumps with flap valves on transported mammalian cells. The 5×5 mm² silicon pump with 20 µm **stroke height** impacts cells causing 35.9 % dead cells compared to 5 % in the control sample. The larger steel pump has less impact, especially with adapted, soft actuation. Further evaluation and the design of adapted pumps can potentially improve cell culture and in vitro cell test applications.

7.1. Introduction

Cell cultures, organ-on-chip or spheroids enable researcher to mimic complex biological processes and cell-cell interactions on a microscale. Today, **microfluidic** chips are in use to culture, analyse, or maintain a specific cell type and function in highly defined environments. Especially in pharmaceutical research, micro systems are of broad interest [191]. **Microfluidic** solutions are even critical for 3D bioprinting of cells [192]. However, cell transport, dosage of additives or culture medium circulation usually require manual handling, tubing, and bulky pumps next to the incubator. The use of micropumps for these tasks enables less manual handling and therefore higher reproducibility, accuracy, and integrability.

To the best of our knowledge, no micropumps of this size have been reported to directly transport living cells. Even though the technology provides many advantages for miniaturized cell culture, the interaction of pump and medium is not yet sufficiently understood. Without further precautions micro diaphragm pumps are likely to harm transported cells due to mechanical stress. For instance, the cell membrane can be slit open on sharp edges inside the micropump and cells can be squashed by the pumping membrane or destroyed by high shear forces.

The piezoelectric micropumps of **Fraunhofer EMFT** offer the possibility for micropumps as consumable with a cost-efficient production by using standard wafer-level silicon processes or inexpensive laser-welded steel foil structures. To enable cell culture applications that make use of these pump technologies, it is of interest to investigate and minimize their influence on living cells.

7.2. Materials and Methods

The experiments in this work are conducted with K562 human chronic myeloid leukaemia cells, which are transported with different micropump types from [Fraunhofer EMFT](#).

7.2.1. Micropumps

In this work we use two types of piezoelectric micro diaphragm pumps with passive check valves: Metal-sheet pumps with a diameter of 20 mm and 2 mm thickness and silicon pumps as small as $5 \times 5 \times 0.6 \text{ mm}^3$ [110, 151].

The pumps consist of a body, valves, and diaphragm with a glued-on piezo ceramic actuator (Figure 7.1). Actuation is based on the indirect piezoelectric effect: an electric field causes a mechanical deformation of the bending actuator [27]. When an alternating high voltage is applied, the diaphragm oscillates vertically, causing fluid movement through the two passive check valves (Figure 7.1). Usually rectangular, sinusoidal, or rectangular signals with 250 Hz sine flanks are used for the actuation of the piezo ceramic.

Flap valves are necessary to prevent backflow, diffusion, and leakage. Additionally, high backpressure capability as well as robust [bubble tolerance](#) are difficult to achieve with valve less, e.g., diffuser/nozzle setups. Hence, for many applications, valves are necessary. We therefore use pumps with passive flap valves (silicon pumps) or spring valves (steel pumps) to pump cell suspension.

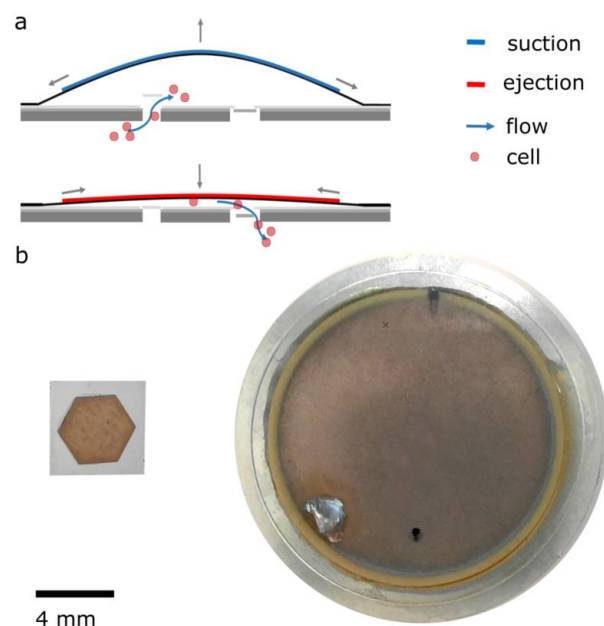


Figure 7.1 [Fraunhofer EMFT](#)'s piezoelectric micro diaphragm pumps; a: working principle with fluid intake at negative voltage and ejection at positive voltage; b: $5 \times 5 \text{ mm}$ silicon pump and the 20 mm diameter steel pump.

In this work, we conduct experiments on one steel micropump and two silicon micropumps. The silicon pumps differ in the pump chamber height: One has chamber height of $20 \mu\text{m}$ (at the lowest actuator position) and a [stroke](#) of approximately $20 \mu\text{m}$ for high flow applications, while the second pump is optimized for [bubble-tolerant](#) dosing and has a chamber height of only $1 \mu\text{m}$ at the lowest actuator position. The upward [stroke height](#) of this pump is $12 \mu\text{m}$. Hence, it constitutes an extremely narrow flow path for the

cells in the solutions. Transport with this pump represents the worst-case strain. The typical flow rates and pressure capability of these devices as well as used actuation signals are summarized in Table 7.1.

Table 7.1 Flow performance and geometry of the used pump types including one stainless-steel pump and two types of silicon pumps

	Steel	Silicon-1 μ m	Silicon-20 μ m
Size in mm³	Ø 20×2	5×5×0.8	5×5×0.8
Chamber Height in μm	10	1	20
Stroke Height in μm	60	12	20
Flow Rate (Water) in μL/min	8700	60	450
Blockingpressure (Water) in kPa	80	55	80
Backpressure (Air) in kPa	35	30	15
Actuation Amplitude in kV/mm	1.9	2.4	2.4
Actuation Frequency in Hz	30	350	350
Waveform	Sine / Rect.	Rect.	Rect.

Even though application with liquid media is aimed, air performance is important as it gives a first indication on self-priming ability and [bubble tolerance](#) [32].

7.2.2. Cell Transport

We conducted all cell-viability pumping experiments with non-adherent K-562 human chronic myeloid leukaemia cells [193] (DSMZ GmbH ; DSMZ no.: ACC 10) of approximately 17 μ m. Prior to the transportation experiment, harvested cells were washed from culture medium and aliquoted with a concentration of approximately 2×10^5 cells/mL.

The experimental setup consists of an inlet reservoir filled with cell suspension, the pump and an outlet reservoir to collect the sample. One millilitre of cell suspension is transported from inlet to outlet reservoir by the pump one single time and not circulated or stressed repeatedly. Different pump actuation signals were tested. Each measurement of a given pump and actuation signal was conducted on three individual cell solution samples (Table 7.2). Between measurements with different actuation signals, the micro-pump was passively flushed with buffer using a syringe to remove all cell residues. The first 2 mL of rinsing solution were collected and analysed for cell residues, which gives an indication of cell agglomeration inside the pump. To prevent falsification of the total number of cells in a sample, the pump is flushed with air before and after rinsing.

Table 7.2 Overview of conducted experiments showing the number of samples transported with a micro-pump type and given actuation waveform

Number of Transported Samples	Steel	Silicon_1 μ m	Silicon_20 μ m
Sinusoidal Actuation	3	-	-
Rectangular Actuation	3	1	3

7.2.3. Propidium iodide cell viability by flow cytometry

All samples were treated with Propidium iodide (PI) solution (Miltenyi Biotec GmbH), a nucleus staining reagent that cannot penetrate the membrane of intact cells, to mark dead cells according to the supplier guidelines. In a typical experiment, 2 μL of PI was added to the previously “Pumped” cells as well to “Non-pumped” cells (negative control) and to cells treated with TritonTM X-100 (Merck) instead of pumping as positive control. Cells were incubated with the PI for 15 minutes before flow cytometry measurements.

We measured all samples successively, starting and ending with a positive and negative control sample to detect errors due to incubation time.

7.2.4. Analysis

The samples were analysed using the MACS Quant Analyzer 10 Optical Flow Cytometer (Miltenyi Biotec GmbH). Data is gated for single cells using the forward scatter height versus forward scatter area.

For each sample, the total number of cells and the percentage of dead cells, indicated by fluorescence intensity in the PI channel are evaluated. While the total number of cells indicates whether a significant amount of cells were stuck inside the micropump and/or fluidic connections, the percentage of dead cells indicates how much mechanical damage occurred during cell transport.

7.3. Results and Discussion

The comparison of control samples measured before and after the pumped cell solution shows no significant difference in terms of dead cells or number of cells.

The number of cells in each sample was compared to the negative control. In combination with the cell density in the rinsing solution this gives information on cell agglomeration within the pump during operation with cell solution. The cell concentration in samples transported with the steel pump is not significantly different than the control sample (Figure 7.2 a). An 8% decrease in cell concentration is detected for samples transported with the high chamber silicon pump. These findings indicate some cell aggregation during the transport of 1 mL cell suspension.

Measurements with the 1 μm chamber silicon pump were aborted after the transport of one out of three samples. The flow rate of the silicon pump dropped to close to 0 $\mu\text{L}/\text{min}$ probably due to an occlusion of the pump. The stroke of the pump is not sufficiently large to transport cells through the low chamber. The number of cells in the sample substantiates this hypothesis with a significant drop in concentration from 199 ± 12 cells/ μL of the control to 29 ± 1 cells/ μL in the pumped sample (Figure 7.2 a).

Analysis of the first 2 mL of rinsing solution confirm these findings (Figure 7.2 b). There are few cells in the passively pushed through buffer after experiments with the steel and the large chamber silicon pump (2 cells/ μL and 5 cells/ μL). Thus, the solution used to rinse the small chamber pump contains 29 cells/ μL , which is as much as was detected in the pumped sample itself.

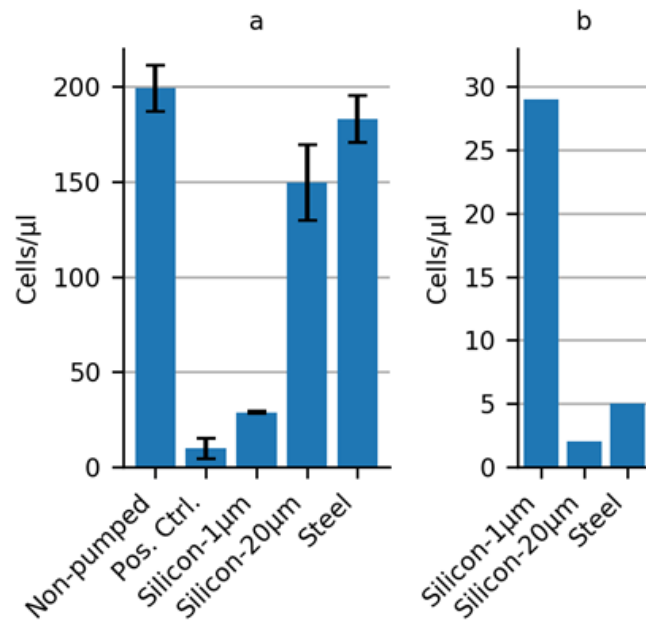


Figure 7.2 Comparison of cell density after transport with a micro diaphragm pump; (a) Cell density in transported as well as control samples, $n=3$; (b) Cell density in the rinsing solution.

The initial cell transport using the steel pumps is conducted with rectangular actuation. This actuation is the most efficient signal form from a fluidic point of view, since the achieved pressure pulse in the pump chamber is maximized and the most fluid is ejected by the pump. Figure 7.3 shows the number of intact cells in samples after transportation with the steel pump with a rectangular actuation signal. 87.1 ± 0.2 % of cells are intact, compared to 95.6 ± 0.7 % in the negative control sample (not pumped cells). There are two probable reasons for the decrease of intact cells: The shear stress in the fluid is high with rectangular actuation signal and the opening and closing impulses on the valves are instant, leading to fast opening with large valve oscillation.

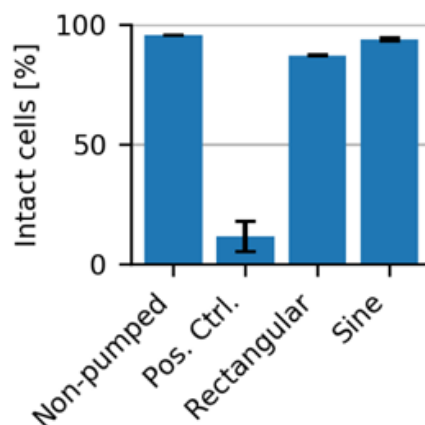


Figure 7.3 Proportion of intact cells after transport with the steel micropump with two different actuation signals, $n=3$

Additionally, a smoother actuation signal was tested to limit the impact on the transported cells. Cell solution transported with sinusoidal actuation show 93.8 ± 0.5 % intact cells, which is very close to the not pumped control sample with 95.6 ± 0.7 % intact cells. Thus, it is possible to reduce the damage on the cell solution significantly simply

by adapting the actuation signal. Damage is reduced, since shear forces in the liquid are reduced and the valve oscillation is minimized due to the steady diaphragm movement. However, the achievable flow is also slightly smaller and especially bubbles that can always occur in fluidic systems are more problematic with sinusoidal actuation, since the smaller pressure peak inside the pump chamber makes it more difficult to eject bubbles from the pump chamber.

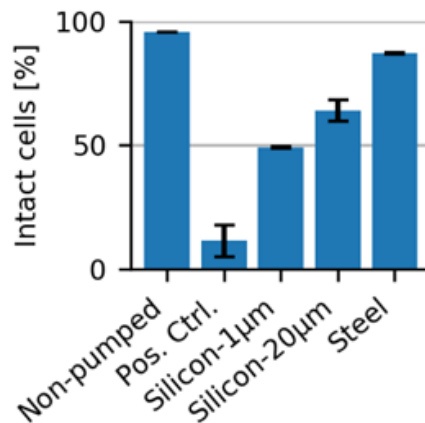


Figure 7.4 Proportion of intact cells after transport with the small pump chamber and large pump chamber silicon pumps compared to the samples transported with the steel pump using rectangular actuation, $n=3$

As expected, the silicon-1µm pump has a large impact on the transported cells. The number of intact cells after transport through this pump, is extremely low with 49.2 ± 0.4 % (Figure 7.4).

The 20µm chamber silicon pump does not occlude and the evaluation of the samples pumped with rectangular actuation shows 64.0 ± 4.2 % intact cells (Figure 7.4). The higher pump chamber already leads to a smaller impact of the transport. However, the damage caused by this silicon pump is significantly more severe than damage caused by the steel micro pump with rectangular actuation.

The steel **stroke volume** is 11.5 µL and significantly larger than the one of the silicon pumps with approximately 50 nL. Therefore, the steel pump enables transport of more fluid with one **actuator stroke** and consequently, less interaction between the cells and the rapid movement of the pump valves or actuator. The surface to volume ratio in the steel pump's chamber is smaller, enabling more cells to pass through the pump with little surface contact compared to the silicon sample. Furthermore, the valves of the silicon pump have sharp edges that might cut cells. Additionally, the valve seat and the flap are in close contact when the valve is shut, since the silicon surface is very smooth and cells are likely to be damaged when caught in a closing valve. The surface of the steel valve is rough and uneven, offering more space for the cell to move before the valve closes. Another important reason for more severe damage is the higher actuation frequency that was chosen to achieve sufficient flow rates in the small silicon pumps (30 Hz membrane oscillation frequency for steel pumps compared to 350 Hz for silicon pumps). This rapid movement leads to high shear and more damage of the cells in the solution.

7.4. Conclusion

This work is the first evaluation of usability of micro diaphragm pumps with passive flap valves for the transport of living cells. The experiments in this work prove a general feasibility of cell transport using piezoelectric micro diaphragm pumps. The

larger steel micropumps enable transport of cell solutions with limited damage to the cells. Especially the use of sinusoidal actuation instead of the fluidically more efficient rectangular actuation decrease the number of dead cells after transport. More complicated actuation signals, such as rectangular actuation with sinusoidal flanks, might combine the advantages of both tested waveforms and offer limited cell death in combination with better fluidic performance. Further experiments are necessary to identify the optimal actuation.

The transport with the considerably smaller silicon pumps causes more cell damage. The silicon-1 μm shows the expected high impact on the cells. It occludes quickly, showing that the actuator is not capable of transporting cell debris out of the cell. In addition to the quick occlusion, it causes considerable mammalian cell damage, as was expected. The 20 μm chamber silicon pump enables cell transport without clogging. However, this pump has a distinct effect on the cell suspension, with more than 1/3 dead cells after transport compared to only 5% of the control sample.

Even if the silicon pump's impact on the transported cells is significantly higher, the device remains interesting for biomedical applications. It is a lot smaller and offers smaller flow rates as well as the possibility to dose smaller volumes accurately. Furthermore, the use as disposable product is more appealing, since production costs can be minimized in large scale MEMS productions. Direct integration into microchips for cell culture is possible. It is therefore of high interest to further study the impact of the pump on the transported cell solution. Prospective experiments to optimize the actuation signal with sinusoidal flanks might help to limit the pump's impact. Additionally, geometrical changes of the valves, pump chamber, fluidic connectors and other system components could reduce the cell damage.

Acknowledgements

This work is part of the Moore4Medical project funded by the ECSEL Joint Undertaking under grant number H2020-ECSEL-2019-IA-876190. Special thanks to Alfred Michelfelder for his work in maintaining the cell cultures.

8. Microfluidic Cell Transport with Piezoelectric Micro Diaphragm Pumps

Bußmann, Agnes^{a,b,*}; Thalsofer, Thomas^{a,c}; Hoffmann, Sophie^a; Daum, Leopold^c; Surendran, Nivedha^a; Hayden, Oliver^c; Hubbuch, Jürgen^b; Richter, Martin^a

^aFraunhofer EMFT Research Institution for Microsystems and Solid State Technologies, Hansastrasse 27d, 80686 Munich, Germany

^bKIT, MAB - Biomolecular Separation Engineering, Fritz-Haber-Weg 2, 76131 Karlsruhe, Germany

^cTUM, TranslaTUM—Central Institute for Translational Cancer Research, Einsteinstrasse 25, 81675 Munich, Germany

* Correspondence: agnes.bussmann@emft.fraunhofer.de; Tel.: +49 89 54759-416

Abstract

The automated transport of cells can enable far-reaching cell culture research. However, to date, such automated transport has been achieved with large pump systems that often come with long fluidic connections and a large power consumption. Improvement is possible with space- and energy-efficient piezoelectric micro diaphragm pumps, though a precondition for a successful use is to enable transport with little to no mechanical stress on the cell suspension. This study evaluates the impact of the **microfluidic** transport of cells with the piezoelectric micro diaphragm pump developed by our group. It includes the investigation of different actuation signals. Therewith, we aim to achieve optimal fluidic performance while maximizing the cell viability. The investigation of fluidic properties proves a similar performance with a hybrid actuation signal that is a rectangular waveform with sinusoidal flanks, compared to the fluidically optimal rectangular actuation. The comparison of the cell transport with three actuation signals, sinusoidal, rectangular, and hybrid actuation shows that the hybrid actuation causes less damage than the rectangular actuation. With a 5% reduction of the cell viability it causes similar strain to the transport with sinusoidal actuation. Piezoelectric micro diaphragm pumps with the fluidically efficient hybrid signal actuation are therefore an interesting option for integrable **microfluidic** workflows.

8.1. Introduction

The detailed experimental analysis of biological systems on a microscale is a common subject of current research. Within the last 30 years, micro fluidic systems developed rapidly and already offer solutions for various experimental setups [194, 195]. Today, analysis on aggressively scaled devices is possible. However, the sample transport either relies on passive capillary forces or requires systems with bulky external pumps for active transport that often have a high power consumption and are connected with long tubing, which leads to a high dead volume [196–199]. The active transport in space-restricted situations, such as in clinical environments, is even more challenging. The integration of micropumps can offer a cost as well as an energy efficient on-chip solution for active sample transport.

Micropumps are not only of interest for the active transport in **microfluidic** setups, but can also offer a possibility to improve three-dimensional (3D) bioprinting. This technique enables the generation of complex structures that are of interest in pharmaceutical

research, regenerative medicine, or the food industry [200, 201]. For instance, the advantages of 3D-cultures compared to 2D-cultures for pharmaceutical research are demonstrated in several studies [202–204] and an industrial use of 3D cultures in pharmaceutical research is expected [200].

Bioprinting is widely researched as treatment of large skin injuries. In particular, large skin lesions can lead to poor healing, infection, or hypertrophic scars [205, 206]. The state-of-the-art treatment is skin transplant from healthy areas. Even though meshing can increase the area of a graft tremendously [207], it is often problematic to harvest sufficient skin. Bioprinting of skin tissue is proposed as possible solution [208] including two main approaches: the generations of grafts in vitro that are cultivated and implanted into the wound and the in situ printing directly into the wound [209].

Fluid transport for the printing process can be more challenging for in situ printing compared to laboratory configurations. Similar to analysis systems, laboratory printing setups often rely on large pump systems. However, a printer used in a hospital environment is easier to imagine as a handheld device with small weight and ergonomic geometry. Hakimi et al. [210] present an in situ handheld skin printer. The device weighs less than 800 g and is able to print different cell materials, which allows for consecutive deposition of dermal and epidermal layers. The printability on rough wound surfaces is already shown in vivo.

Micro diaphragm pumps are a possible solution for active cell transport in the presented applications. There is a large amount of research conducted on micropumps and several actuation mechanisms have emerged [27, 100, 211]. A common actuation principle is piezoelectric actuation. It is popular due to its energy-efficiency, high attained forces, large range of applicable frequencies, and precise control [73]. Another common pump type is the electromagnetically actuated pump, which also allows for energy efficient actuation [82].

Energy-efficiency and the possibility for low-cost production as well as small size [100] make micropumps an ideal **microfluidic** actuator for cell transport, even in disposable application. However, currently there is little information on the interaction of micropumps with the dosed medium. In particular, cell solution is not usually transported and analysed. The only work known to the authors that discusses cell transport with a micro diaphragm pump describes the viability of cells after passage through an electromagnetic pump with diffuser nozzle valves [212]. Yamahata et al. [212] show their pump to be well adapted for cell transport, since the viability of both the tested Jurkat cells as well as the more delicate 5D10 hybridoma cells remains high after pumping. However, the fluidic performance of the pump is lower than observed for other micropumps: the $33 \times 22 \text{ mm}^2$ pump can transport $400 \mu\text{L}/\text{min}$ and shows a **blockingpressure** of 12 mbar [112]. The low backpressure capability is most likely partly caused by the diffuser nozzle valves. These valves additionally limit **bubble tolerance**, though the pump is able to transport bubbles without backpressure due to its **compression ratio** over 0.2 [112].

Even though a diffuser nozzle valve design is most likely less destructive for cells, it limits the fluidic performance of a pump system. The backpressure capability, **bubble tolerance**, and ability to transport fluids with a high viscosity such as bioinks can be improved with passive valves, e.g., flap or spring valves. However, the impact of such valves that constitute moving parts with sharp edges and a risk of squeezing the cells between the valve and valve seat is unknown to date. To enable cell transport for in situ bioprinting or on chip analysis application with high performance micropumps, we investigated the influence of our piezoelectric micro diaphragm pumps with spring valves on viable cell

suspensions. The aim of the presented work is to examine the feasibility of cell transport with a micropump including passive valves to enable future developments of **microfluidic** devices with integrated automated fluid transport.

8.2. Materials and Methods

The pumps used for cell transport in this work are **Fraunhofer EMFT**'s stainless steel pumps. A fluidic characterisation of the samples is conducted before and after the cell transport experiments.

8.2.1. Piezoelectric Micro Diaphragm Pumps

A detailed evaluation of the pump type used in this work is given by Bußmann, Durasiewicz et al. [213]. The devices have a diameter of 20 mm and a height of 1.5 mm. The pumps consist of a stainless-steel pump body and a glued on piezoelectric disc actuator (PIC 151, diameter of 16 mm; thickness of 200 μm). The pump body includes two passive spring valves and the actuator diaphragm. All components are laser welded to the base plate. The pump chamber has a diameter of 18 mm and a height of approximately 100 μm to 150 μm , depending on the mechanical stress generated during the welding process and the electric tension applied during the mounting process of the piezoceramic actuator. The valves of the pump are 5 mm apart.

Fluid transport bases on the indirect piezoelectric effect (Figure 8.1). The exposure of the piezoelectric ceramic to an alternating high voltage signal leads to an oscillatory diaphragm movement. The resulting periodic expansion and reduction of the chamber volume in combination with the flow restriction of the passive spring valves leads to a directed fluid transport. The passive flap valves limit backflow and enable a high back-pressure capability as well as high **bubble tolerance**. Therefore, they are indispensable for the fluidic performance of the micropump.

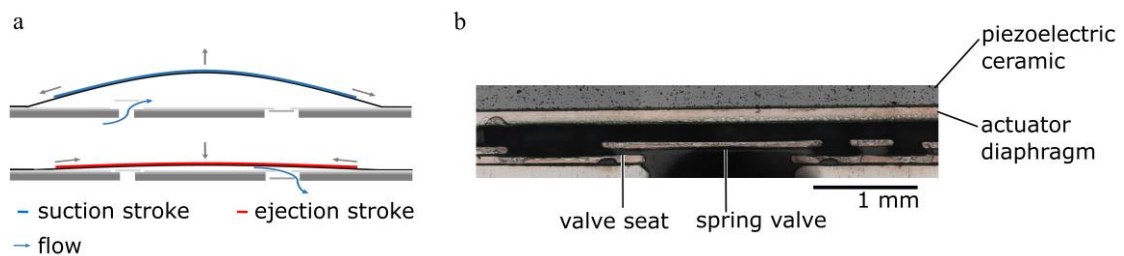


Figure 8.1 Piezoelectric micro diaphragm pump. (a) Functional principle: A negative field moves the bending actuator upwards and sucks liquid through the passive inlet valve into the pump chamber. A positive electric field moves it towards the chamber bottom and pushes the fluid through the outlet valve. Figure adapted from Bußmann et al. [213]. (b) Section of the pump's inlet valve including the spring valve and the valve seat that form the valve gap that is approximately 300 μm long and in the open state of the valve 50 μm high

8.2.1.1. Actuator Stroke Measurements

The **actuator stroke** is an important metric for micro membrane pumps. It is measured optically using a white light profilometer (Fries Research and Technology, Bergisch Gladbach, Germany, sensor range: 3 mm, sensitivity: 30 nm). A voltage sweep is executed ranging from 0.4 kV/mm to 2 kV/mm (amplifier SVR 500-3, piezosystem jena GmbH, Jena, Germany) and the respecting actor positions are detected. The sweep is repeated multiple times. Repetitive tests of the same pump show a measurement accuracy of 2 μm .

8.2.1.2. Fluidic Characterisation

The pumps are characterized with both air as well as deionised (DI) water at room temperature. The actuation signal for these measurements is a sinusoidal alternating voltage from -0.4 kV/mm to 1.5 kV/mm, which equals -80 V to 300 V for the 200 μm thick actuator. Water flow is measured with Coriflow sensors (Bronkhorst, Kamen, Germany ML120V00: range 0.8 $\mu\text{L}/\text{min}$ to 500 $\mu\text{L}/\text{min}$, accuracy: $\pm 0.2\%$ and Bronkhorst MINI CORI-FLOW M14: range 0.5 mL/min to 167 mL/min, accuracy: $\pm 0.2\%$). The backpressure for both water and air characterisation is set with a pressure controller (Mensor, San Marcos, TX, USA CPC3000: range -50 kPa to 200 kPa, accuracy: ± 0.05 kPa). During water measurements, the differential pressure over the pumps is measured with two piezoresistive pressure sensors (TDK Electronics, Munich, Germany, EPCOS Gauge pressure transducers AKR 1.000 C40: range 0.0 kPa– 100 kPa, accuracy: ± 0.6 kPa).

When transporting liquid media, it is always possible that small bubbles occur and the pump needs to be able to transport them through the chamber. We therefore test the pump's backpressure capability with air at actuation frequencies for liquid transport (30 and 60 Hz). The pressure is increased by 2.5 kPa until the flow reaches zero.

Water characterisation of the pumps includes the frequency dependant flow at a constant pressure of 14 kPa in the range from 1 Hz to 50 Hz, the pressure dependant flow in the range from 0 kPa to 50 kPa, and pressure dependant leakage in the range from 5 kPa to 50 kPa.

8.2.1.3. Single Stroke Characterisation

We evaluate the pump's **single stroke volume** with DI water in a gravimetric measurement depicted in Figure 8.2. It is based on a setup introduced by Thalhofer et al. [214]. The inlet reservoir is placed on a precision scale (Sartorius, Göttingen, Germany, MC410S, resolution 100 μg) with the inlet tube immersed free-hanging in the liquid at all times. The pump, which is placed next to the balance, transports liquid from the inlet reservoir to the outlet. The actuation signal is triggered using an automated protocol. The single stroke signal is amplified with the SVR 500–3 (piezosystem jena GmbH, Jena, Germany). The fluid reservoirs are covered with Nitto SWT 10+R to minimize drift caused by condensation or evaporation.

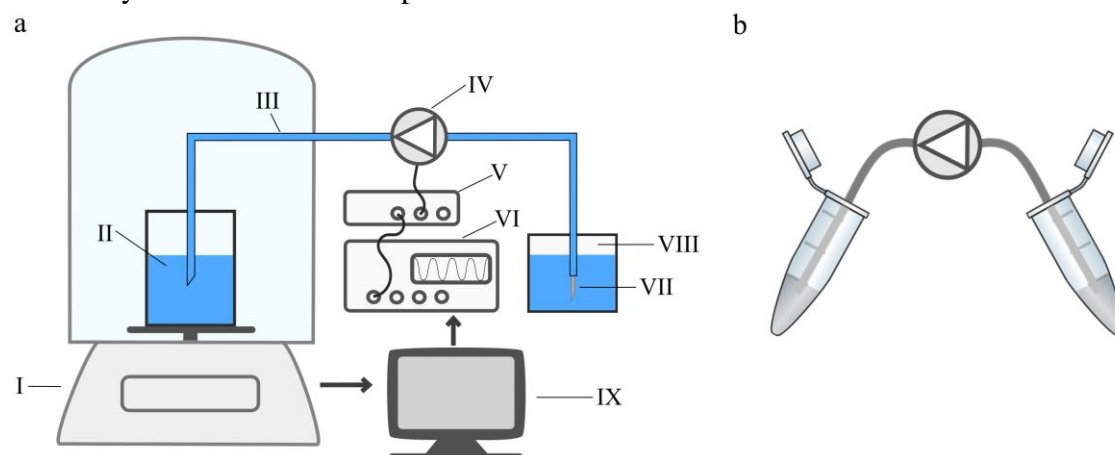


Figure 8.2 (a) Experimental setup of the gravimetric measurement to determine the **single stroke volume** for different actuation signals including a balance (I), the inlet reservoir (II), silicone tubing (III), the micro diaphragm pump (IV) driven with a piezo amplifier (V) and signal generator (VI), an outlet capillary (VII), and pressure equalized reservoir (VIII), as well as automated control and data acquisition (IX); (b) Setup of the cell transport experiments with an inlet- and outlet reservoir as well as the pump connected with silicone tubing. A picture of the two experimental setups is available in Figure B.1 in Appendix B.

The weight of the outlet reservoir is detected before and after the dosage of one single stroke in order to calculate the dosed **single stroke volume** from the weight difference. The sampling frequency is 1 Hz and does not affect the measurement, since we detect the total weight of a single stroke and do not depict the time dependant weight change during the stroke. To account for the drift of the balance, we perform five scale measurements before a single pump stroke is performed with defined waveform and frequency. After an eight seconds break, another five post-trigger scale measurements are recorded. The weight difference before and after the pump stroke is evaluated and corrected for the average drift that is calculated based on the five consecutive measurements before and after the trigger.

8.2.2. Cell Transport

Experiments with cells are conducted with two different cell lines cultivated in suspension culture: K-562 human chronic myeloid leukaemia cells [193] (DSMZ GmbH, Braunschweig, Germany; DSMZ no.: ACC 10) of approximately 17 μm diameter and Jurkat T cell leukaemia cells [215] (DSMZ GmbH, Braunschweig, Germany; DSMZ no.: ACC 282) of approximately 13 μm diameter.

For the transport experiments, harvested cells are washed and aliquoted in buffer (autoMACS Running Buffer; Miltenyi Biotec B.V. & Co. KG; Bergisch Gladbach, Germany) to approximately 6×10^4 cells/mL. Individual samples of 500 μL each are prepared in reaction vessels. One sample of each culture bottle is set aside and not transported for the negative control. Another sample is set aside as positive control and, before staining, is treated with TritonTM X-100 (Merck KGaA, Darmstadt, Germany), which disrupts the cells' membrane. Cells are transported with five different actuation settings as indicated in Table 8.1. Three individual samples are transported per setting and pump, leading to a total of 15 samples per setting. Results are averaged over all transported samples for each setting.

Table 8.1 Used actuation signals for the transport of cells. The waveforms are described in further detail in Section 8.3.1.2 and depicted the Figure.

	Waveform	Frequency in Hz	Abbreviation
Setting 1	Rectangular	15	Re_15
Setting 2	Sinusoidal	15	Sin_15
Setting 3	Rectangular with 60 Hz sinusoidal flanks (hybrid actuation)	15	Srs_15
Setting 4	Rectangular	60	Re_60
Setting 5	Sinusoidal	60	Sin_60

The experimental setup for the cell transport is depicted in Figure 8.2 b. The pump's inlet and outlet are connected with the inlet and outlet reservoir using flexible tubing with 4 cm length and 1.4 mm inner diameter. The inlet reservoir contains 500 μL of cell solution. To assure sufficient resuspension of cells, each reservoir is agitated carefully prior to transport that is completed in less than ten seconds. The cells are transported with the desired setting and collected in a reaction vessel. The solution is pumped one single time and not circulated or transported repeatedly. For cleaning, we passively flush the pumps with 20 mL buffer (autoMACS Running Buffer; Miltenyi Biotec B.V. & Co.

KG; Bergisch Gladbach, Germany) between samples with different actuation signals. After flushing, 500 μL of rinsing solution are collected and analysed for the number of cells to assure that the following sample is not influenced by remaining cells in the pump.

8.2.2.1. Propidium Iodide Cell Viability by Flow Cytometry

To evaluate the amount of intact and dead cells, samples are stained with propidium iodide (PI) solution (Miltenyi Biotec B.V. & Co. KG; Bergisch Gladbach, Germany), a nucleus staining agent that is not able to penetrate an intact membrane of viable cells. To each sample, including the positive control and “Non-pumped” samples (negative control), 6 μL PI is added and incubated for 15 min. All samples are washed and distributed to a 96 well plate for automatic flow cytometry measurements with the MACS Quant Analyzer 10 Optical FlowCytometer (Miltenyi Biotec B.V. & Co. KG; Bergisch Gladbach, Germany). To account for time effects, the positive and negative control are analysed both before and after all other samples with no visible change.

The collected data are gated for single cells using the height versus forward scatter area. The samples for a given actuation signal are averaged over all five pumps. For comparison of two sample groups that include 15 individual samples with approximately 30,000 cells each, we use a two-tailed *t*-test with a *p*-value of 0.02.

8.3. Results and Discussion

Cell transport with very limited available space is a challenging task. Both damage on the cells caused by the pump as well as pump degradation due to cell transport are possible. With a detailed experimental consideration, we intend to clarify possible influences and provide the basis for further improvements.

8.3.1. Pump Characterisation

Micro diaphragm pump characterisation includes the evaluation of the general properties of the pump as well as an investigation of the single stroke with different actuation mechanisms. The later generates information on the fluidic efficiency of each actuation and allows us to adapt the actuation signal to a fluidically optimal transport with less influence on the cells.

8.3.1.1. General Micro Diaphragm Pump Characterisation

To estimate the impact of cell transport on the diaphragm pump itself, all devices are characterized prior to and after the cell transport. It is possible for cells to accumulate in the pump chamber as well as in the dead volume around the valves and therefore lead to a pump degradation. A change in **stroke** or passive as well as active flow characteristics allows for better understanding of failure mechanisms.

The exact movement of the diaphragm is a crucial part of the pump’s functionality. A typical **stroke** measurement is shown in Figure 8.3 a, with the clear piezoelectric hysteresis. The **stroke height** determines the **stroke volume** and therefore the achievable flow rate of the system. The **stroke** measurement allows to detect mechanical constraints to the actuator’s movement. The average total **stroke** after cell transport is $81.7 \pm 3.9 \mu\text{m}$ and not significantly changed compared to the initial average **stroke** of $82.4 \pm 3.4 \mu\text{m}$ (Figure 8.3 b). These findings indicate that cells do not agglomerate in the chamber and block the actuator movement.

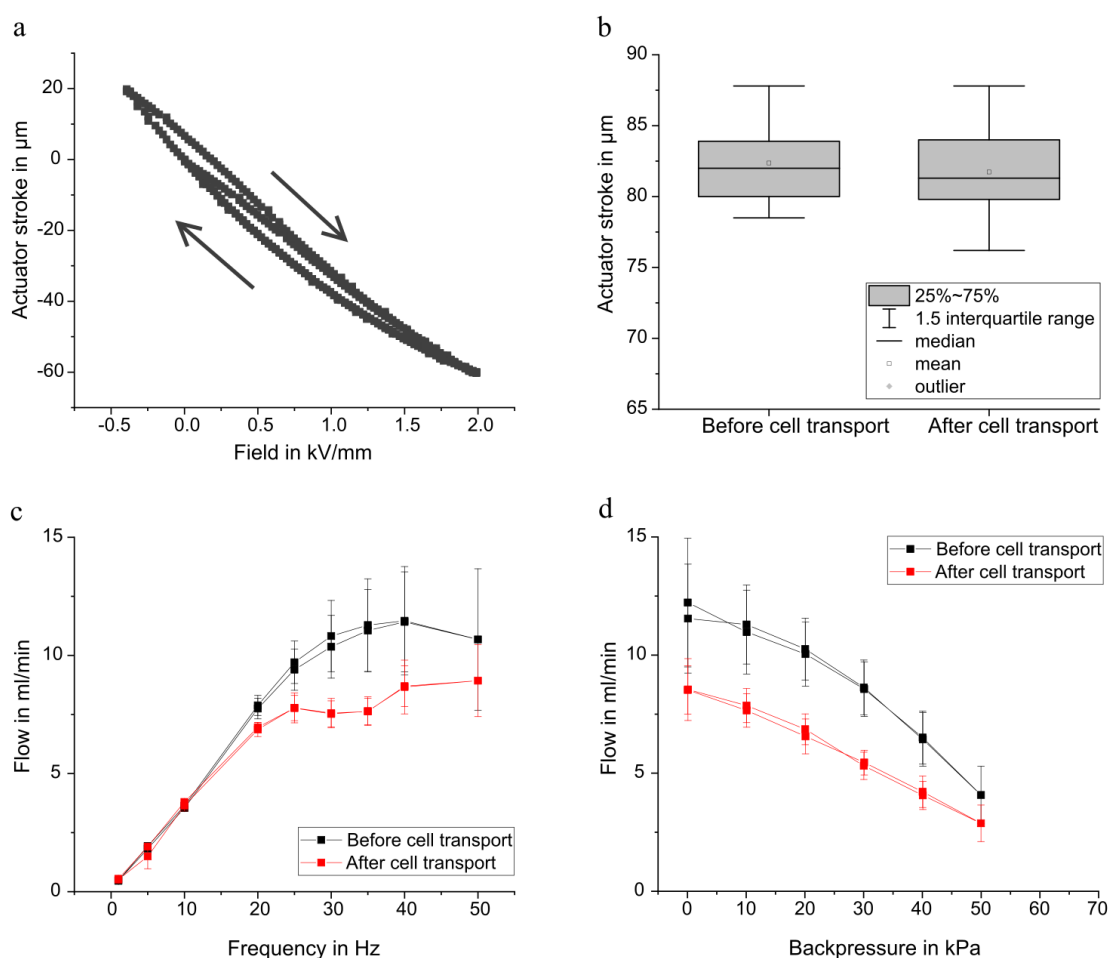


Figure 8.3 Mechanical and fluidical characterization of the tested micro diaphragm pumps. (a) The actuator displacement shows the typical piezoelectric hysteresis. Adapted from Bußmann et al. [213]; (b) There is no change in the total stroke height before and after the cell transport; (c) The frequency-dependant flow rate with 14 kPa backpressure at $-80/300 \text{ V}$ (corresponding to $-0.4/1.5 \text{ kV/mm}$) sinusoidal actuation remains nearly unchanged in the linear regime, but changes for high frequencies. The maximal achievable flow rate after cell transport is smaller; (d) Backpressure dependant flow rate at $-80/300 \text{ V}$ sinusoidal actuation with 30 Hz .

Figure 8.3 shows the frequency dependant flow rate of the used steel micro-pumps. The flow increases linearly with the frequency until dynamic damping effects in the chamber become dominant and the curve plateaus. In the non-linear regime, the flow strongly depends on the fluidic periphery [216]. Therefore, a performance comparison should take place in the linear regime. The flow prior to cell transport experiments matches the expectation based on former pump batches [213]. After cell transport, the average flow up to 10 Hz is equal to the flow before the exposure to cell solution. The ability to achieve the same flow at low frequencies indicates no significant change in the behaviour of the passive flap valves. Low frequencies with sinusoidal actuation lead to a slow actuator movement and therefore low pressure gradients. The valves are opened and closed comparatively slowly with low force. A bad valve quality is therefore often visible in the low frequency range. The assumption of constant valve performance before and after the cell transport is substantiated by the leakage rates, which only changed for one out of six pumps. The leakage rate at 50 kPa differential pressure of the pumps before cell transport is below 30 $\mu\text{L/min}$ for all samples. After transport, it remains unchanged for all but one pump that shows a drastically increased leakage rate of 260 $\mu\text{L/min}$. This

increase is potentially caused by fibres caught in the passive flap valves that were visible in the optical inspection and probably transported into the pump during use outside of the clean room environment. The leakage measurement always detects the leakage over both, the inlet as well as the outlet valve. If only one valve is sufficiently tight, the overall leakage is small. Significant backflow in active pump mode is still possible, if the other valve is leaking.

For higher frequencies, the average flow decreases and the end of the linear region is lower. A volume change in the chamber, due to agglomeration of cells or particles, is a possible explanation for the detected change in the fluidic performance. Furthermore, increased leakage through the passive flap valves can change the flow behaviour. However, as described above, increased leakage has a large influence on the flow at small frequencies and would be visible in the linear range.

The decrease in flow for higher frequencies after cell transport compared to the initial performance is also visible in the backpressure measurements of the pumps. With 30 Hz, sinusoidal actuation, the flow at 0 kPa is approximately 3 mL/min lower after the cell transport. The extrapolated **blocking pressure** however remains unchanged with approximately 70 kPa before and after cell transport. This indicates the same stiffness of the actuator and therefore no degradation of the ceramic itself or the adhesive connection during the experiments.

8.3.1.2. Single Stroke Characterisation

The single stroke measurement with varying actuation signals allows to estimate the fluidic efficiency of the transport. A single actuator stroke requires approximately 2 mJ and single stroke power consumption of the pump itself (without driving electronics) is independent of the waveform and frequency [213]. From the energy required for one pump stroke and the volume transported per stroke, we can calculate the power consumption per dosed volume. Since the energy per stroke is constant, it depends on the **single stroke volume** that again depends on the actuation signal.

A perfectly rectangular actuation generates the fastest actuator movement and therefore the fastest pressure built-up. Consequently, the actuation of the passive flap valves is rapid and backflow through insufficiently closed valves is minimized [68]. A lower flank steepness, as is the case for sinusoidal actuation, leads to a slower pressure built-up and slow opening and closing of the passive valves. It therefore allows a portion of the transported fluid to move backwards through the valves [68]. A steeper flank therefore leads to a higher **stroke volume**. However, the fast actuator movement also increases the strain on both, the pump as well as the dosed medium, since it leads to high mechanical stress in the piezoelectric actuator and increases the fluidic shear stress

A trade-off between fluidic efficiency and strain on pump and medium can be a hybrid actuation based on a rectangular waveform with sinusoidal flanks. Figure 8.4 shows the resulting waveform in comparison to other waveforms: the hybrid signal is a mix between a rectangular signal with a given frequency and a sinusoidal signal of a higher frequency. In order to evaluate which flank is appropriate, we determined the **single stroke volume** for several actuation frequencies with varying flanks. A frequency dependence of the **single stroke volume** is expected due to fluidic damping in the chamber at higher frequencies and flow rates. Figure 8.4 b depicts the dependence of the **single stroke volume** on the actuation frequency and flank steepness. The **single stroke volume** is reduced for 50 Hz actuation frequency compared to slower actuation, whereas it is independent of the actuation frequency up to 20 Hz.

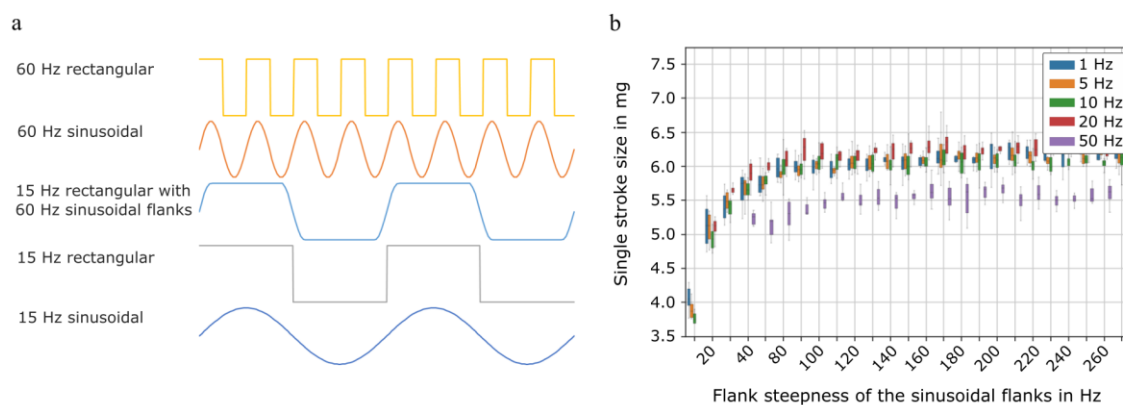


Figure 8.4 (a) Comparison of the different actuation signal chosen for cell transport. The hybrid signal of 15 Hz rectangular actuation with 60 Hz sinusoidal flanks is a mix of the depicted 15 Hz rectangular waveform and the 60 Hz sinusoidal waveform. (b) Single stroke volume transported by a micropump dependent on the actuation frequency and the steepness of the sinusoidal flanks.

For all tested frequencies, the **single stroke volume** plateaus for sufficiently steep flanks. The required flank steepness depends on the actuation frequency. While for actuation with 1 to 20 Hz, a flank steepness of approximately 60 Hz is sufficient, the **single stroke volume** at 50 Hz only plateaus at steeper flanks of approximately 90 Hz. The results are reproducible for all four evaluated pumps. These results indicate that the fluid transport is as efficient with sufficiently steep flanks as it is with rectangular actuation, however, the flank steepness needs to be comparatively high for higher actuation frequencies. The resulting flow rate for specific waveforms is verified with the measurement of the frequency dependant flow rate. Up to 25 Hz actuation frequency, the hybrid signal achieves the same flow rate as the rectangular signal. The experimental results are presented in Figure B.2 in the Appendix. Based on these findings, a 15 Hz hybrid signal with 60 Hz sinusoidal flank is chosen as one of the signals used for cell transport. This allows to compare the impact when the pump is actuated with sinusoidal, rectangular, or the hybrid signal.

8.3.2. Cell Transport

Viable cells are sensitive to their environment, and transport with a micro diaphragm pump can damage them in different ways. A first important indicator to assess the feasibility of cell transport with micro diaphragm pumps is the recovery rate of cells after transport. Neither the total cell concentration nor the percentages of cells within the gate deviate significantly between the negative control sample and the transported samples. Cells therefore do not accumulate within the pump, which corresponds well to the results of the electromechanical and fluidic characterisation of the pumps presented above.

8.3.2.1. Consideration of Effects Influencing the Cell Viability

Pumping can have a mechanical impact on the transported cells due to moving parts in the flow path. For instance, cells can get caught in between the valve and its seat. However, this scenario is unlikely: one pump stroke, and therefore one opening and closing motion of the valves, transports approximately 10 μL of fluid. The total fluid volume between the valve and its seat when the valve starts closing is calculated based on the valve geometry: the surface of the valve seat of 0.23 mm^2 and a valve opening of maximal 50 μm . It is approximately 0.01 μL for each valve. Therefore, if we assume that the cells are uniformly distributed and that all cells that are between the valve and its seat when

the valve starts closing get caught in the valve, this would only affect 0.2% of the transported cells. We thus assume that the damage caused by hard-hard touch squeezing is neglectable.

It is also imaginable that cells become damaged when they come into contact with sharp edges. In particular, the etched valve structure or the drilled inlet and outlet access constitute such sharp edges. However, fluid flow around the cells causes fluidic drag thus their fluidic resistance is high and the cells move towards the middle of the flow path. Hence, the cells likely flow around the edges without contact. The effect is already shown by Ozbey et al. [217] who observe cells moving towards the centre of the channel in laminar flow.

A likely influence on the cell viability is the experienced fluidic shear stress. Studies discuss the impact of shear on non-adherent cells and indicate that the size as well as the deformability of a cell have an influence on its behaviour when subjected to shear stress [217–219].

To generate a first understanding of the shear force the cells are subjected to when passing through the pump, we consider the analytic description of a strongly simplified model. We aim to compare the influence of specific geometries in the pump, e.g., chamber and valves, as well as different actuation signals. We do not intend to give a quantitative analysis of shear forces.

The valve as well as the pump chamber have a high aspect ratio: The valve seat is 300 μm long and the valve opens 50 μm ; the pump chamber is approximately 100 μm to 150 μm high (in the upwards position of the actuator) and we consider the distance of 5000 μm between the two valve openings as the gap length. We assume laminar gap flow in these geometries. Furthermore, for simplicity, we only consider the liquid medium itself and do not specifically calculate the velocity of the cells in this flow. This strong simplification allows a first comparison of geometries and actuation signals.

The shear stress of the laminar flow is given by

$$\sigma = \eta \frac{\partial v_x}{\partial z} \quad (8.1)$$

with the viscosity of the liquid η and the flow velocity v_x . Furthermore, the velocity profile of the laminar gap flow is parabolic

$$v_x(z) = \frac{\Delta p}{2\eta L_{gap}} (h_{gap}z - z^2) \quad (8.2)$$

and depends on the pressure difference Δp , the gap length L_{gap} , the gap height h_{gap} , and the viscosity of the liquid η . When the pump is active, the movement of the actuator diaphragm generates the pressure difference Δp that drives the fluid through the gap and therewith generates the fluidic shear forces. The maximal pressure that the bending actuator can achieve is its **blocking pressure**. This pressure is generated when the actuator is subjected to a rectangular actuation and the movement is extremely fast. Since the maximal pressure occurs during this fast actuator displacement, the pressure peak is independent of the actuation frequency for rectangular actuation. The maximal pressure difference depends on the bending actuator's geometry and used material and can be calculated with the analytical model presented by Herz et al. [155].

For sinusoidal actuation, the voltage change and therewith the actuator movement is considerably slower than for rectangular actuation. The time constant of the actuator movement and the fluid movement through the passive valves therefore converge and the maximal pressure peak decreases. Since the speed of actuator movement depends on the

actuation frequency for sinusoidal actuation, the generated pressure difference is also a function of the actuation frequency. Similarly, for the hybrid signal, the maximal pressure depends on the speed of the actuator's movement and therefore on the sinusoidal flank steepness of the signal. Based on the model by Herz et al. [155] the analytic description of the pressure peak of the sinusoidal actuation can be derived. However, the equation cannot be solved analytically and a numerical description will be part of future work. However, the analytical model allows for a qualitative comparison that shows that the shear force is maximal for rectangular actuation and minimal for sinusoidal actuation with a small frequency. Due to the relation between the maximal pressure and the flank steepness, the pressure difference and therewith the shear forces in this model are equal for sinusoidal actuation with 60 Hz and the hybrid signal with 60 Hz sinusoidal flanks.

To identify the most relevant pump geometries, the shear stress in the valve σ_{valve} and the chamber $\sigma_{chamber}$ are compared for rectangular actuation. For the simplified model, we assume gap flow in the valve as well as in the pump chamber as described above. Furthermore, we assume that the maximal pressure difference applies to both the chamber and the valve, even if in reality the pressure is split.

$$\sigma = \frac{\Delta p}{2L_{gap}} (h_{gap} - 2z) \quad (8.3)$$

$$\sigma_{max} = \sigma|_{z=0} = \frac{h_{gap}}{2L_{gap}} \Delta p \quad (8.4)$$

Based on Equation 8.4 and the geometry of the flow path (the valve seat length $L_{valve} = 300 \mu\text{m}$ and valve opening $h_{valve} = 50 \mu\text{m}$, as well as pump chamber length $L_{chamber} = 5000 \mu\text{m}$ and pump chamber height $h_{chamber} = 100$ to $150 \mu\text{m}$), the ratio of shear in the chamber and the valve can be estimated with

$$\frac{\sigma_{chamber}}{\sigma_{valve}} = \frac{L_{valve}}{L_{chamber}} \frac{h_{chamber}}{h_{valve}} \quad (8.5)$$

and is approximately 0.12 to 0.18. As can be seen from Formula 8.5, the ratio is independent of the pressure difference. The estimation shows that the shear stress at the valve unit is larger compared to the shear stress in the pump chamber. To further reduce the impact of the pump on cells, it is thus necessary to adapt the valve geometry to reduce the occurring shear stress in this area.

8.3.2.2. Viability of K-562 and Jurkat Cells after Transport

In this preliminary study, we only detect the immediate influence of the pump on the cells, since we measure the percentage of intact cells compared to the negative control. The influence of the transport on the long-term viability of the cells are not yet examined and will be part of future studies.

Both cell types are impacted by the pumping process. For K-562 cells, the non-pumped (negative) control samples contains $89.9 \pm 2.6\%$ intact cells; for Jurkat cells it contains $88.6 \pm 5.2\%$ intact cells. Figure 8.5 shows the change of the percentage of intact cells due to transport with the micro diaphragm pump with different actuation signals. The mean percentage of intact cells is slightly lower for all transported samples compared to the non-pumped control and the decrease is significant with $p \leq 0.02$.

The various actuation signals cause different damage of the K-562 cells. The largest decrease of intact cells is caused by the actuation with 60 Hz and the use of sinusoidal

or rectangular actuation does not have a significance influence on the impact. With an average of 75.4% intact cells, there are 14.5 percentage points less intact cells compared to the non-pumped control. A significantly lower damage ($p \leq 0.02$) is caused by sinusoidal actuation with 15 Hz, which is the smoothest actuation. The mean percentage of intact cells is $85.4 \pm 4.6\%$ and therefore only 4.5 percentage points lower than the non-pumped control. The smaller impact can be due to the overall lower flow rate and thus reduced shear force. Furthermore, the maximal speed of the diaphragm and therewith the maximal pressure difference is decreased and evokes a smaller maximal pressure gradient. The average damage caused by a rectangular actuation with 15 Hz shows, that the faster actuator movement causes more damage. However, the difference is only significant with $p \leq 0.05$. As described above, for rectangular actuation, the maximal pressure difference does not depend on the actuation frequency. Therefore, the analytical model cannot explain the different impact of 60 Hz and 15 Hz rectangular actuation on the transported cells. However, the average overall flow rate and thus average shear in the pump and periphery are larger for 60 Hz actuation. The transport with the hybrid signal (15 Hz rectangular signal with 60 Hz sinusoidal flanks: srs_15) imposes a slower actuator movement compared to 15 Hz rectangular actuation while maintaining the fluidic performance. The impact on the cells is also slightly reduced, but the difference is not significant.

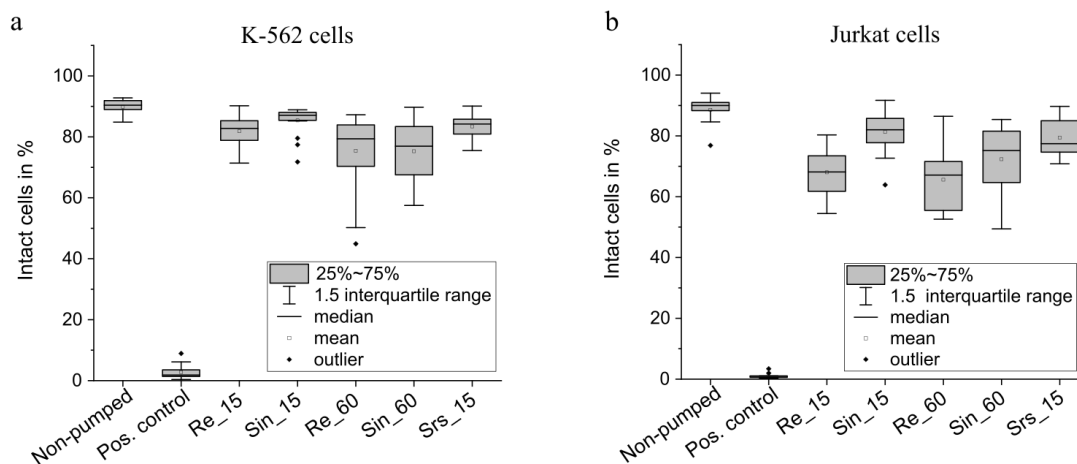


Figure 8.5 Percentage of viable cells after gating for single cells in the control samples as well as in the transported cell solution for K-562 cells (a) and Jurkat cells (b). Data for each actuation type include 15 individual samples.

The impact of the pump on Jurkat cells is more pronounced. The diameter of the two cell lines is similar, though the deformability is different. Since the deformability determines the path of the cell in the fluidic channel [218], the increased impact on Jurkat cells can among others be caused by a difference in the experienced fluidic shear stress. The largest decrease of intact cells occurs after transport with a rectangular actuation of 60 Hz, which is the most stressful actuation. It generates the fastest actuator movement, highest pressure peak and the highest overall flow. On average, $65.6 \pm 10.3\%$ of cells stay intact after this transport, nearly one quarter of cells less than the control. A similar large impact (no significant difference, $p \geq 0.05$) is caused by rectangular actuation with only 15 Hz ($68.0 \pm 8.0\%$). As described above, the maximal pressure peak and therefore the maximal fluidic shear stress caused by the pressure peak that pushes fluid through the valve channel, do not depend on the applied frequency for rectangular actuation. The similar reduction of viable cells for 15 Hz and 60 Hz rectangular actuation indicates that this maximal shear stress has a significant influence on the transported cells. For both

actuation frequencies, sinusoidal actuation causes less damage with $81.3 \pm 7.6\%$ intact cells for 15 Hz actuation and $72.3 \pm 10.3\%$ for 60 Hz. However, the sinusoidal actuation with a frequency of 60 Hz still stresses the cells and the impact is not significantly different to rectangular actuation ($p \geq 0.05$). The influence of the transport with hybrid actuation (15 Hz rectangular actuation with 60 Hz sinusoidal flanks) on the cells is very similar to the 15 Hz sinusoidal actuation and the difference is not significant with $p \geq 0.05$. According to the analytical model described above, the generated pressure peak and imposed shear are the same for the hybrid actuation and 60 Hz sinusoidal actuation, since the flank steepness of the two signals is equal. The different impact of the hybrid actuation and 60 Hz sinusoidal actuation indicate that not only the maximal experienced shear, but also the average overall flow rate impact the cells. The average flow is higher for the 60 Hz sinusoidal actuation than for the hybrid signal (Figure B.2, Appendix B).

Overall, the transport with 15 Hz hybrid signal has a similar impact on the cells as the transport with sinusoidal actuation (Figure 8.5) while maintaining the fluidic performance of rectangular actuation as shown by the comparison of the [single stroke volume](#) as well as the flow characterisation presented in Figure B.2, Appendix B. The hybrid actuation therefore offers the possibility of efficient cell transport while minimizing the damage. However, for both cell types, the impact is still significant with approximately 7.3 and 4.6 percentage points less intact cells compared to the control sample for Jurkat and K-562 cells respectively. It is thus necessary to further optimize the pump systems with respect to the exact valve geometry, the pump chamber, as well as the inlet and outlet channel.

8.4. Conclusion

Overall, the standard characterisation of the pumps before and after cell transport shows a small degradation but no complete loss of functionality. It is important to notice that during the transportation experiments the pumps were not used in a cleanroom environment and therefore not only exposed to cell solution but also to contamination such as fibres. The optical examination of the valves did show fibres in several pumps. Hence, it is not possible to distinguish degradation caused by cells from other influences and further evaluations are necessary to assess possible pump degradation. In preliminary experiments we plan to evaluate the particle resistance of the micro diaphragm pumps with the transport of polystyrene particles, before we evaluate the influence of cells.

Furthermore, a more detailed investigation of the pump's impact on the cells is necessary. In this preliminary experiment, we only evaluated immediate damage to the cells by staining. However, a long-term effect, e.g., reduced activity, is very likely. We will therefore conduct further evaluation including cell activity assays and long-term evaluation.

Overall, the results on pump performance as well as the impact on the cells are very promising. The impact on the cells can be further minimized with the optimization of the pump's geometry. The analytical estimation of shear forces in the pump shows higher shear forces in the valve gap compared to the chamber. To reduce this shear stress, an optimisation towards larger valve opening can be envisaged by a reduction of the stiffness of the flap valve. Furthermore, shear stress can be reduced by adapting the channel size of the inlet and outlet as well as the pump chamber geometry in terms of structure or

height. With those measures we expect to further limit the damage caused by the pump and enable the development of improved and miniaturized transport systems.

Data Availability Statement

The [actuator stroke](#), fluidic test, and simulation data that support the findings of this study are available in Fordatis–Research Data Repository of Fraunhofer-Gesellschaft with the identifier <https://fordatis.fraunhofer.de/handle/fordatis/233> (accessed 26.11.2021).

Acknowledgments

This research is part of the Moore4Medical project, which has received funding within the Electronic Components and Systems for European Leadership Joint Undertaking (ECSEL JU) in collaboration with the European Union’s H2020 Framework Programme (H2020/2014–2020) and National Authorities, under grant agreement H2020-ECSEL-2019-IA-876190 www.moore4medical.eu (accessed 26.11.2021).

Special thanks to Alfred Michelfelder for his work in maintaining the cell cultures.

9. Particle Tolerance of Metal Micro Diaphragm Pumps

Bußmann, Agnes^{a,b}, Surendran, Nivedha^a, Hoffmann, Sophie^a

^aFraunhofer EMFT Research Institution for Microsystems and Solid State Technologies, Hansastrasse 27d, 80686 Munich, Germany

^bKIT, MAB - Biomolecular Separation Engineering, Fritz-Haber-Weg 2, 76131 Karlsruhe, Germany

Abstract

Micropumps present the prospect of improvement for numerous **microfluidic** applications, since they can offer a solution for size, energy, or cost constraints. However, many fluidic tasks, especially in biomedical application, involve the transport of fluids that contain particles, debris, cells, or even fibres. Unfortunately, micropumps are specifically sensitive to any type of solid object in the transported solution, since they have narrow fluid paths and fragile small structures. To enable a reliable use, a detailed experimental analysis of the particles' impact is necessary. This work is an experimental investigation with highly concentrated polystyrene particle solution with 1 μm and 16 μm diameter particles as a model system. An optical investigation of the valve structure before and after transport shows deposition in corners and curves. Additional deposition within the pump chamber is indicated by a reduced **actuator stroke** after the transport of 16 μm particles. The degradation of the pumps is also visible in the flow characteristics: the overall flow rate and achievable backpressure decreases and leakage rates increase severely. Once again, the impact of 16 μm particles is more severe. The preliminary experiments show a large impact of the particle transport. However, no tested pump fails completely. Based on this experiments, geometric adaptations of the pumps can be developed that allow for more reliable particle transport.

9.1. Introduction

Micro diaphragm pumps offer the possibility of miniaturisation and automatization of biomedical **microfluidic** applications, and even enable the development of completely new approaches. Most of these applications up until today rely on capillary forces, bulky external pump systems or manual handling. Examples are the transport of samples within micro total analysis systems (**μTAS**) [194, 195], transport of cell culture medium, reagents and test substances in cell culture [220], or three dimensional bioprinting for pharmaceutical research, medical application, or the food industry [200, 201].

The advantages of micropumps for those applications are evident: they allow to manufacture economic disposable devices, omit the need for bulky pump systems and long connecting tubing, enable automatization and consequently reduce the need of manual handling (outside the incubator), are energy as well as space efficient, and precise. However, the biomedical field is a challenging environment for **microfluidic** actuation. The transported medium is usually a solution composed of many substances and even smaller or larger particles. Furthermore, handling outside of a clean room environment, e.g., when sampling solutions, makes the occurrence of contaminations such as particles or fibres likely. In the case of automated cell culture or three dimensional bioprinting, the transport of cell debris or cell solution is necessary.

To enable a reliable use within biomedical application, micropumps have to be capable of transporting the medium at hand including all contained substances. However, particles, cells and contaminations can interfere with the functionality of a micro diaphragm pump, since it is often extremely miniaturized and thus the fluid path is often narrow. Furthermore, micropumps usually contain fragile, small structures. It is therefore necessary to investigate possible interaction between the transported medium and the pump to evaluate failure mechanisms and implement mitigation methods.

In this study, we experimentally evaluate the particle tolerance of EMFT's piezoelectric metal diaphragm pumps. Therewith, we enable a detailed analysis of the pumps' capability to transport particle-laden fluids. The aim of this first experimental investigation is to understand failure patterns and enable improvements of the pump towards a more reliable transport of fluids other than deionised water and gas.

9.2. Materials and Methods

All experiments are conducted with Fraunhofer EMFT's stainless-steel pumps that are described in detail by Bußmann et al. [213]. The pumps with a diameter of 20 mm consist of a steel pump body that includes two passive spring valves (inlet and outlet) and an actuator diaphragm. Using a two-component epoxy adhesive, a piezoelectric disc actuator (PIC 151, $d = 16 \text{ mm}$, $t = 200 \text{ }\mu\text{m}$) is glued to the metal diaphragm.

The pumping principle is depicted in Figure 9.1 a. The indirect piezoelectric effect causes the piezoelectric ceramic to contract and expand when it is subjected to an alternating high voltage field. This length variation leads to an oscillatory bending movement of the actuator diaphragm, which expands and compresses the pump chamber. The flow constraint by the passive spring valves leads to a directed fluid transport.

For the fluidic and electromechanics evaluations, the pumps are mounted into test housings. These polycarbonate cases are equipped with O-ring sealings to prevent leakage past the pump. For electrical contact, a custom-made PCB is integrated and soldered to the ceramic, and screwed stainless-steel barbs enable easy fluidic connection.

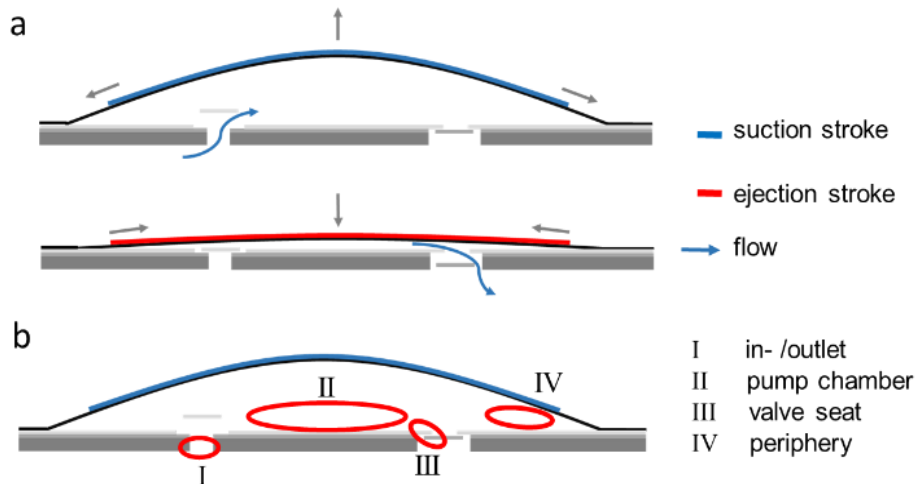


Figure 9.1 Schematic of the piezoelectrically driven metal micro diaphragm pump; (a) An alternating high voltage signal leads to an oscillatory diaphragm movement. In combination with passive flow valves, that leads to directed fluid transport; (b) Particles can agglomerate in the valve openings (I), the chamber (II), between the valve and its seat (III), or in the periphery of the pump chamber (IV) and decrease the fluidic performance.

Due to the pump's geometry, there are several areas where particles can impair the devices functionality (Figure 9.1 b). Agglomeration within the periphery of the chamber (IV) blocks the diaphragm movement and therewith limits the **stroke volume** of the pump. In this case, the detected **actuator stroke** in the optical measurement (Chapter 9.2.1) is reduced. Similar accounts for agglomerates in the middle of the chamber (II). Accumulated particles in the chamber or in the flow channels (I) increase the flow resistance during fluid transport. Consequently, the maximal achievable flow rate gets reduced. Furthermore, particles can impair the functionality of the passive flap valves. Caught between the valve and its seat, they can cause valve sticking that inhibits sufficient opening and therefore hinders throughflow. Additionally, pinned particles cause a remaining gap of the valve, which results in backwards leakage during the actuator's movement and reduces the achieved flow rate. In addition, passive reverse leakage in turned off state can increase.

9.2.1. Optical Examination of the Valve Structure

The passive spring valves of the micro diaphragm pump are crucial for its functionality. A large initial gap leads to leakage during the suction and ejection stroke and impairs the directed fluid transport. Particles can accumulate in the valve structures, increase leakage, cause valve sticking or increase the flow resistance even in the open valve state. To distinguish different failure mechanisms when transporting particle-laden fluids, an optical investigation of the valves complements the investigation of the fluidic performance and **actuator stroke** measurements.

For the optical investigation, pumps are disassembled from their test housing. To prevent contamination, the disassembly as well as the optical investigation take place under clean, laminar air flow. The valves are imaged individually with a Leica reflected light microscope (equipped with a DMC5400 camera, LED 5000 light, M205 C sample table). For comparison, valves are investigated before and after the particle transport, as well as after cleaning of the pump. The camber is not imaged, since its optical inspection is a destructive examination, and sample preparation likely affects the particle allocation, geometry of the valves, and actuator position.

9.2.2. Stroke measurements

The movement of the bending actuator gives a first indication on the pump's functionality. The distance between the highest and lowest turning point of the pump's actuator diaphragm is called **stroke height**. Particles that agglomerate in the pump chamber can block the actuator movement and thus reduce the fluidic performance of the **micro-fluidic** actuator.

The stroke measurement is the optical detection of the actuator's position when subjected to a quasi-static voltage (amplifier SVR 500-3, piezosystem jena GmbH). The movement is detected with a white light profilometer (Fries Research and Technology; sensor range: 3 mm; maximal resolution 30 nm). The actuation voltage is cycled automatically two times from -80 V to 400 V to track the piezoelectric hysteresis. Measurement automatization implies constant time steps between measurements and thus reduces the impact of piezoelectric time effects. The voltage range is extended compared to the standard actuation voltage of the piezoelectric ceramic (-80/300 V), to detect abnormalities just after the normal range of movement. Due to inaccuracies when positioning the pump, the overall accuracy of the detected stroke is $\pm 2 \mu\text{m}$.

9.2.3. Fluidic test

To investigate the impact of particle transport on the fluidic performance of the micro diaphragm pump, a detailed experimental characterization of its properties is conducted before and after particle transport, as well as after manual cleaning of the samples. The fluidic characterization includes in the listed order the measurement of leakage, frequency dependent active flow, and pressure dependent active flow. Table 9.1 gives an overview of the used actuation amplitude, frequency, and applied backpressure. All active measurements are conducted with sinusoidal pump actuation.

Table 9.1 Flow characterisation of the metal micro diaphragm pumps. When actuated, the pumps are driven with a sinusoidal voltage signal.

Measurement	Amplitude in V	Frequency in Hz	Pressure in kP
Leakage	-	-	0 to 5
Frequency dependent flow	-80/300	1 to 50	14
Pressure dependent flow	-80/30	30	0 to 50

The test setup consists of an inlet reservoir that is pressure compensated via a filter, silicone tubing for fluidic connections, a Coriflow sensor (Bronkhorts ML120V00: range 0.8 $\mu\text{L}/\text{min}$ to 500 $\mu\text{L}/\text{min}$, accuracy: $\pm 0.2\%$), the tested pump, and a pressurized outlet reservoir (pressure controller: Mensor CPC3000: range -0.5 bar to 2 bar, accuracy: ± 0.05 kPa). The pump is placed behind the flow sensor to prevent any particles remaining in the pump from reaching the sensor. However, this setup lowers the maximal detected flow, since the flow sensor depicts a fluidic resistance, and the suction of the pump is less powerful than its ejection. This reduction is unproblematic for the conducted study, since only changes in the performance are investigated and it is not our aim to evaluate the maximal achievable performance of a pump type.

9.2.4. Particle Transport

To investigate the influence of particle-laden solution on the micropumps, they transport a polystyrene particle solution for a given time in a loop. After this defined strain, the standard characterisation is repeated.

As depicted in Figure 9.2, the pump moves the particle-laden fluid from a reservoir and transports it back into the same reservoir. The transport is effectuated for 10 min. There is enough sample volume and the used tubing is connected in a way that no air enters the pump chamber. The functionality of the pump is verified at the beginning and the end of the experiment: Priming is actively performed by the pump itself and the timer only started if the pump is able to self-prime, and after the duration of transport the inlet is removed from the reservoir and the sample volume that remains in the pump is actively ejected into the reservoir proving that the pump is still functional. The electric actuation of the pump during the particle transport is achieved with a miniaturized hand-held electronic developed at [Fraunhofer EMFT](#). This enables the parallel actuation of 10 pumps and allows for a statistically relevant investigation.

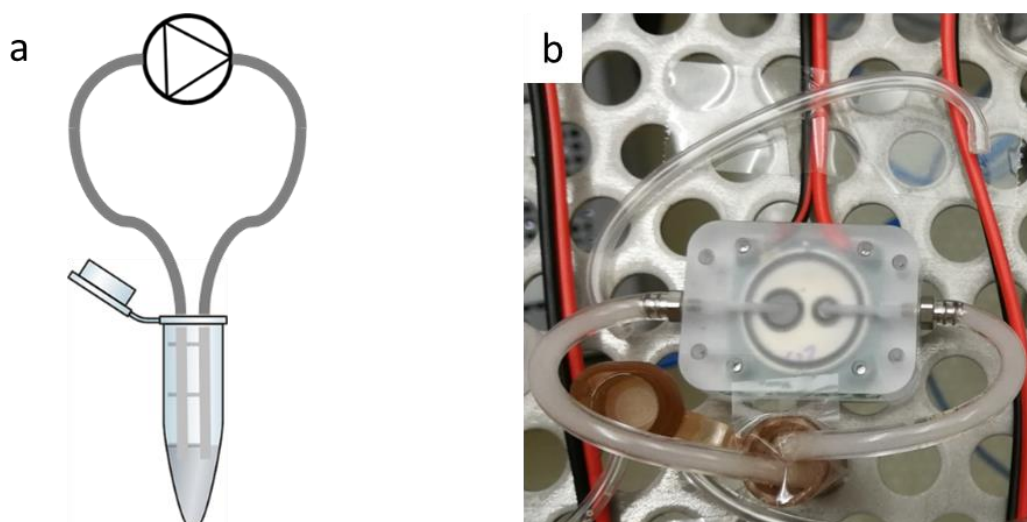


Figure 9.2 Fluidic setup for the transport of particle solution; (a) schematic depiction of the reservoir, fluidic connections and the pump; (b) photograph of the setup. The pump moves the fluid in a circle with a constant actuation with a 15 Hz sinusoidal voltage signal of -80/300 V.

The model particles chosen for this investigation are polystyrene beads of different size (Table 9.2). The advantage of polystyrene is the flexibly and precisely adjustable size of the beads. The small sized beads of approximately 1 μm diameter are chosen to investigate if there is a size limit up until that no damage is caused. Particles over 1 μm can easily be filtered without adding an enormous flow resistance with the added filter. The larger particles of approximately 16 μm diameter are investigated, since they are similar to the size of the transported cells described in Chapter 7 and 8.

Table 9.2 Overview of the used particle solution and number of pumps used for the transport of the respective particles

Particle Diameter	Particle Concentration	Nr of Pumps	Transport Duration
$0.97 \pm 0.03 \mu\text{m}$	5 % w/v	12	10 min
$16.6 \pm 0.28 \mu\text{m}$	10 % w/v	5	10 min

An important reason for the choice of polystyrene as model system is that the density of polystyrene ($\rho = 1.05 \text{ g/cm}^3$) is very close to the density of water. Therefore, the beads only precipitate extremely slowly and with sufficient agitation, as created by the pumping, not at all. The solution of polystyrene particles contains Tween® 20 to prevent spontaneous agglomeration.

9.3. Results and Discussion

The 17 pumps used in this investigation are characterised before and after the transport of particles. The detailed optical, electromechanical and fluidical characterisation helps to understand failure mechanisms.

9.3.1. Optical Valve Inspection

Imaging of the valves is the first characterisation. After the particle transport, the optical inspection takes place before any of the other measurements, since especially the flow characterisation during which the pump is flushed with clean DI water, can alter the distribution of particles within the valve structures. Before the transport of particles, the

valve structures are examined for contamination. Especially any fibres or residues of silicon tubing that can interfere with the passive spring valves functionality are of interest and would lead to the exclusion of the sample from the study. None of the pumps show any foreign material within the valves (Figure 9.3).

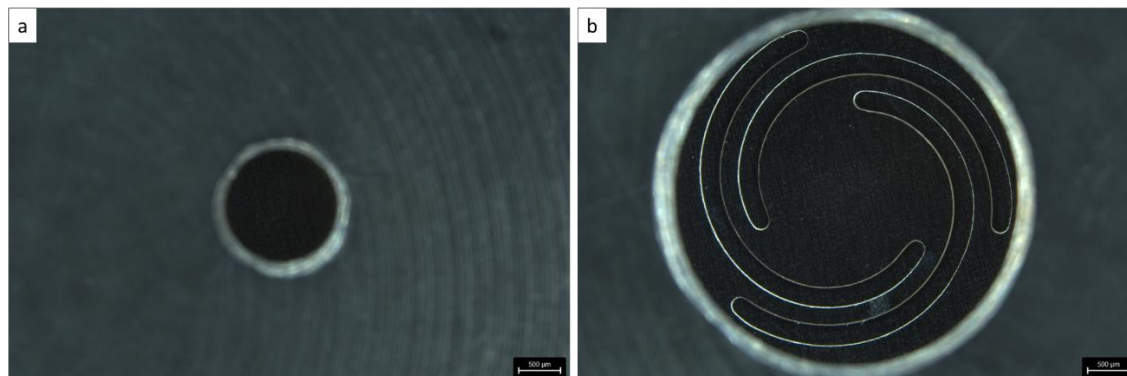


Figure 9.3 Exemplary inlet (a) and outlet (b) valve of a steel micro diaphragm pump (pump P32009-187) before particle transport. The scale bar represents 500 μm .

The optical inspection after the transport of particles reveals a strong deposition (Figure 9.4). Especially fine curves, as well as edges are affected. However, also flat surfaces, e.g., the surface of the spring valves show an aggregation of particles.

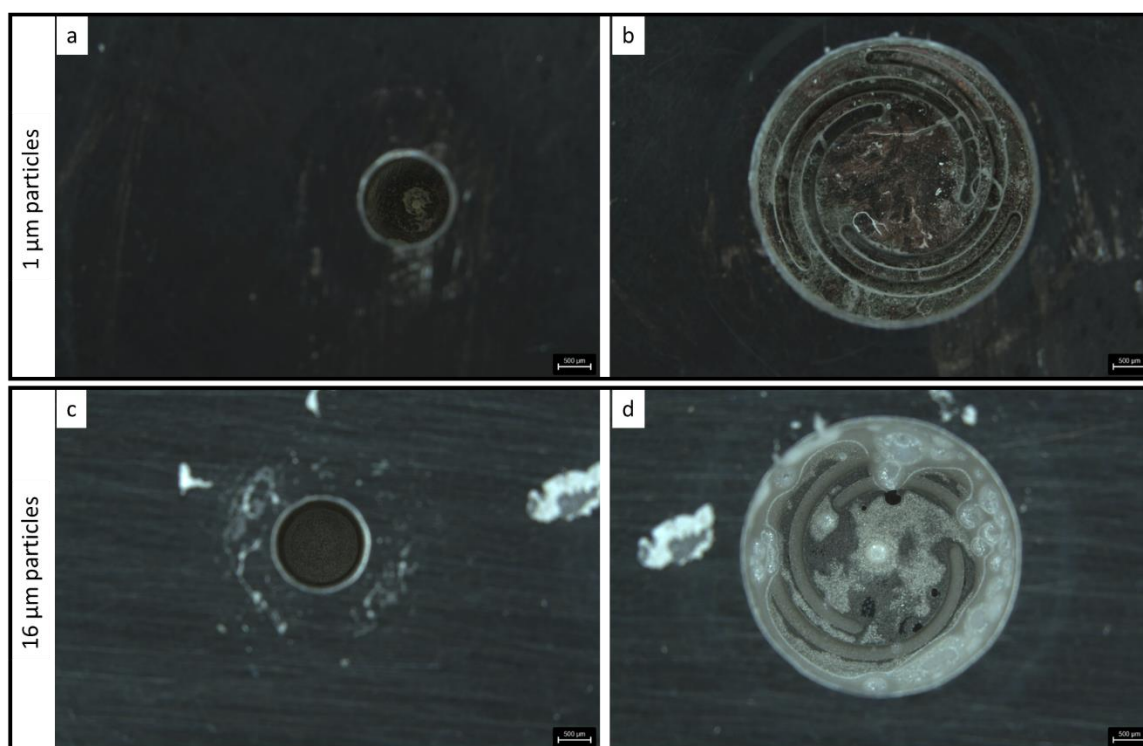


Figure 9.4 Exemplary images of the valve structures of two pumps after the transport of particle-laden solution. (a) inlet of P32009-214 that transported 1 μm particles; (b) outlet of P32009-214 (1 μm particles); (c) inlet of P32009-247 that transported 16 μm particles; (d) outlet of P32009-247 (16 μm particles). Deposition within edges and corners is clearly visible. The scale bars represent 500 μm .

Generally, the deposition of particles is less severe for the 1 μm polystyrene particle solution. The deposited particle layer appears thinner and moreover, the stainless-steel surface is visible in many areas. The distribution of particles is most common in corners and similar for all twelve tested pumps. The investigation of the five pumps that

transported a solution of 16 μm particles shows a larger deviation between individual pumps (Figure 9.5)

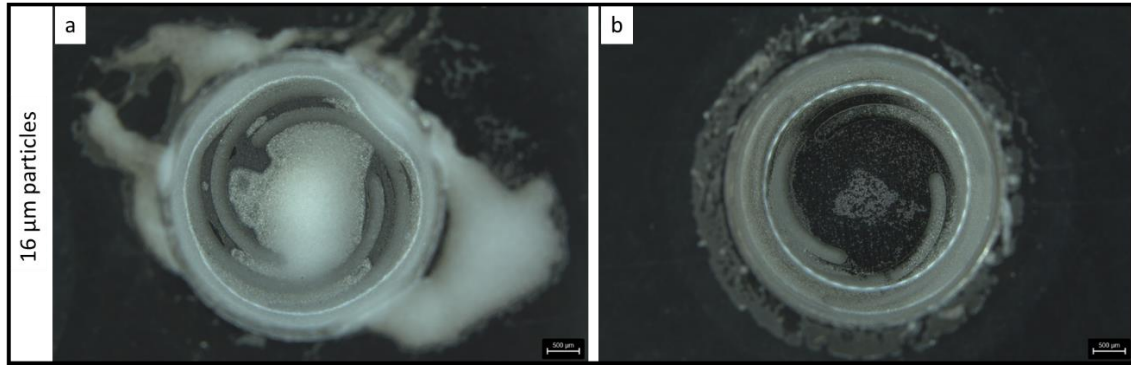


Figure 9.5 Difference in particle deposition between individual pumps after the transport of 16 μm polystyrene particles, (a) P32009-200, (b) P32009-193; the scale bars represent 500 μm

The large differences between individual pumps become apparent in the optical **actuator stroke** measurement as well as the decrease in fluidic performance of individual devices. Pumps that show many deposited particles within their valve structure tend to have a higher loss in fluidic performance.

9.3.2. Actuator Stroke Measurement

The first indication for the functionality of the micro diaphragm pump is its **actuator stroke**. It is undesirable for the pump to show a touchdown, which is the mechanical blocking of the actuator diaphragm when it reaches the chamber bottom before the maximal positive actuation voltage is applied. None of the tested pumps show actuator blocking or other abnormalities in the actuator movement. The transport of particles with a diameter of approximately 1 μm does not interfere with the **actuator stroke**, while the larger particles with a diameter of approximately 16 μm damages the pump severely (Table 9.3).

Table 9.3 Change in the **actuator stroke** after the transport of 1 μm particles and 16 μm particles respectively

Particles	Nr of pumps	Stroke Height Before Transport	Stroke Height After Transport
\varnothing 1 μm	12	$72 \pm 11 \mu\text{m}$	$69 \pm 9 \mu\text{m}$
\varnothing 16 μm	5	$67 \pm 4 \mu\text{m}$	$29 \pm 8 \mu\text{m}$

Even with the small sample size of only five pumps for the transport of large particles, the loss in **actuator stroke** is extremely significant. The reduction of stroke is likely caused by mechanical blocking. The voltage dependant hysteresis of the actuator shows a slight bend and the subsequent severely reduced slope leads the large reduction of **stroke**.

9.3.3. Flow Characterisation

To evaluate the performance of a micro diaphragm pump, detailed flow characterisation is necessary. The performance in general depends on the pump design as well as the quality of the individual parts. There are different effects that can decrease the flow

performance of a micro diaphragm pump. A loss in **actuator stroke** reduces the volume transported per stroke and due to direct proportionality, the achieved flow rate. Furthermore, the flow rate can be reduced due to increased leakage in the valves.

A reduced **stroke** is visible already without backpressure and for any frequency within the linear flow regime. An increased leakage of the valves can remain unrecognized if the flow rate is only measured without applied backpressure and a sufficiently high frequency. The impact of a small degradation of the valves is more severe on transport with lower frequencies of a sinusoidal signal, since the pressure peak in the chamber that actuates the passive valves is less pronounced. Additionally, applied backpressure increases this effect, since a larger pressure peak is necessary to eject the volume from the chamber. The flow reduction at low sinusoidal actuation frequencies adds information to the leakage measurement: While the passive leakage measurement detects the leakage over both valves and therefore mostly evaluates the tighter valve (with better quality), the flow measurement is affected already by one bad valve and adds information on the inferior valve.

The transport of particles increases the passive leakage of the investigated micro-pumps. After 10 min of transporting 1 μm polystyrene particles, the leakage of the twelve pumps increases in average by 50 %. The influence of 16 μm particles on the five used pumps is more severe with a leakage increase of in average 130 %.

The flow characterisation shows a degradation that corresponds well to the earlier findings. After transport of the 1 μm particles, the pumps did not show a significant decrease in the **stroke height** and a less severe increase of leakage rates. Consequently, the influence of the particle transport on the achieved flow without backpressure is small (Figure 9.5 a). However, an increase of pressure shows a stronger decrease of flow and the achievable backpressure is reduced to 50 kPa compared to approximately 75 kPa of the clean pumps. The decrease of the achievable backpressure substantiates the findings of the leakage measurements.

Once again, the impact of the larger particles is more severe (Figure 9.5 b): The flow at 0 kPa backpressure is already significantly reduced with a mean achieved flow of approximately half the initial value. These findings correspond well to the **stroke height** that was also reduced by approximately half. Furthermore, the decrease of the flow with the applied backpressure is substantial and the average flow reaches already zero at 10 kPa backpressure. The large leakage rates of the valves impede fluid transport against pressure.

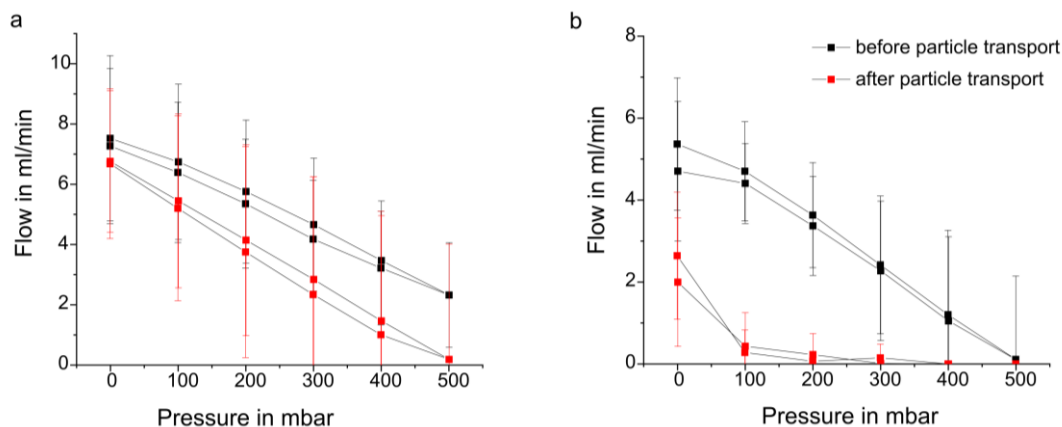


Figure 9.6 Backpressure characterisation before and after the transport of 1 μm (a) and 16 μm (b) particles. The error bars depict the standard deviation of twelve (a) and five (b) pumps respectively.

9.4. Discussion and Conclusion

The presented evaluation of the particle tolerance of our piezoelectric micro diaphragm pumps on the model of polystyrene particles of approximately 1 μm and 16 μm diameter shows a considerable impact on the **microfluidic** device. In our experimental characterisation we detect a more severe influence of larger particles that cause an **actuator stroke** and flow rate decrease to half of the initial values. After the transport of the larger particles, pumping against backpressure is nearly impossible due to the severe impact on the valves and thus evident increase in leakage rates. The optical evaluation of the valves substantiates these findings as it shows a more severe particle deposition after the transport of larger particles. The impact of smaller particles is less pronounced with no significant reduction of the **actuator stroke** or the flow rate at 0 kPa backpressure. However, the capability of the pumps to transport fluid against backpressure is reduced and zero flow is already reached at 50 kPa compared to 75 kPa of the clean devices.

It is important to notice that our experiment was set up deliberately challenging: The concentration of particles in solution is high with 5 %w/v and 10 %w/v for the small and large particles respectively, and a lower concentration would cause less degradation in the same time period. That concentration corresponds to 9×10^7 beads/ μL for the 1 μm diameter particles and 4.4×10^4 beads/ μL for the large particles. As a comparison, the cell transport in Chapter 7 and 8 was conducted with cell solution containing 200 cells/ μL and thus approximately a 200 times lower concentration. However, the cell concentration for bioprinting application can go up to 10^4 cells/ μL [221–223], which is why the pumps were subjected to a respectively high particle concentration.

The experimental analysis shows that larger particles cause more damage and provoke different failure mechanisms than smaller particles, such as the decrease of **actuator stroke**. However, also small particles cause degradation, especially of the passive spring valves. In subsequent development steps a more detailed understanding of these effects is necessary. In follow up experiments, we are going to evaluate if there is an upper limit of the particle concentration that the pumps can still transport without occlusion and significant increase in leakage. Since deposition effects strongly depend on the time, a long-term evaluation of the transport of particles has to be included into the experiments. Both, large and small particles are of interest in smaller concentrations, since the concentration limit for cell transport can be estimated with the larger particles, while a maximal supportable contamination with small debris can be estimated using the particles with a diameter of 1 μm . In addition to different particle concentrations, the particle geometry has to be varied for a more detailed understanding of the impact on the pumps and their reliability in specific applications. For example, fibres can be caught in the valves and there-with lead to more severe damage than individual particles.

A long-term aim of the device development is the adaptation towards more particle, fibre and contamination tolerance. To that end, geometric adaptations are necessary. The number of sharp edges needs to be reduced. For example, an angular drilled hole for the inlet and outlet can decrease corners with little flow and high tendency for particle deposition. In addition, such an adaptation can increase the achievable flow rate of the pump, since it lowers the fluidic resistance of the flow path. Furthermore, it would be advantages to increase the pump chamber height and minimize areas of little to no flow. This adaptation is more problematic, since it negatively influences the fluidic properties of the pump. A higher pump chamber (up until the outer periphery of the chamber) decreases the **compression ratio** remarkably and thus interferes with the ability of the device

to transport gas and liquid-gas mixtures. A possibility can be the implementation of a rip structure, that guides the flow and enables easier transport of particles within structured channels on the chamber bottom without decreasing the **bubble tolerance** significantly.

Overall, the presented experiments prove the feasibility of particle transport even in high concentrations. However, the degradation of the micropumps demands for further development steps to increase their robustness against contamination and enable a reliable long-term use in applications with demanding media.

Acknowledgement

This work is part of the Moore4Medical project funded by the ECSEL Joint Undertaking under grant number H2020-ECSEL-2019-IA-876190. www.moore4medical.eu

Data availability

The **actuator stroke**, fluidic test, and optical evaluation data that support the findings of this study are available in Fordatis – Research Data Repository of Fraunhofer-Gesellschaft with the identifier <https://fordatis.fraunhofer.de/handle/fordatis/228>

10. Conclusion and Outlook

Despite the evident possibility to improve medical treatment, micropumps are not commonly used in medical devices, and the industrialization of diaphragm pumps is still pending. A detailed analysis of the requirements for biomedical applications and the existing research on [microfluidic](#) actuators reveals open research questions that need to be addressed before a safe and reliable use is possible. The aim of this work is to advance the biomedical application of piezoelectric micro diaphragm pumps. This actuation principle is of particular interest, since it achieves high forces, high actuation frequencies, is easy to use, and is energy-efficient.

There are two major reasons that hinder the medical application of micropumps. To begin with, the implementation of a new dosing method is a large technological step. Such an enormous change requires a large initial investment to cover the development, implementation, as well as approval of the device. Furthermore, micropump research in literature mostly stays superficial, and presented devices have not been fully optimized. For instance, there is few to no data available concerning the reliability, dosing [precision](#), or the interaction between the pump and dosed medium. To address this shortcoming, this work includes detailed experimental investigations of [Fraunhofer EMFT](#)'s micropumps and improves the devices for biomedical applications.

The piezoelectric actuator is a central element of the micro diaphragm pump and needs to be well understood to enable targeted pump design and reliable use. Consequently, the first part of this thesis addresses this component, initially by itself (Chapter 3) and subsequently as part of the micro diaphragm pump (Chapter 4). The results of the experimental investigation of the [large-signal](#) piezoelectric behaviour allows for a more accurate pump design. In future work, the investigation of thermal effects can be integrated into the experimental setup. Therewith, both the thermal expansion of the disc actuator and the temperature-dependent change in piezoelectric elongation can be examined. This information is crucial if the pump is used at temperatures other than ambient temperature, since the difference in thermal expansion between the ceramic and actuator diaphragm change the position of the diaphragm and therewith fluidic properties of the pump. Furthermore, the initial position of the diaphragm depends on the elongation of the ceramic and the diaphragm material during the curing process. This elongation is composed of two parts: the piezoelectric elongation caused by the applied voltage offset and the thermal expansion. The extension of experimental possibilities to investigate thermal effects thus enable further understanding of the production process and more precise pump design and manufacturing.

An important finding of the disc actuator characterisation is the [coercive field](#) at which the polarisation of the piezoelectric ceramic changes its direction. This knowledge is necessary to investigate possible depolarisation caused by the negative amplitude of the pump's actuation signal. As a technological standard, no more than 30% of the negative [coercive field](#) is applied to piezoelectric actuators. However, an extension of the negative actuation of the pumps leads to an overproportional increase in flow rate due to the unsymmetrical elongation curve. The achievable improvement is especially useful for medical applications, where a high margin of safety is necessary. Evaluations presented in Chapter 4 show significant improvements of the flow rate, especially with applied backpressure, where an increase of 260 % is achieved. Long-term evaluations show no depolarisation for up to one million cycles with a negative field of up to 90 % of the [coercive field](#) strength. However, in addition to depolarisation, failure can also occur due to piezo cracking and delamination of the adhesive layer. Therefore, in future a detailed evaluation

is necessary for each specific application, especially since failure mechanisms can also depend on the periphery, e.g., backpressure or temperature.

Based on the insights of the thesis' first part, it is possible to further extend the actuation signal of EMFT's $5 \times 5 \times 0.6 \text{ mm}^3$ silicon micropump towards negative voltages. A detailed experimental analysis of the pump that is presented in Chapter 5 reveals a resulting flow rate of $74 \pm 6 \text{ } \mu\text{L}/\text{min}$ and an achievable backpressure of $12.5 \pm 0.8 \text{ kPa}$, which lends itself particularly well to subcutaneous delivery of drug solution. Furthermore, our study proves high precision compared to macroscopic, commercially available dosing units. Therefore, it can even be suitable to dose higher concentrated medication. Nevertheless, additional evaluations are necessary to investigate if the change in drug concentration influences the dosing accuracy and if the resulting higher viscosity can be transported without additional limitations. Furthermore, the study reveals need of improvement: the change from water to insulin solution causes an increased problem with air in the fluid path. The development of a pump that is not only bubble-tolerant but also doses independent of bubbles is consequently an important open topic. To this end, the compression ratio needs to be increased. Additionally, a hydrophilic surface treatment of the fluid path can facilitate priming.

The study of the dosing precision is the base for the development of a closed-loop-controlled dosing unit. The combination of the silicon micropump, higher concentrated insulin solution, and a space-efficient capacitive volume control in the drug reservoir that is developed in the dissertation of Thomas Thalsofer, will allow the development of an innovative patch pump. With a projected diameter of 30 mm and only a few millimetres in height, the planned system is extremely small compared to state of the art dosing units. This patch pump can thus improve the patients' comfort significantly.

While small silicon micro diaphragm pumps are suitable for drug delivery requiring small volumes, a high-volume delivery or hydraulic implants that need higher flow rates require larger micropumps. These applications have so far been addressed by Fraunhofer EMFT's steel micropumps. However, implantation requires artefact-free imaging, which makes the transfer of the technology from steel to titanium necessary. In addition to these technical requirements, the application in medical devices is inhibited by the large initial effort to implement a new technology. To address these two hinderances, a titanium-based microfluidic technology platform is developed and presented in Chapter 6. A flexible combination of the micro diaphragm pump with two types of active micro diaphragm valves enables the development of several medical devices based on the same platform. Therewith, costs for the initial implementation of the technology as well as regulatory efforts can be divided. The introduced platform allows the automatization of manually operated state-of-the-art implants. With such improved implants, the target group for a specific treatment can be significantly enlarged, e.g., artificial sphincter implants for women or elderly people with limited agility. Therefore, this work is a considerable step towards the industrialisation and widespread application of microfluidic devices in medical treatment.

Detailed experimental analysis of the piezoelectrically actuated pump and valves shows that the technology is suitable for biomedical applications. Nevertheless, further improvements can increase the number of achievable implants and devices. For instance, a higher blocking pressure is necessary for some hydraulic applications. To this end, the actuator needs to be stiffer, which is possible with a thicker actuator diaphragm and ceramic disc actuator. It is important to note that such changes limit the maximal achievable flow rate. An additional drawback is the high actuation voltage of up to 500 V required for the thicker piezoelectric actuator. To lower the actuation voltage would have many advantages: it guarantees a safe use within the human body, enables easier medical device

approval, and simplifies the electric actuation unit. Therefore, the development of multi-layer actuation can be extremely beneficial. Due to the specific requirements in terms of geometry, elongation and achievable force, the multilayer disc actuator needs to be custom-developed for a specific pump.

To allow a flexible usage, the pump introduced within the technology platform presented in Chapter 6 needs to function under various environmental conditions, as well as with different transported media. For instance, the operation of the pump in an automated cell culture system can require the transport of test substances. Furthermore, the transport of cells can be necessary in specific applications. To extend the pump's field of application towards automated cell culture, this thesis investigates the pump's impact on cells and vice versa. Preliminary experiments described in Chapter 7 show that transport with rectangular actuation reduces the percentage of viable cells by approximately 8 %, while sinusoidal actuation is less harmful leading to a reduction of approximately 2 %. Unfortunately, sinusoidal actuation is less efficient for fluid transport. To limit the impact without a significant loss in fluidic performance, a mixed actuation signal is tested: a rectangular wave with sinusoidal flanks. The experimental characterisation of the single [stroke volume](#) of the pump presented in Chapter 8 shows a constant [stroke volume](#) when applying sufficiently steep flanks. Therefore, we use a 15 Hz rectangular wave with 60 Hz sinusoidal flanks for cell transport and compare its influence on cell viability. The mean impact on the cell solution samples transported with different actuation signals indicate that higher frequencies are generally more harmful. The least impact is detected after transport with 15 Hz sinusoidal actuation and the difference of cell viability in samples transported with the mixed signal is not statistically significant. The adaptation of the actuation signal thus improves the cell transport with EMFT's metal micropump without reducing the fluidic efficiency.

The presented study evaluates the viability of the cells directly after transport and does not analyse the long-term effect, i.e., the activity of the cells after a given period. This detailed investigation is necessary for each specific cell type in a given application. Besides the improvement of the actuation signal investigated in Chapter 8, geometric adaptations of the pump design can further reduce the pump's impact in future. To limit the shear stress to which the cells are subjected, it is advisable to omit 90 ° angles and increase the height of flow paths. Nevertheless, an increased height of the pump chamber decreases the [compression ratio](#). This geometric adaptation is thus a trade-off between a robust [bubble tolerance](#) and a decrease in shear. Furthermore, adaptations of the passive flap valves can reduce the pump's influence on cells. For this complicated geometry, a detailed fluid mechanical simulation as well as experimental investigation are necessary to minimize the pump's impact while maintaining the required fluidic performance. It is imaginable that flap valves instead of spring valves are beneficial due to a more directed fluid flow and a reduced number of sharp edges and moving geometries.

To allow a safe and reliable use of micro diaphragm pumps in biomedical applications, it is not only necessary to limit the pump's impact on the transported medium, but also vice versa. Depending on the exact pump type, the surface in contact with the medium is completely made of silicon, steel or titanium and chemical interactions with these materials have to be considered. For example, the transport of alkaline solution with silicon pumps is restricted. In addition to chemical interaction, the pumps can be damaged physically by solids, e.g., fibres, cells, or particles in the transported fluid. Micro diaphragm pumps are sensitive to solid material in the fluid, since flow paths are narrow and

fragile structures such as the valves can be damaged. To gain a better understanding of the particle tolerance of metal micro diaphragm pumps, this subject is experimentally evaluated using polystyrene particles as described in Chapter 9. Experiments with 16 μm particles in a concentration of approximately 4.4×10^4 beads/ μL simulate the strain of a cell-printing application. Additionally, experiments with a solution with 1 μm polystyrene allow to determine an upper bound for the particle size that limits the impact on the pumps. For both sizes, the optical valve inspection shows a particle deposition not only in corners and curves, but also on flat structures. The deposition is more distinct for larger particles. The higher impact of larger particles is also visible in the [actuator stroke](#) reduction as well as in the loss of fluidic performance. The experiments show that both the large and small particles impact the pump significantly. However, the 1 μm particles cause less severe damage. Nevertheless, no pump failed completely during the course of the experiment. For short-term application, the experimental evaluation of different particle concentrations can offer additional information about the amount of supportable particles in solution. Furthermore, the change of the tested particle geometry is necessary to additionally evaluate the pump's compatibility with solids in solution. This is particularly the case for fibres, since they can get caught in the valve more easily than particles.

The transport of particle solution described above reveals geometric adaptations of the pump design that can increase the pump's particle tolerance. The beads mostly deposit in areas of little to no fluid movement. Hence, to avoid angles and narrow curves can decrease the sensitivity of the pump to particles. Sharp edges can be avoided for instance with angled boreholes for the inlet and outlet connections. However, particle deposition is also visible in the small structures of the valve foil itself. To avoid edges there is unrealistic, since the valve foils are chemically edged and postprocessing is impractical. However, an adapted overall geometry, such as a change from spring valves to flap valves, might limit the number of susceptible locations. In addition to the avoidance of sharp edges, it can be helpful to decrease narrow flow paths within the pump chamber. This can be achieved with a higher pump chamber as described above.

The experimental analysis, device development and design, as well as actuation improvement presented in this thesis are a valuable contribution to the advance of the biomedical application of micropumps. The introduced studies allow for a basic understanding of the challenging biomedical environment, emphasize crucial properties and necessary considerations and build the basis for detailed reliability studies for specific applications.

11. References

1. Jenke CW, Kibler S, Gao Y, Hollot A, Neuhann T, Kirchhof B, Montag B, Geiger M, Neitzel J, Kutter, C., Richter, M. (2014) Optimiation of a piezoelectric micropump actuator for medical application in glaucoma and phthisis therapy. Actuator 2014, 14th International Conference on New Actuators & 8th International Exhibition on Smart Actuators and Drive Systems. Conference Proceeding
2. Marziale L, Lucarini G, Mazzocchi T, Gruppioni E, Castellano S, Davalli A, Sacchetti R, Pistolesi D, Ricotti L, Menciassi A (2018) Artificial Sphincters to Manage Urinary Incontinence: A Review. Artificial organs. Doi:10.1111/aor.13164
3. Henry Anhalt and Nancy J.V. Bohannon Insulin Patch Pumps: Their Development and Future in Closed-Loop Systems
4. The Diabetes Control and Complications Trial Research Group (1997) Hypoglycemia in the Diabetes Control and Complications Trial. Diabetes. Doi:10.2337/diab.46.2.271
5. Doyle EA, Weinzimer SA, Steffen AT, Ahern JAH, Vincent M, Tamborlane WV (2004) A Randomized, Prospective Trial Comparing the Efficacy of Continuous Subcutaneous Insulin Infusion With Multiple Daily Injections Using Insulin Glargine. Diabetes Care. Doi:10.2337/diacare.27.7.1554
6. Jeitler K, Horvath K, Berghold A, Gratzner TW, Neeser K, Pieber TR, Siebenhofer A (2008) Continuous subcutaneous insulin infusion versus multiple daily insulin injections in patients with diabetes mellitus: systematic review and meta-analysis. Diabetologia. Doi:10.1007/s00125-008-0974-3
7. Zisser HC, Bevier W, Dassau E, Jovanovic L (2010) Siphon effects on continuous subcutaneous insulin infusion pump delivery performance. Journal of diabetes science and technology. Doi:10.1177/193229681000400112
8. Laubner K, Singler E, Straetener J, Siegmund T, Päch G, Seufert J (2019) Comparative Dose Accuracy of Durable and Patch Insulin Pumps Under Laboratory Conditions. Diabetes technology & therapeutics. Doi:10.1089/dia.2019.0089
9. Bowen JL, Allender CJ (2016) A Comparative Pulse Accuracy Study of Two Commercially Available Patch Insulin Infusion Pumps. Eur Endocrinol. Doi:10.17925/EE.2016.12.02.79
10. Jahn LG, Capurro JJ, Levy BL (2013) Comparative dose accuracy of durable and patch insulin infusion pumps. Journal of diabetes science and technology. Doi:10.1177/193229681300700425
11. Youan B-BC (2004) Chronopharmaceutics: gimmick or clinically relevant approach to drug delivery? Journal of controlled release official journal of the Controlled Release Society. Doi:10.1016/j.jconrel.2004.05.015
12. Lévi F, Focan C, Karaboué A, La Valette V de, Focan-Henrard D, Baron B, Kreutz F, Giacchetti S (2007) Implications of circadian clocks for the rhythmic delivery of cancer therapeutics. Advanced drug delivery reviews. Doi:10.1016/j.addr.2006.11.001
13. Levi F, Zidani R, Misset J-L (1997) Randomised multicentre trial of chronotherapy with oxaliplatin, fluorouracil, and folinic acid in metastatic colorectal cancer. The Lancet 350(9079):681–686
14. Chen TC, Napolitano GR, Adell F, Schönthal AH, Shachar Y (2015) Development of the Metronomic Biofeedback Pump for leptomeningeal carcinomatosis: technical note. Journal of neurosurgery. Doi:10.3171/2014.10.JNS14343
15. Markland AD, Richter HE, Fwu C-W, Eggers P, Kusek JW (2011) Prevalence and trends of urinary incontinence in adults in the United States, 2001 to 2008. The Journal of urology. Doi:10.1016/j.juro.2011.03.114

16. Matsushita K, Chughtai BI, Maschino AC, Lee RK, Sandhu JS (2012) International variation in artificial urinary sphincter use. *Urology*. Doi:10.1016/j.urol-ogy.2012.04.065
17. Reagan-Shaw S, Nihal M, Ahmad N (2008) Dose translation from animal to human studies revisited. *FASEB journal official publication of the Federation of American Societies for Experimental Biology*. Doi:10.1096/fj.07-9574LSF
18. Alzet osmotic pumps (2020) DURECT Corporation. <https://www.alzet.com/>. Accessed 14 Aug 2020
19. Innovative drug infusion technology for laboratory animals iPrecio. <https://www.iprecio.com/>. Accessed 14 Aug 2020
20. Low Cost Infusion Pumps for Veterinary and Laboratory Use Infuse Disk. <http://medecell.com/products.htm>. Accessed 14 Aug 2020
21. Wang Y-N, Fu L-M (2018) Micropumps and biomedical applications – A review. *Microelectronic Engineering*. Doi:10.1016/j.mee.2018.04.008
22. Tsai N-C, Sue C-Y (2007) Review of MEMS-based drug delivery and dosing systems. *Sensors and actuators. A, Physical*. Doi:10.1016/j.sna.2006.06.014
23. J B Steen and O Iversen (1969) A high precision micropump. *Journal of Physics E: Scientific Instruments* (2):419–420
24. Schubert W, Baurischmidt P., Nagel J., Thull R., Schaldach M. (1980) An implantable artificial pancreas. *Medical and Biological Engineering and Computing*. Doi:10.1007/BF02443331
25. Smits JG (1990) Piezoelectric micropump with three valves working peristaltically. *Proceedings of the 5th International Conference on Solid-State Sensors and Actuators and Eurosensors III*. Doi:10.1016/0924-4247(90)85039-7
26. Spencer WJ, Corbett WT, Dominguez LR, B. D. Shafer (1978) An electronically controlled piezoelectric insulin pump and valves. *IEEE Transactions on Sonics and Ultrasonics*. Doi:10.1109/T-SU.1978.31006
27. D_J_Laser_2004_J._Micromech._Microeng._14_R35
28. Farideh Abhari ,Haslina Jaafar and Nurul Amziah Md Yunus (2012) A Comprehensive Study of Micropumps Technologies. *International Journal of Electrochemical Science* (9765 - 9780, Vol. 7)
29. Nguyen N-T, Huang X, Chuan TK (2002) MEMS-Micropumps: A Review. *J. Fluids Eng*. Doi:10.1115/1.1459075
30. Nisar A, Afzulpurkar N, Mahaisavariya B, Tuantranont A (2008) MEMS-based micropumps in drug delivery and biomedical applications. *Sensors and Actuators B: Chemical*. Doi:10.1016/j.snb.2007.10.064
31. Regulation (EU) 2017/745 of the European Parliament and of the Council of 5 April 2017 on medical devices, amending Directive 2001/83/EC, Regulation (EC) No 178/2002 and Regulation (EC) No 1223/2009 and repealing Council Directives 90/385/EEC and 93/42/EEC. <http://data.europa.eu/eli/reg/2017/745/oj>
32. Richter M, Linnemann R, Woias P (1998) Robust design of gas and liquid micropumps. *Sensors and actuators. A, Physical*. Doi:10.1016/S0924-4247(98)00053-3
33. Kamecke U, Waldenmaier D, Haug C, Ziegler R, Freckmann G (2019) Establishing Methods to Determine Clinically Relevant Bolus and Basal Rate Delivery Accuracy of Insulin Pumps. *Journal of diabetes science and technology*. Doi:10.1177/1932296818788349
34. Pankhurst P, Abdollahi ZM (2016) Evaluation of a novel portable micro-pump and infusion system for drug delivery. *IEEE Engineering in Medicine and Biology Society. Annual Conference*. Doi:10.1109/EMBC.2016.7590740

35. Maillefer D, van Lintel H, Rey-Mermet G, Hirschi R A high-performance silicon micropump for an implantable drug delivery system. Technical Digest. IEEE International MEMS 99 Conference. Doi:10.1109/MEMSYS.1999.746886
36. Masufumi Yoshida, Louis D. Lowry (1984) Hydrostatic pressure measurement of endolymph and perilymph in the guinea pig cochlea. American Journal of Otolaryngology. Doi:10.1016/S0196-0709(84)80007-1
37. Liu G, Shen C, Yang Z, Cai X, Zhang H (2010) A disposable piezoelectric micropump with high performance for closed-loop insulin therapy system. Sensors and actuators. A, Physical. Doi:10.1016/j.sna.2010.06.030
38. Wallen JJ, Barrera EV, Ge L, Pastuszak AW, Carrion RE, Perito PE, Hakky TS (2018) Biomechanical Comparison of Inflatable Penile Implants: A Cadaveric Pilot Study. The journal of sexual medicine. Doi:10.1016/j.jsxm.2018.05.014
39. Kim L, Toh Y-C, Voldman J, Yu H (2007) A practical guide to microfluidic perfusion culture of adherent mammalian cells. Lab on a Chip. Doi:10.1039/b704602b
40. Chappell MA, Payne SJ (2006) A physiological model of the release of gas bubbles from crevices under decompression. Respiratory physiology & neurobiology. Doi:10.1016/j.resp.2005.10.006
41. Wang Y, Lee D, Zhang L, Jeon H, Mendoza-Elias JE, Harvat TA, Hassan SZ, Zhou A, Eddington DT, Oberholzer J (2012) Systematic prevention of bubble formation and accumulation for long-term culture of pancreatic islet cells in microfluidic device. Biomedical Microdevices. Doi:10.1007/s10544-011-9618-3
42. Chandrasekaran A, Packirisamy M (2012) Experimental investigation of cavitation behavior in valveless micropumps. J. Micromech. Microeng. Doi:10.1088/0960-1317/22/12/125019
43. Sung JH, Shuler ML (2009) Prevention of air bubble formation in a microfluidic perfusion cell culture system using a microscale bubble trap. Biomedical Microdevices. Doi:10.1007/s10544-009-9286-8
44. Fu T, Ma Y (2015) Bubble formation and breakup dynamics in microfluidic devices: A review. Chemical Engineering Science. Doi:10.1016/j.ces.2015.02.016
45. Jaspe J, Hagen SJ (2006) Do protein molecules unfold in a simple shear flow? Biophysical journal. Doi:10.1529/biophysj.106.089367
46. Thomas CR, Geer D (2011) Effects of shear on proteins in solution. Biotechnology letters. Doi:10.1007/s10529-010-0469-4
47. Nayak A, Dutta AK, Belfort G (2008) Surface-enhanced nucleation of insulin amyloid fibrillation. Biochemical and biophysical research communications. Doi:10.1016/j.bbrc.2008.01.159
48. Wang W, Nema S, Teagarden D (2010) Protein aggregation--pathways and influencing factors. International journal of pharmaceuticals. Doi:10.1016/j.ijpharm.2010.02.025
49. Biddlecombe JG, Smith G, Uddin S, Mulot S, Spencer D, Gee C, Fish BC, Bracewell DG (2009) Factors influencing antibody stability at solid-liquid interfaces in a high shear environment. Biotechnology progress. Doi:10.1002/btpr.211
50. Wang W, Roberts CJ (2018) Protein aggregation - Mechanisms, detection, and control. International journal of pharmaceuticals. Doi:10.1016/j.ijpharm.2018.08.043
51. Frachon T, Bruckert F, Le Masne Q, Monnin E, Weidenhaupt M (2016) Insulin Aggregation at a Dynamic Solid-Liquid-Air Triple Interface. Langmuir the ACS journal of surfaces and colloids. Doi:10.1021/acs.langmuir.6b03314
52. Geller AI, Shehab N, Lovegrove MC, Kegler SR, Weidenbach KN, Ryan GJ, Budnitz DS (2014) National estimates of insulin-related hypoglycemia and errors leading to emergency department visits and hospitalizations. JAMA internal medicine. Doi:10.1001/jamainternmed.2014.136

53. Yong PL, Olsen L, McGinnis JM (eds) (2010) *Value in Health Care: Accounting for Cost, Quality, Safety, Outcomes, and Innovation*, Washington (DC)
54. Mishra MK, Dubey V, Mishra PM, Khan I (2019) MEMS Technology: A Review. *JERR*. Doi:10.9734/jerr/2019/v4i116891
55. Vaezi M, Seitz H, Yang S (2013) A review on 3D micro-additive manufacturing technologies. *Int J Adv Manuf Technol*. Doi:10.1007/s00170-012-4605-2
56. Gietzelt T, Jacobi O, Piottter V, Ruprecht R, Hausselt J (2004) Development of a micro annular gear pump by micro powder injection molding. *J Mater Sci*. Doi:10.1023/B:JMSC.0000017774.64153.d9
57. Baumans V (2005) Science-based assessment of animal welfare: laboratory animals. *Revue Scientifique Et Technique-Office International Des Epizooties* 24(2):503
58. International Electrotechnical Commission (2016) *Medical electrical equipment - Part 2-24: Particular requirements for basic safety and essential performance of infusion pumps and controllers: IEC 60601-2-24:2012*
59. Pleus S, Kamecke U, Waldenmaier D, Freckmann G (2019) Reporting Insulin Pump Accuracy: Trumpet Curves According to IEC 60601-2-24 and Beyond. *Journal of diabetes science and technology*. Doi:10.1177/1932296818806509
60. Freckmann G, Kamecke U, Waldenmaier D, Haug C, Ziegler R (2019) Accuracy of Bolus and Basal Rate Delivery of Different Insulin Pump Systems. *Diabetes Technol Ther*. Doi:10.1089/dia.2018.0376
61. Borot S, Franc S, Cristante J, Penfornis A, Benhamou P-Y, Guerci B, Hanaire H, Renard E, Reznik Y, Simon C, Charpentier G (2014) Accuracy of a new patch pump based on a microelectromechanical system (MEMS) compared to other commercially available insulin pumps: results of the first in vitro and in vivo studies. *Journal of diabetes science and technology*. Doi:10.1177/1932296814543946
62. Zisser H, Breton M, Dassau E, Markova K, Bevier W, Seborg D, Kovatchev B (2011) Novel methodology to determine the accuracy of the OmniPod insulin pump: a key component of the artificial pancreas system. *Journal of diabetes science and technology*. Doi:10.1177/193229681100500627
63. Wackerle M, Richter M, Woias P, Goldschmidtböing F (2000) Sub-nl flow measurement method for microfluidic actuators. Borgmann, H.: *Actuator 2000. 7th International Conference on New Actuators and International Exhibition on Smart Actuators and Drive Systems*. Conference proceedings. Bremen: Messe Bremen Ges., 2000, pp. 507-510
64. Pečar B, Resnik D, Možek M, Aljančič U, Dolžan T, Amon S, Vrtačnik D (2013) Triton X-100 as an effective surfactant for micropump bubble tolerance enhancement. *Electronic Components and Materials* 43(2):103–110
65. Jenke C, Pallejà Rubio J, Kibler S, Häfner J, Richter M, Kutter C (2017) The Combination of Micro Diaphragm Pumps and Flow Sensors for Single Stroke Based Liquid Flow Control. *Sensors*. Doi:10.3390/s17040755
66. Ashraf MW, Tayyaba S, Afzulpurkar N (2011) Micro Electromechanical Systems (MEMS) Based Microfluidic Devices for Biomedical Applications: diffuser nozzle micro pump micropump. *International journal of Molecular Sciences*. Doi:10.3390/ijms12063648
67. Mohith S, Navin Karanth P, Kulkarni SM (2019) Recent trends in mechanical micro-pumps and their applications: A review. *Mechatronics*. Doi:10.1016/j.mechatronics.2019.04.009
68. Jenke C, Kager S, Richter M, Kutter C (2018) Flow rate influencing effects of micro-pumps. *Sensors and actuators. A, Physical*. Doi:10.1016/j.sna.2018.04.025
69. Zengerle R, Richter M (1994) Simulation of microfluid systems. *J. Micromech. Microeng*. Doi:10.1088/0960-1317/4/4/004

70. Richter M, Leistner H, Congar Y, Drost A, Kibler S, Röhl S, Wackerle M (2019) Piezoelektrisch angetriebene Silizium Mikropumpe der Baugröße 3,5x3,5x0,6 mm³: piezoelectric silicone micro pump sized 3.5x3.5x0.6 mm³. Proceedings Mikro System Technik Kongress 2019
71. Kittel C, McEuen P, John Wiley & Sons (2004) Introduction to Solid State Physics: Chapter 16: Dielectrics And Ferroelectrics, pp. 481. John Wiley & Sons
72. Crawley EF, Luis J de (1987) Use of piezoelectric actuators as elements of intelligent structures. AIAA Journal. Doi:10.2514/3.9792
73. Lai B-K, Kahn H, Phillips SM, Heuer AH (2004) A Comparison of PZT-Based and TiNi Shape Memory Alloy-Based MEMS Microactuators. Ferroelectrics. Doi:10.1080/00150190490460867
74. Zhang Z, Chen S, Wang S, Kan J, Wen J, Yang C (2018) Performance evaluation and comparison of a serial–parallel hybrid multichamber piezoelectric pump. Journal of Intelligent Material Systems and Structures. Doi:10.1177/1045389X18758181
75. He X, Bian R, Lin N, Xu W, Deng Z, Yang S (2019) A novel valveless piezoelectric micropump with a bluff-body based on Coanda effect. Microsyst Technol. Doi:10.1007/s00542-018-4215-5
76. Pečar B, Križaj D, Vrtačnik D, Resnik D, Dolžan T, Možek M (2014) Piezoelectric peristaltic micropump with a single actuator. J. Micromech. Microeng. Doi:10.1088/0960-1317/24/10/105010
77. Benard WL, Kahn H, Heuer AH, Huff MA (1997) A titanium-nickel shape-memory alloy actuated micropump. Proceedings of the Transducers '97 1
78. Benard WL, Kahn H, Heuer AH, Huff MA (1998) Thin-film shape-memory alloy actuated micropumps. J. Microelectromech. Syst. 7(2):245–251
79. Lexcellent C (2013) Shape-Memory Alloys Handbook. Materials Science Series. Wiley; iste
80. Zainal MA, Sahlan S, Ali MSM (2015) Micromachined shape-memory-alloy microactuators and their application in biomedical devices. Micromachines. Doi:10.3390/mi6070879
81. Rusli MQ, Chee PS, Arsat R, Lau KX, Leow PL (2018) Electromagnetic actuation dual-chamber bidirectional flow micropump. Sensors and actuators. A, Physical. Doi:10.1016/j.sna.2018.08.047
82. Shen C-Y, Liu H-K (2010) Innovative Composite PDMS Micropump with Electromagnetic Drive. Sensors and Materials 22(2):85–100
83. Zengerle R, Richter A, Sandmaier H (1992) A micro membrane pump with electrostatic actuation. Proceedings of the Micro Electro Mechanical Systems '92
84. Uhlig S, Gaudet M, Langa S, Schimmanz K, Conrad H, Kaiser B, Schenk H (2018) Electrostatically driven in-plane silicon micropump for modular configuration. Micromachines. Doi:10.3390/mi9040190
85. Xu T-B, Su J (2005) Development, characterization, and theoretical evaluation of electroactive polymer-based micropump diaphragm. Sensors and actuators. A, Physical. Doi:10.1016/j.sna.2005.01.020
86. Xu T-B, Cheng Z-Y, Zhang QM (2002) High-performance micromachined unimorph actuators based on electrostrictive poly(vinylidene fluoride–trifluoroethylene) copolymer. Appl. Phys. Lett. Doi:10.1063/1.1448661
87. Mirfakhrai T, Madden JD, Baughman RH (2007) Polymer artificial muscles. Materials Today. Doi:10.1016/S1369-7021(07)70048-2
88. Annabestani M, Fardmanesh M (2019) Ionic Electro active Polymer-Based Soft Actuators and Their Applications in Microfluidic Micropumps, Microvalves, and Mixers: A Review. arXiv: Applied Physics

89. Bar-Cohen Y, Anderson IA (2019) Electroactive polymer (EAP) actuators—background review. *Mech Soft Mater*. Doi:10.1007/s42558-019-0005-1
90. Seung-Mo Ha, Woong Cho, Yoomin Ahn (2009) Disposable thermo-pneumatic micropump for bio lab-on-a-chip application. *Microelectronic Engineering*. Doi:10.1016/j.mee.2008.12.046
91. Bodén R, Lehto M, Simu U, Thornell G, Hjort K, Schweitz J-Å (2006) A polymeric paraffin actuated high-pressure micropump. *Sensors and actuators. A, Physical*. Doi:10.1016/j.sna.2005.11.068
92. Forouzandeh F, Zhu X, Alfadhel A, Ding B, Walton JP, Cormier D, Frisina RD, Borkholder DA (2019) A nanoliter resolution implantable micropump for murine inner ear drug delivery. *Journal of controlled release official journal of the Controlled Release Society*. Doi:10.1016/j.jconrel.2019.01.032
93. Svensson S, Sharma G, Ogden S, Hjort K, Klintberg L (2010) High-Pressure Peristaltic Membrane Micropump With Temperature Control. *J. Microelectromech. Syst*. Doi:10.1109/JMEMS.2010.2076784
94. Ogden S, Klintberg L, Thornell G, Hjort K, Bodén R (2014) Review on miniaturized paraffin phase change actuators, valves, and pumps. *Microfluid Nanofluid*. Doi:10.1007/s10404-013-1289-3
95. Ullakko K, Wendell L, Smith A, Müllner P, Hampikian G (2012) A magnetic shape memory micropump: contact-free, and compatible with PCR and human DNA profiling. *Smart Mater. Struct*. Doi:10.1088/0964-1726/21/11/115020
96. Piotter V (2019) In: *Handbook of Metal Injection Molding*. Elsevier, pp 333–360
97. Piotter V, Klein A, Plewa K, Beyerlein KR, Chapman HN, Bajt S (2018) Development of a ceramic injection molding process for liquid jet nozzles to be applied for X-ray free-electron lasers. *Microsyst Technol*. Doi:10.1007/s00542-017-3493-7
98. Zhou S, Hrymak AN, Kamal MR (2018) Microinjection molding of polypropylene/multi-walled carbon nanotube nanocomposites: The influence of process parameters. *Polym Eng Sci*. Doi:10.1002/pen.24682
99. Yunas J, Mulyanti B, Hamidah I, Mohd Said M, Pawinanto RE, Wan Ali WAF, Subandi A, Hamzah AA, Latif R, Yeop Majlis B (2020) Polymer-based MEMS electromagnetic actuator for biomedical application: A review. *Polymers*. Doi:10.3390/polym12051184
100. Bußmann AB, Grünerbel LM, Durasiewicz CP, Thalhoffer TA, Wille A, Richter M (2021) Microdosing for drug delivery application—A review. *Sensors and Actuators A: Physical*. Doi:10.1016/j.sna.2021.112820
101. Cazorla P-H, Fuchs O, Cochet M, Maubert S, Le Rhun G, Fouillet Y, Defay E (2016) A low voltage silicon micro-pump based on piezoelectric thin films. *Sensors and actuators. A, Physical*. Doi:10.1016/j.sna.2016.09.012
102. Richter M, Wackerle M, Kibler S, Biehl M, Koch T, Müller C, Zeiter O, Nuffer J, Halter R (2013) Miniaturized drug delivery system TUDOS with accurate metering of microliter volumes. *SENSOR, International Conference on Sensors and Measurement Technology*, 16, AMA Conferences, 2013, 2013, pp.420-425
103. Wang J, Yang Z, Liu Y, Shen Y, Chen S, Yu J (2018) The effect of surface wettability on the performance of a piezoelectric membrane pump. *AIP Advances*. Doi:10.1063/1.5017993
104. Ma HK, Chen RH, Hsu YH (2015) Development of a piezoelectric-driven miniature pump for biomedical applications. *Sensors and actuators. A, Physical*. Doi:10.1016/j.sna.2015.08.003
105. Trenkle F, Haeberle S, Zengerle R (2011) Normally-closed peristaltic micropump with re-usable actuator and disposable fluidic chip. *Sensors and Actuators B: Chemical*. Doi:10.1016/j.snb.2009.12.069

106. Zhang Z, Kan J, Wang S, Wang H, Wen J, Ma Z (2013) Flow rate self-sensing of a pump with double piezoelectric actuators. *Mechanical Systems and Signal Processing*. Doi:10.1016/j.ymsp.2013.08.012
107. Fuchs O, Fouillet Y, Maubert S, Cochet M, Chabrol C, David N, Médal X, Campagnolo R (2012) A novel volumetric silicon micropump with integrated sensors. *Microelectronic Engineering*. Doi:10.1016/j.mee.2012.04.036
108. L. Grünerbel, A. Bußmann, O. Zett (2019) Optimization of micropump flow rate by phase dependent coupling: Hochflussoptimierung von Mikromembranpumpen durch phasengesteuerte Kopplung. *Proceedings Mikro System Technik Kongress 2019*:758–761
109. Peng T, Guo Q, Yang J, Xiao J, Wang H, Lou Y, Liang X (2019) A high-flow, self-filling piezoelectric pump driven by hybrid connected multiple chambers with umbrella-shaped valves. *Sensors and Actuators B: Chemical*. Doi:10.1016/j.snb.2019.126961
110. Leistner H, Wackerle M, Congar Y, Anheuer D, Roehl S, Richter M (2021) In: Schlaak H (ed) *Actuator 2021: International Conference and Exhibition on New Actuator Systems and Applications GMM conference*, February 17-19, 2021, online event. VDE Verlag GmbH, Berlin, Offenbach, pp 113–116
111. Zhang HJ, Qiu CJ (2006) A TiNiCu Thin Film Micropump Made by Magnetron Co-Sputtered Method. *Materials Transactions*. Doi:10.2320/matertrans.47.532
112. Yamahata C, Lotto C, Al-Assaf E, Gijs MAM (2005) A PMMA valveless micropump using electromagnetic actuation. *Microfluid Nanofluid*. Doi:10.1007/s10404-004-0007-6
113. Tandon V, Kang WS, Robbins TA, Spencer AJ, Kim ES, McKenna MJ, Kujawa SG, Fiering J, Pararas EEL, Mescher MJ, Sewell WF, Borenstein JT (2016) Microfabricated reciprocating micropump for intracochlear drug delivery with integrated drug/fluid storage and electronically controlled dosing. *Lab on a Chip*. Doi:10.1039/c5lc01396h
114. Wang C, Park J (2020) Magnetic micropump embedded in contact lens for on-demand drug delivery. *Micro and Nano Syst Lett*. Doi:10.1186/s40486-019-0101-x
115. Yan B, An D, Wang X, DeLong BJ, Kiourti A, Dungan K, Volakis JL, Ma M, Guo L (2019) Battery-free implantable insulin micropump operating at transcutaneously radio frequency-transmittable power. *Med Devices Sens*. Doi:10.1002/mds3.10055
116. Xia F, Tadigadapa S, Zhang QM (2006) Electroactive polymer based microfluidic pump. *Sensors and actuators. A, Physical*. Doi:10.1016/j.sna.2005.06.026
117. Hiraoka M, Fiorini P, O’Callaghan J, Yamashita I, van Hoof C, Beeck M op de (2012) Miniature conductive polymer actuators for high pressure generation in lab on chip systems. *Sensors and actuators. A, Physical*. Doi:10.1016/j.sna.2011.08.024
118. Johnson DG, Borkholder DA (2016) Towards an Implantable, Low Flow Micropump That Uses No Power in the Blocked-Flow State. *Micromachines*. Doi:10.3390/mi7060099
119. Yang Y-J, Liao H-H (2009) Development and characterization of thermopneumatic peristaltic micropumps. *J. Micromech. Microeng*. Doi:10.1088/0960-1317/19/2/025003
120. Saren A, Smith AR, Ullakko K (2018) Integratable magnetic shape memory micropump for high-pressure, precision microfluidic applications. *Microfluid Nanofluid*. Doi:10.1007/s10404-018-2058-0
121. Barker S, Rhoads E, Lindquist P, Vreugdenhil M, Muellner P (2016) Magnetic Shape Memory Micropump for Submicroliter Intracranial Drug Delivery in Rats. *Journal of Medical Devices*. Doi:10.1115/1.4034576

122. Smith AR, Saren A, Järvinen J, Ullakko K (2015) Characterization of a high-resolution solid-state micropump that can be integrated into microfluidic systems. *Microfluid Nanofluid*. Doi:10.1007/s10404-014-1524-6
123. Waldschik A, Büttgenbach S (2010) Micro gear pump with internal electromagnetic drive. *Microsyst Technol*. Doi:10.1007/s00542-010-1028-6
124. Iacovacci V, Tamadon I, Rocchi M, Dario P, Mencias A (2019) Toward Dosing Precision and Insulin Stability in an Artificial Pancreas System. *Journal of Medical Devices* 13(1)
125. Vinayakumar KB, Nadiger G, Shetty VR, Dinesh NS, Nayak MM, Rajanna K (2017) Packaged peristaltic micropump for controlled drug delivery application. *The Review of scientific instruments*. Doi:10.1063/1.4973513
126. Cobo A, Sheybani R, Tu H, Meng E (2016) A Wireless Implantable Micropump for Chronic Drug Infusion Against Cancer. *Sensors and actuators. A, Physical*. Doi:10.1016/j.sna.2016.01.001
127. Khalil Moussi, Abdullah Bukhamsin, Jurgen Kosel (2019) Implantable 3D Printed Drug Delivery System. *Proceedings of Transducers 2019 - EUROSENSORS XXXIII*
128. Chappel E, Mefti S, Lettieri G-L, Proennecke S, Conan C (2014) High precision innovative micropump for artificial pancreas. *Microfluidics, BioMEMS, and Medical Microsystems XII*. Doi:10.1117/12.2036068
129. Shikida Y, Mizobuchi M, Inoue T, Hamada T, Ogata H, Koiwa F, Shibata T (2018) Effect of Continuous Intravenous Calcium Loading on Fibroblast Growth Factor 23 in Normal and Uremic Rats. *Calcified tissue international*. Doi:10.1007/s00223-018-0440-2
130. Streijger F, So K, Manouchehri N, Gheorghe A, Okon EB, Chan RM, Ng B, Shortt K, Sekhon MS, Griesdale DE, Kwon BK (2018) A Direct Comparison between Norepinephrine and Phenylephrine for Augmenting Spinal Cord Perfusion in a Porcine Model of Spinal Cord Injury. *Journal of neurotrauma*. Doi:10.1089/neu.2017.5285
131. Beverungen H, Klaszky SC, Klaszky M, Côté M-P (2020) Rehabilitation Decreases Spasticity by Restoring Chloride Homeostasis through the Brain-Derived Neurotrophic Factor-KCC2 Pathway after Spinal Cord Injury. *Journal of neurotrauma*. Doi:10.1089/neu.2019.6526
132. Withey SL, Doyle RJ, Porter EN, Bergman J, Kangas BD (2020) Discrimination learning in oxycodone-treated nonhuman primates. *Drug and alcohol dependence*. Doi:10.1016/j.drugalcdep.2019.107778
133. Robble MA, Holloway IL, Ridener E, Webber CJ, Caine SB, Meloni E, Desai RI, Carlezon WA (2020) Differential effects of nicotine and nicotine withdrawal on fear conditioning in male rats. *The international journal of neuropsychopharmacology*. Doi:10.1093/ijnp/pyaa024
134. Tan T, Watts SW, Davis RP (2011) Drug Delivery: Enabling Technology for Drug Discovery and Development. *iPRECIO Micro Infusion Pump: Programmable, Refillable, and Implantable*. *Frontiers in pharmacology*. Doi:10.3389/fphar.2011.00044
135. Woias P (2005) Micropumps—past, progress and future prospects. *Sensors and Actuators B: Chemical*. Doi:10.1016/j.snb.2004.02.033
136. iPRECIO Programmable Infusion Pump (2020) DURECT Corporation. <https://www.alzet.com/iprecio-pump/iprecio-overview/>. Accessed 11 Nov 2020
137. Herz M, Richter M, Wackerle M (2016) Method for manufacturing a bending transducer, a micro pump and a micro valve, micro pump and micro valve (US9410641B2). <https://patents.google.com/patent/US9410641B2/en>
138. Huang FS, Kan JW, Zhang ZH, Ma ZH, Wang SY, Cheng GM (2013) Fabrication and Performance of a Double-Chamber Serial Piezoelectric Micropump. *AMR*. Doi:10.4028/www.scientific.net/AMR.655-657.1164

139. Yan B, Li B, Kunecke F, Gu Z, Guo L (2015) Polypyrrole-Based Implantable Electroactive Pump for Controlled Drug Microinjection. *ACS applied materials & interfaces*. Doi:10.1021/acsami.5b04551
140. Bianchi F, Conan C (2010) Drug delivery device with a module for preventing fibrillation downstream of its reservoir (US 8,257,308 B2)
141. Chappel E, Conan C, Mefti S, Cannehan F, Lettieri G-L, Proennecke S, Zanotti L, Ferrera M, Merassi A, Oggioni L (2012) Infusion Micro-Pump Development Using MEMS Technology. HAL archives ouvertes
142. Geipel A, Doll A, Goldschmidtboing F, Jantscheff P, Esser N, Massing U, Woias P (2006) In: 19th IEEE International Conference on Micro Electro Mechanical Systems. IEEE, pp 786–789
143. Liu B, Yang J, Zhang Z, Yang J, Li D (2018) A phase change microactuator based on paraffin wax/expanded graphite/nickel particle composite with induction heating. *Sensors and actuators. A, Physical*. Doi:10.1016/j.sna.2018.04.006
144. Chee PS, Minjal MN, Leow PL, Ali MSM (2015) Wireless powered thermo-pneumatic micropump using frequency-controlled heater. *Sensors and actuators. A, Physical*. Doi:10.1016/j.sna.2015.06.017
145. Schabmueller CGJ, Koch M, Mokhtari ME, Evans AGR, Brunnschweiler A, Sehr H (2002) Self-aligning gas/liquid micropump. *J. Micromech. Microeng.* Doi:10.1088/0960-1317/12/4/313
146. Dumont-Fillon D, Tahriou H, Conan C, Chappel E (2014) Insulin Micropump with Embedded Pressure Sensors for Failure Detection and Delivery of Accurate Monitoring. *Micromachines*. Doi:10.3390/mi5041161
147. Zhu R, Wallrabe U, Woias P, Wapler M, Mescheder U (2019) Semi-rigid ring-shaped electrode dielectric electroactive polymer membrane as buckling actuator. *J. Micromech. Microeng.* Doi:10.1088/1361-6439/ab078d
148. Maillefer D, Gamper S, Frehner B, Balmer P, van Lintel H, Renaud P (2001) A high-performance silicon micropump for disposable drug delivery systems. *Technical Digest. MEMS 2001. 14th IEEE International Conference on Micro Electro Mechanical Systems (Cat. No. 01CH37090):413–417*
149. Schneeberger N, Blondel A, Boutaud B, Chappel E, Maillefer D, Schneider V (2004) Disposable Insulin Pump-A Medical Case Study. *DTIP of MEMS & MOEMS:25–27*
150. Khalil Moussi, Mohammed AIDajani, Jurgen Kosel Miniaturized Drug Delivery System for Biomedical Applications
151. Wald C, Richter M, Holzer M, Weigl M (2013) Concept of a novel stainless-steel micro pump for applications in medicine and biotechnology. *Mikrosystemtechnik Kongress 2013*
152. Bruno BP, Fahmy AR, Stürmer M, Wallrabe U, Wapler MC Properties of piezoceramic materials in high electric field actuator applications
153. Richter M, Kruckow J (2010) Pump arrangement comprising a safety valve (US20100290935A1). <https://patents.google.com/patent/US8382452B2/en>
154. Amirouche F, Zhou Y, Johnson T (2009) Current micropump technologies and their biomedical applications. *Microsyst Technol*. Doi:10.1007/s00542-009-0804-7
155. Herz M, Horsch D, Wachutka G, Lueth TC, Richter M (2010) Design of ideal circular bending actuators for high performance micropumps. *Sensors and actuators. A, Physical*. Doi:10.1016/j.sna.2010.05.018
156. M. Richter, M. Wackerle, Y. Congar, A. Drost, J. Häfner, S. Röhl, S. Kibler, J. Kruckow, C. Kutter Miniaturisierung von Mikromembranpumpen für die Integration in Mobilfunkgeräte
157. Zisser H, Jovanovic L (2006) OmniPod Insulin Management System: patient perceptions, preference, and glycemic control. *Diabetes Care*, 2006:2175

158. Zisser HC (2010) The OmniPod Insulin Management System: the latest innovation in insulin pump therapy. *Diabetes therapy research, treatment and education of diabetes and related disorders*. Doi:10.1007/s13300-010-0004-6
159. Luis G. Jahn, Ph.D., Jorge J. Capurro, M.Sc., and Brian L. Levy, M.D. (2013) Comparative Dose Accuracy of Durable and Patch Insulin Infusion Pumps (7):1011–1020
160. Kargov A, Werner T, Pylatiuk C, Schulz S (2008) Development of a miniaturised hydraulic actuation system for artificial hands. *Sensors and Actuators A: Physical* 141(2):548–557
161. Solanki P (2014) Aortic Counterpulsation: C-Pulse and Other Devices for Cardiac Support. *Journal of Cardiovascular Translational Research*. Doi:10.1007/s12265-014-9548-6
162. Siracusano S, Fondacaro L, Melega E (2020) In: Siracusano S, Dodi G, Pennisi M, Gozzi C, Pastore AL, Cerruto MA (eds) *Complications of Surgery for Male Urinary and Fecal Incontinence*. Springer International Publishing, Cham, pp 43–53
163. Schrag H-J, Padilla FF, Doll A, Goldschmidtboing F, Woias P, Hopt UT (2004) German Artificial Sphincter System-GASS: Entwicklung und in vitro Evaluation eines neuen vollimplantierbarer hochintegrativen Neosphinkters zur Therapie der hochgradigen Stuhlinkontinenz / Development of a novel and highly integrated sphincter prosthesis for therapy of major fecale incontinence based on piezotechnology. *Biomedical Engineering / Biomedizinische Technik*. Doi:10.1515/BMT.2004.051
164. Sefton MV, Lusher HM, Firth SR, Waher MU (1979) Controlled release micropump for insulin administration. *Annals of Biomedical Engineering*. Doi:10.1007/BF02364120
165. Oh K, Ahn C (2006) A Review of Microvalves. *J. Micromech. Microeng* 16:13–39
166. Qian J-Y, Hou C-W, Li X-J, Jin Z-J (2020) Actuation Mechanism of Microvalves: A Review. *Micromachines* 11(2):172
167. Zaehring S, Menacher M, Kirchner P, Schwesinger N (eds) (2010) Design of a normally closed piezoelectric micro valve
168. Ramanamurthy PV, Ahrens R, Karmalkar S (2007) Piezoelectric microvalve. 0019-5596
169. Eui-Hyeok (EH) Yang, Choonsup Lee and Juergen Mueller (ed) (2003) Normally-closed, leak-tight piezoelectric microvalve under ultra-high upstream pressure for integrated micropulsion. *IEEE*
170. Rogge T, Rummler Z, Schomburg WK (2004) Polymer micro valve with a hydraulic piezo-drive fabricated by the AMANDA process. *Sensors and Actuators A: Physical* 110(1-3):206–212
171. Chen S, Lu S, Liu Y, Wang J, Tian X, Liu G, Yang Z (2016) A normally-closed piezoelectric micro-valve with flexible stopper. *AIP Advances* 6(4):45112
172. Wald C, Richter, Martin (2015) Low-Cost Edelstahl- Mikropumpen zur Probenzufuhr eines miniaturisierten Gassensorsystems zur Brandfrüherkennung. *Low-Cost Stainless Steel Micro Pumps for miniaturized early fire detection systems*, 2015th edn. VDE-Verl., Berlin
173. Bussmann A, Gruenerbel L Increasing piezo micro diaphragm pump performance by optimizing piezo actuation. *Smart Systems Integration 2019. Conference Proceedings*:1–4
174. Buchli R, Boesiger P, Meier D (1988) Heating effects of metallic implants by MRI examinations. *Magn. Reson. Med.* 7(3):255–261
175. Holton A, Walsh E, Anayiotos A, Pohost G, Venugopalan R (2002) Comparative mri compatibility of 316l stainless steel alloy and nickel–titanium alloy stents: Original article technical. *Journal of Cardiovascular Magnetic Resonance* 4(4):423–430

176. Klocke A, Kemper J, Schulze D, Adam G, Kahl-Nieke B (2005) Magnetic field interactions of orthodontic wires during magnetic resonance imaging (MRI) at 1.5 Tesla. *Journal of Orofacial Orthopedics/Fortschritte der Kieferorthopädie* 66(4):279–287
177. Brunette DM, Tengvall P, Textor M, Thomsen P (2012) *Titanium in medicine: material science, surface science, engineering, biological responses and medical applications*. Springer Science & Business Media
178. Sidambe AT (2014) Biocompatibility of Advanced Manufactured Titanium Implants—A Review. *Materials*. Doi:10.3390/ma7128168
179. Khorasani AM, Goldberg M, Doeven EH, Littlefair G (2015) Titanium in Biomedical Applications—Properties and Fabrication: A Review. *J Biomater Tissue Eng*. Doi:10.1166/jbt.2015.1361
180. Jiang G, Zhou DD (2010) In: Zhou D, Greenbaum E (eds) *Implantable Neural Prostheses 2*. Springer New York, New York, NY, pp 27–61
181. Blasco-Tamarit E, Igual-Muñoz A, Antón JG, García-García DM (2009) Galvanic corrosion of titanium coupled to welded titanium in LiBr solutions at different temperatures. *Corrosion Science*. Doi:10.1016/j.corsci.2009.02.023
182. Nakahara K, Yamamoto M, Okayama Y, Yoshimura K, Fukagata K, Miki N (2013) A peristaltic micropump using traveling waves on a polymer membrane. *J. Micro-mech. Microeng*. Doi:10.1088/0960-1317/23/8/085024
183. Rapp R, Schomburg, Schomburg WK, Schulz j, Stark W (1994) LIGA micropump for gases and liquids. *Sensors and Actuators A: Physical*. Doi:10.1016/0924-4247(94)85030-5
184. Guo T, Meng T, Li W, Qin J, Tong Z, Zhang Q, Li X (2014) UV-driven microvalve based on a micro–nano TiO₂/SiO₂ composite surface for microscale flow control. *Nanotechnology* 25(12):125301
185. Veiga C, Davim JP, Loureiro AJR Properties and Applications of Titanium Alloys: A brief Review. *Rev. Adv. Mater. Sci.* 2012(32):133–148
186. Durasiewicz C, Bußmann A, Kibler S, Wald C (2019) Experimental Characterisation and Simulation of Piezoelectric Titanium Micropumps and Titanium Microvalves. *Fordatis - Research Data Repository of Fraunhofer-Gesellschaft* 2019:<http://dx.doi.org/10.24406/fordatis/74>
187. Leyens C, Peters M, Kumpfert J (2003) *Titanium and Titanium Alloys: Fundamentals and Applications*. Wiley & Sons
188. Chen Z, Gandhi U, Lee J, Wagoner RH (2016) Variation and consistency of Young's modulus in steel. *Journal of Materials Processing Technology*. Doi:10.1016/j.jmatprotec.2015.08.024
189. Doll AF, Wischke M, Geipel A, Goldschmidtboeing F, Ruthmann O, Hopt UT, Schrag H-J, Woias P (2007) A novel artificial sphincter prosthesis driven by a four-membrane silicon micropump. *Sensors and actuators. A, Physical*. Doi:10.1016/j.sna.2007.03.025
190. Zengerle R, Ulrich J, Kluge S, Richter M, Richter A (1995) A bidirectional silicon micropump. *Sensors and actuators. A, Physical*. Doi:10.1016/0924-4247(96)80088-4
191. Wu M-H, Huang S-B, Lee G-B (2010) Microfluidic cell culture systems for drug research. *Lab on a Chip*. Doi:10.1039/b921695b
192. Yan Q, Dong H, Su J, Han J, Song B, Wei Q, Shi Y (2018) A Review of 3D Printing Technology for Medical Applications. *Engineering*. Doi:10.1016/j.eng.2018.07.021
193. Drexler HG (1994) Leukemia cell lines: in vitro models for the study of chronic myeloid leukemia. *Leukemia research*. Doi:10.1016/0145-2126(94)90103-1
194. Kurniawan YS (2019) Micro Total Analysis System Application for Biomedicals: A Mini-Review. *BJSTR*. Doi:10.26717/BJSTR.2019.12.002294

195. Patabadige DEW, Jia S, Sibbitts J, Sadeghi J, Sellens K, Culbertson CT (2016) Micro Total Analysis Systems: Fundamental Advances and Applications. Analytical chemistry. Doi:10.1021/acs.analchem.5b04310
196. Gregory N, Bancroft, Vassilios I, Sikavitsas, and Antonios G. Mikos Technical Note: Design of a Flow Perfusion Bioreactor System for Bone Tissue-Engineering Applications
197. Khait L, Hecker L, Radnoti D, Birla RK (2008) Micro-perfusion for cardiac tissue engineering: development of a bench-top system for the culture of primary cardiac cells. Annals of Biomedical Engineering. Doi:10.1007/s10439-008-9459-2
198. Chung BG, Flanagan LA, Rhee SW, Schwartz PH, Lee AP, Monuki ES, Li Jeon N (2005) Human neural stem cell growth and differentiation in a gradient-generating microfluidic device. Lab on a Chip. Doi:10.1039/b417651k
199. Tourovskaia A, Figueroa-Masot X, Folch A (2005) Differentiation-on-a-chip: a microfluidic platform for long-term cell culture studies. Lab on a Chip. Doi:10.1039/b405719h
200. Elemoso A, Shalunov G, Balakhovsky YM, Ostrovskiy AY, Khesuani YD (2020) 3D Bioprinting: The Roller Coaster Ride to Commercialization. Int J Bioprint. Doi:10.18063/ijb.v6i3.301
201. Gu Z, Fu J, Lin H, He Y (2020) Development of 3D bioprinting: From printing methods to biomedical applications. Asian J Pharm Sci. Doi:10.1016/j.ajps.2019.11.003
202. Ozbolat IT, Peng W, Ozbolat V (2016) Application areas of 3D bioprinting. Drug discovery today. Doi:10.1016/j.drudis.2016.04.006
203. Peng W, Unutmaz D, Ozbolat IT (2016) Bioprinting towards Physiologically Relevant Tissue Models for Pharmaceuticals. Trends in biotechnology. Doi:10.1016/j.tibtech.2016.05.013
204. Peng W, Datta P, Ayan B, Ozbolat V, Sosnoski D, Ozbolat IT (2017) 3D bioprinting for drug discovery and development in pharmaceuticals. Acta biomaterialia. Doi:10.1016/j.actbio.2017.05.025
205. Butzelaar L, Ulrich MMW, van der Mink Molen AB, Niessen FB, Beelen RHJ (2016) Currently known risk factors for hypertrophic skin scarring: A review. Journal of plastic, reconstructive & aesthetic surgery JPRAS. Doi:10.1016/j.bjps.2015.11.015
206. Wang Y, Beekman J, Hew J, Jackson S, Issler-Fisher AC, Parungao R, Lajevardi SS, Li Z, Maitz PKM (2018) Burn injury: Challenges and advances in burn wound healing, infection, pain and scarring. Advanced drug delivery reviews. Doi:10.1016/j.addr.2017.09.018
207. Henderson J, Arya R, Gillespie P (2012) Skin graft meshing, over-meshing and cross-meshing. International journal of surgery (London, England). Doi:10.1016/j.ijso.2012.08.013
208. Yan W-C, Davoodi P, Vijayavenkataraman S, Tian Y, Ng WC, Fuh JYH, Robinson KS, Wang C-H (2018) 3D bioprinting of skin tissue: From pre-processing to final product evaluation. Advanced drug delivery reviews. Doi:10.1016/j.addr.2018.07.016
209. Skardal A, Mack D, Kapetanovic E, Atala A, Jackson JD, Yoo J, Soker S (2012) Bioprinted amniotic fluid-derived stem cells accelerate healing of large skin wounds. Stem cells translational medicine. Doi:10.5966/sctm.2012-0088
210. Navid Hakimi, Richard Cheng, Lian Leng, Mohammad Sotoudehfar, Phoenix Qing Ba, Nazihah Bakhtyar, Saeid Amini-Nik, Marc G. Jeschke, Axel Günther Handheld skin printer: in situ formation of planar biomaterials and tissues
211. Mohith S, Karanth PN, Kulkarni SM (2019) Experimental investigation on performance of disposable micropump with retrofit piezo stack actuator for biomedical application. Microsyst Technol. Doi:10.1007/s00542-019-04414-2

212. Yamahata C, Vandevyver C, Lacharme F, Izewska P, Vogel H, Freitag R, Gijs MAM (2005) Pumping of mammalian cells with a nozzle-diffuser micropump. *Lab on a Chip*. Doi:10.1039/b504468e
213. Bußmann AB, Durasiewicz CP, Kibler SHA, Wald CK (2021) Piezoelectric titanium based microfluidic pump and valves for implantable medical applications. *Sensors and Actuators A: Physical*. Doi:10.1016/j.sna.2021.112649
214. Thalhofer T, Bussmann A, Durasiewicz C, Hayden O (2021) In: *ACTUATOR; International Conference and Exhibition on New Actuator Systems and Applications 2021*, pp 1–4
215. Schneider U, Schwenk H-U, Bornkamm G (1977) Characterization of EBV-genome negative “null” and “T” cell lines derived from children with acute lymphoblastic leukemia and leukemic transformed non-Hodgkin lymphoma. *International Journal of Cancer*
216. Zengerle R, Geiger W, Richter M, Ulrich J, Kluge S, Richter A (1995) Transient measurements on miniaturized diaphragm pumps in microfluid systems. *Sensors and actuators. A, Physical*. Doi:10.1016/0924-4247(94)00961-G
217. Ozbey A, Karimzadehkhoei M, Kocaturk NM, Bilir SE, Kutlu O, Gozuacik D, Kosar A (2019) Inertial focusing of cancer cell lines in curvilinear microchannels. *Micro and Nano Engineering*. Doi:10.1016/j.mne.2019.01.002
218. Connolly S, McGourty K, Newport D (2020) The in vitro inertial positions and viability of cells in suspension under different in vivo flow conditions. *Scientific reports*. Doi:10.1038/s41598-020-58161-w
219. Huber D, Oskoei A, Casadevall I Solvas X, Andrew d, Kaigala GV (2018) Hydrodynamics in Cell Studies. *Chemical reviews*. Doi:10.1021/acs.chemrev.7b00317
220. Daniszewski M, Crombie DE, Henderson R, Liang HH, Wong RCB, Hewitt AW, Pébay A (2018) Automated Cell Culture Systems and Their Applications to Human Pluripotent Stem Cell Studies. *SLAS technology*. Doi:10.1177/2472630317712220
221. Votanopoulos KI, Mazzocchi A, Sivakumar H, Forsythe S, Aleman J, Levine EA, Skardal A (2019) Appendiceal Cancer Patient-Specific Tumor Organoid Model for Predicting Chemotherapy Efficacy Prior to Initiation of Treatment: A Feasibility Study. *Annals of surgical oncology*. Doi:10.1245/s10434-018-7008-2
222. Joung D, Truong V, Neitzke CC, Guo S-Z, Walsh PJ, Monat JR, Meng F, Park SH, Dutton JR, Parr AM, McAlpine MC (2018) 3D Printed Stem-Cell Derived Neural Progenitors Generate Spinal Cord Scaffolds. *Advanced functional materials*. Doi:10.1002/adfm.201801850
223. Christopher D. Lindsay, Julien G. Roth, Bauer L. LeSavage, Sarah C. Heilshorn (2019) Bioprinting of stem cell expansion lattices. *Acta biomaterialia*. Doi:10.1016/j.actbio.2019.05.014

Abbreviations

CP	conjugated polymers
EAB	extra-aortic balloon
EAP	electro active polymer
FEM	finite-element-modelling
FKM	fluorocarbon
Fraunhofer EMFT	Einrichtung für Mikrosysteme Festkörpertechnologien (Fraunhofer EMFT Research Institution for Microsystems and Solid State Technologies)
iEAP	ionic electro active polymer
IPMC	ionic polymer-metal composite
MEMS	micro electro mechanical system
MRI	magnetic resonance imaging
MSM	magnetic shape memory
NC	normally closed
NO	normally open
PANI	polyaniline
PPy	polypyrrole
PZT	lead zirconate titanate

Glossary

actuator stroke	Movement of the pump's piezoelectric bending actuator. The distance between the highest and lowest point is the stroke height.
blocking pressure	Maximal achievable backpressure of the micro diaphragm pump when transporting incompressible media
bubble independence	Capability of a pump to transport bubbles without deviation of the flow rate
bubble tolerance	Capability of a pump to transport bubbles without failure
coercive field	Electric field, where the polarisation of a piezoelectric ceramic changes its direction.
compression ratio	Ratio of displaced volume to the dead volume in the pump chamber
dosing accuracy	Deviation of the mean value from a target value
dosing precision	Scattering of repeated measurements under the same conditions
dosing stability	Flow rates susceptibility to environmental parameters such as pressure, temperature, or medium's viscosity, as well as steady dosing over time
freeflow	Unrestricted throughflow caused by an overpressure at the pump's inlet
large-signal	Input signal above the limit for linear transmission of non-linear systems. In this thesis, voltages that drive the piezoelectric ceramic in its non-linear regime.
large-signal behaviour	Behaviour of a non-linear transmission system with input signal up to their maximum value. In this thesis, the electromechanical properties of the piezoelectric ceramic with an actuation voltage up to the saturation field.
microdosing	Dosage of small amounts of fluids in the range of nano- or microliter
microfluidics	The science of fluid flow at small length scales (micrometre scale) or with small volume flow ($\mu\text{l}/\text{min}$)
pretension technique	Process of the piezoelectric ceramic actuator mounting. The application of an electric voltage offset during glue curing

	leads to a bulged-up pump chamber and increased compression ratio.
stroke height	Distance between the highest and lowest position of the actuator diaphragm
(single) stroke volume	Displaced volume with a single actuator movement

Appendix

A. Supplementary Material Chapter 5

Table A.1 Overview of the material necessary for the manufacturing of the silicon micropump

Item	Description
Monocrystalline silicon wafer (n-doped, 100)	Base material for manufacturing the silicon micropump consisting (two valve wafers and one actuator wafer)
Piezoelectric disc	PIC 252; base material forming the bending actuator together with the actuator wafer
2k-epoxy glue	EPOTEK 353 ND-T, to attach the disc actuator to the pump body
O-ring	FKM material that seals the fluidic periphery with the micropump housing
Soft sealing	Costume made FKM sealing prevent leakage between the silicon micropump and the housing
Micropump housing	Special developed PEEK assembly to house the silicon micropump
Filter frit	Stainless steel filter at the inlet of the micropump housing, blocking particles larger than 5 μm
Capillaries	PEEK capillaries with 1 mm inner diameter
M1 screw	Standard screw to clamp the silicon micropump to the housing with its cover

B. Supplementary Material Chapter 8

Experimental Setup for Cell Transport and Gravimetric Measurement

The setup for cell transport experiments (Figure B.1 a) is simple with the pump being connected with flexible tubing with the inlet and outlet reservoir. The gravimetric setup was evaluated in a preliminary setup as shown in Figure B.1 b. In this setup, the pump transports liquid from the inlet reservoir on the balance towards an outlet next to it. The actuation signal of the pump is verified with an oscilloscope. This setup was improved for the experiments in this work as shown in Figure 8.2.

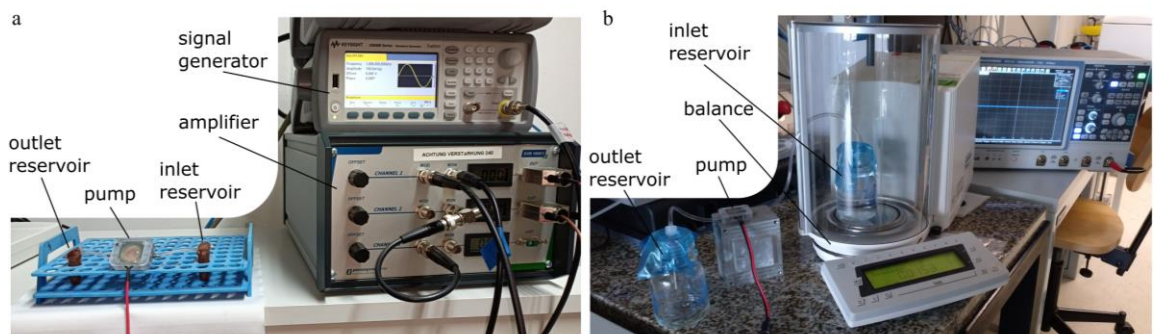


Figure B.1(a) Experimental setup of the cell transport including an inlet and outlet reservoir as well as the electric actuation of the pump; (b) Preliminary gravimetric setup to detect the single stroke volume of the piezoelectric micropump. The setup was slightly improved for the final experiments.

Flow Characterisation with Different Actuation Waveforms

The mean frequency dependant flow rate of five pumps shows an influence of the actuation waveform (Figure B.2). The rectangular actuation and the hybrid actuation (rectangular with 60 Hz sinusoidal flanks) show a similar flowrate up to 25 Hz actuation frequency. For higher frequencies, the rectangular signal achieves clearly higher flow. However, a rectangular actuation can damage the actuator ceramic especially during long term use with liquid media, which is why the hybrid signal can be a good tradeoff. The increase of flow rate compared to sinusoidal actuation is 16% for 15 Hz, which is the frequency used for cell transport.

The periphery has an influence on the flowrate, especially for higher actuation frequencies. Since the flow characterisation takes place in a large setup with comparatively long tubes and sensors that depict a flow resistance, the real flow rate during cell transport (with short tubes and no additional elements) is potentially even higher for the transport with 60 Hz.

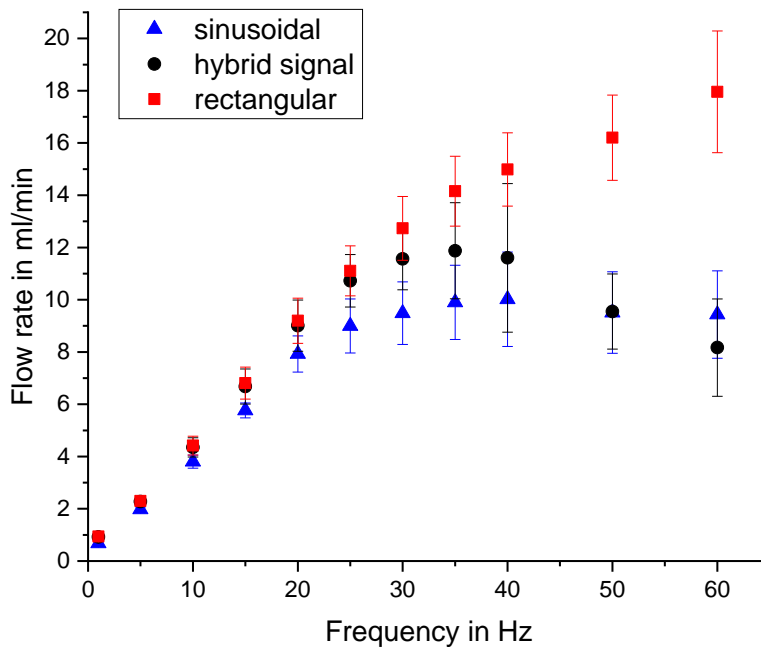


Figure B.2 Comparison of the fluidic performance of the tested micropump type with different actuation signals. Frequency dependent flow rate at 14 kPa backpressure and an actuation amplitude of $-89/300$ V. The compared waveforms are a rectangular wave, sinusoidal wave, and a hybrid signal that consist of a rectangular waveform with 60 Hz sinusoidal flanks as has been used for cell transport. The error bars depict the standard deviation of five individual pumps.